The Degradation of Pigments in the Water Column and Sediments of the Bermuda Rise

A Thesis presented

by

Ashley B. Cohen

to

The Graduate School

in Partial Fulfillment of the

Requirements

for the Degree of

Master of Science

in

Geosciences

Stony Brook University

December 2014

ProQuest LLC.
789 East Eisenhower Parkway
P.O. Box 1346
Ann Arbor, MI 48106 - 1346

Stony Brook University

The Graduate School

Ashley B. Cohen

We, the thesis committee for the above candidate for the

Master of Science degree, hereby recommend

acceptance of this thesis

Dr. Robert Aller - Thesis Advisor
Professor, School of Marine and Atmospheric Sciences

Dr. Cindy Lee - Thesis Advisor
Professor, School of Marine and Atmospheric Sciences

Dr. Troy Rasbury - Thesis Committee Chair
Professor, Department of Geosciences

This thesis is accepted by the Graduate School

Charles Taber
Dean of the Graduate School

Abstract of the Thesis

The Degradation of Pigments in the Water Column and Sediments of the Bermuda Rise

by

Ashley B. Cohen

Master of Science

in

Geosciences

Stony Brook University

2014

The export of particulate carbon from the surface ocean into deeper water and to the seabed is a critical component of the carbon cycle. The concentrations and compositions of particulate pigments collected at different depths and sinking at different settling velocities can be used as a proxy for biologically mediated processes important to the early degradation of OM. By knowing what processes the compositional and quantitative changes in the particulate pigments represent, the POM cycle of the BaRFlux area can be better understood. It is important to understand the POM cycle because deposition of OM to the seabed is the only way that OM is sequestered. The removal of POM from the marine POM cycle is especially important to understand in subtropical gyre areas like the BaRFlux site because:

1. subtropical gyres are areas of downwelling, and therefore POM transport to the deep ocean and may increase as global warming continues, and

2. the flux of CO_2 to the ocean is increasing from rising levels of atmospheric CO_2, and CO_2 removed by the biological pump will lessen processes like ocean acidification.

This thesis examines the early degradation of chloropigments in the sediment and water column in the Bermuda Rise area of the Sargasso Sea. Water column particulate samples were collected with in-situ pumps, Niskin bottles, and Indented Rotating Sphere (IRS) sediment traps, and sediment was collected by box cores during 2011-2013 to record seasonal patterns in quantity and quality of particulate pigments as a function of water column depth and particle size. Chl-a, Chl-b, and pheopigments were separated and quantified using reverse-phase High Performance Liquid Chromatography (HPLC).

The comparison of data from in-situ pumps and Niskin bottles indicates that collection method significantly affects particulate pigment data concentrations. Niskin bottle data showed total pigment concentrations 10 times greater than in-situ pump pigment concentrations at shallow depths. At depths below the euphotic zone, Niskin bottle and in-situ pump concentrations both appear similar because the particulate pigment concentrations were below the detection limit. For the BaRFlux study area, the differences in Niskin bottle and pump data are most likely from: 1. the biased particle distribution due to sampling a small volume of seawater with Niskin bottles in an area of dilute particle concentration; 2. the greater retention efficiency of picophytoplankton on Niskin GF/F filters than 1-μm in-situ pump microquartz filters.

The compositional changes seen in small suspended particulate pigments over depth is consist with small suspended particles being consumed by shallow water zooplankton and then increasingly altered by microbial activity with increasing depth. The composition of small and large particulate pigments were compared to determine if aggregation-disaggregation was an important process. Larger suspended particulate pigments were nearly 100% Chl-a over depth and distinct from smaller suspended particulate pigments other than samples from May or June, during which particle exchange may be more important. The comparison of particulate pigment data to CTD beam transmissivity profiles suggests that the nepheloid layer consists of small suspended particulate matter rather than large particles.

Sediment trap samples were compositionally enriched in pheopigments relative to smaller bottle and pump samples, indicative of enrichment with more rapidly sinking larger zooplankton fecal pellets. The mole% of chlorophyll-a labile pigment increased with increasing settling velocity, suggesting aggregation may increase the settling velocity of particles enough to escape zooplankton feeding. The particulate pigment composition of seafloor sediment collected in August was compositionally distinct from that of suspended and sinking particulate pigments and was nearly 100% pheophorbide-a, indicating POM degradation by feeding macrobenthos.

Contents

List of Figures

List of Tables

Acknowledgements

I sincerely thank my two advisors, Dr. Cindy Lee and Dr. Robert Aller for all of their patience and guidance not only in the making of this thesis but in teaching a classical sedimentologist like myself geochemistry from first principles. All of the suggested literature and informal conversations have made me truly love this field. I would also like to especially thank Carolina Cisternas-Novoa, Dr. Cindy Lee's PhD student. Carolina was invaluable in getting me trained on the laboratory equipment and data analysis procedures. Carolina and our undergraduate assistant, Anthony Ciaverella, were also very helpful by periodically running my samples for me.

I thank my fiancé, Adith Ramamurti, who taught me how to code in Python and typeset documents in LaTeX. He was a very patient reader and editor, as well. Without these, the calculations and thesis writing processes would have been more arduous. His advice and support was invaluable in helping me succeed.

I would like to thank all of the participants from the School of Marine and Atmospheric Sciences in the National Science Foundation funded BaRFlux Project. Everyone was extremely informative and willing to get me up to speed. The collection of particulate pigment samples from 2011-2013 provided me with samples to learn how to use reverse phase HPLC and to study the geochemistry of the Particulate Organic Matter in the open ocean.

I am appreciative of Dr. Troy Rasbury's time in reading this thesis and in leading my thesis committee, especially at such a busy time of year.

My friends have been an amazing support system during the creation of this thesis, which was juggled with many other academic and personal obligations. They truly helped me manage my stress more efficiently and assisted me in seeing situations positively when I got overwhelmed.

1 Introduction

Understanding the quantity and composition of Particulate Organic Matter (POM) present in the reservoirs of the marine POM cycle will help us better understand the specific processes that connect reservoirs and to create more accurate geochemical models, especially for elucidating the impact of future climate change on the marine POM cycle. Examining the mechanisms of POM cycling using organic biomarkers is useful because specific chemical compositions can be attributed to specific degradation reactions or other chemical changes.

The deposition of OM at depth by the biological pump is how OM is removed from the marine POM cycle. The degradation of POM as it sinks from the euphotic zone towards the sediment-water interface can be examined by several different types of biomarkers, including lipids, amino acids, and pigments. Here I examine the early diagenesis of Chl-a in the water column and sediment of the Bermuda Rise. The study of the early Chl-a degradation pathways can trace not just how much POM has been altered, but *how* it has been altered.

After presenting preliminary background information about the production and flux of POM in the open ocean and the Chl-a degradation pathways, I will describe chemical and spectroscopic methods used to analyze samples taken during cruises between 2011 and 2013 to the oligotrophic Bermuda Rise region as part of the BaRFlux project. Results of the sample analyses from water column Niskin bottles and in-situ pumps, sediment traps, and sediment box cores will be presented and compared with previous studies. The comparison of particulate chloropigments in suspended and sinking particles and deposited particulate pigments in sediment will be used to discuss the following questions:

1. What are the dominant degradation pathways of particulate pigments between production in the euphotic zone and post depositional alteration?

2. How do the sampling techniques used to collect particulate pigments affect its quantification?

3. Is particle exchange is a significant process in the OM cycle in the Bermuda Rise?

4. What is the role of the nepheloid layer in the early degradation and sequestration of POM?

5. What does the difference in pigment quantity and quality in sinking and suspended particulate pigments suggest about the role of settling velocity in the OM cycle?

2 Background

2.1 Particulate Organic Matter Production and Flux to the Sea Floor

Because sinking POM is the means by which the ocean's biological pump sequesters OC, the flux and composition of sinking particulate pigments has been of great interest to oceanographers and geochemists for over seventy years. The efficiency of the biological pump depends on both the export of sinking particles from the euphotic zone and their diagenetic alteration as they descend through the mesopelagic zone and the deep sea [Buesseler et al., 2007b, Wakeham et al., 2009]. The change in the quantity and quality of chloropigments as a function of both depth and settling velocity has been studied to better understand the degradation processes that selectively degrade particles at different depths and sinking at different rates [Wakeham et al., 2009, Lee et al., 2000]. Several government funded global scale studies, for example, the United States Joint Global Ocean Flux Survey (USJGOFS), Mediterranean Flux study (MedFlux), and Vertical Transport in the Global Ocean study (VERTIGO) have been conducted to better understand these processes.

POM includes living and detrital organic matter. In marine settings, POM is predominantly produced in the euphotic zone and is transformed biologically, chemically, and physically as it sinks towards the sediment-water interface, where it undergoes further diagenesis. Although the chemical composition of POM is the major influence on its bioavailability, the time it spends in the water column and at the sediment seawater interface also matters. The physical properties of particle size and density can determine how quickly a particle can sink through the water column, and those properties can change through aggregation-disaggregation processes. In addition to biological consumption and aggregation-disaggregation, chemical reactions can alter POM through sorption and photoxidation [Wakeham and Lee, 1988, Emerson and Hedges, 2008]. Due to these processes, only about 1-10% of the POM produced in the euphotic zone reaches the seafloor [Wakeham and Lee, 1988, Honjo et al., 1980]. In sediment with an active benthic community, the labile fraction of POM that does reach the sediment-water interface is rapidly consumed [Bianchi et al., 1988a, Reuss et al., 2005]. Degradation is enhanced if the loose "floc" becomes resuspended. This resuspended floc, can form a benthic boundary layer, and is common in some areas during autumn and winter due to storm activity [Louda et al., 2000].

2.1.1 Suspended vs. Sinking Particles

It is important to understand the relationship between suspended and sinking particles because the exchange of OM between these particle types links OM production in the upper ocean to OM removal by deposition at depth. The relationship between particle size/density and sinking rate has led to the operational definition of "suspended" and "sinking" POM, which are collected by Niskin Bottles or in-situ pumps and sediment traps, respectively. These two POM types are chemically distinct [Liu et al., 2009], and

have different sources and transport mechanisms. [Wakeham and Canuel, 1988, Abramson et al., 2010]. However, there are major questions about the extent to which these particles exchange with one another, and the processes by which they do that.

The inconclusiveness of the "particle exchange debate" mostly stems from the questionable accuracy of different collection methods in different hydrodynamic and biogeochemical settings. Shallow sediment traps can be inefficient in some areas, particularly where currents are strong [Peterson et al., 2005, Buesseler et al., 2007a]. The selective leaching of certain compounds into trap supernatant from particles after collection has also been a problem in deep sediment traps deployed for long periods of time [Buesseler et al., 2007a].

McCave [1975] estimated that sinking particulates larger than 100 μm should make up over half of the resuspended particulate pigments in the nepheloid layer. Because large particles are rare relative to smaller particles in the ocean, the relatively small volume of seawater collected with a Niskin bottle has very little chance of containing many large sinking particulate pigments. Niskin bottle samples will therefore have a sampling bias towards a smaller average particle size. In-situ pumps are used to minimize this bias (e.g., Bishop et al. [1978]). By pumping large volumes of seawater through a filter, the probability of large particle collection increases. Moored sediment traps have also been used to collect sinking particulate pigments [Honjo et al., 1980].

Suspended particle data may be biased by the sample filtration and handling method, e.g., by Niskin bottles or by in-situ pumps. In-situ pumps vacuum-filter large volumes of seawater onto a stacked 70-μm Nitex mesh filter and 1-μm microquartz filter. Niskin bottles are lowered into the water column and seal a small amount of seawater inside, after which they are shaken, transferred into containers through a spigot, and filtered onto 0.7 μm GF/F filters. There has been significant disagreement between the POM measurements in samples collected by Niskin bottles and by in-situ pumps at the same location, depth, and time [Altabet et al., 1992].

Differences in post-collection handling, filtration pressure, and filter material properties between these two collection methods have been examined in many studies, e.g., [Altabet et al., 1992, Liu et al., 2005]. Generally, samples collected with Niskin bottles have resulted in concentration data 2-3 times greater than samples collected by in-situ pumps. This difference seems to be most pronounced in shallow samples and decreases with depth. Several processes have been suggested to explain these differences, including the filter retention efficiency of different primary producers, sorption errors, and pressure differences.

The sorption of DOC to filters can result in the overestimation of POC in samples [Gardner et al., 2003]. Because Niskin bottles collect a much smaller amount of seawater relative to the filter area they pass through, the overestimation of POC is much greater than for in-situ pump filters, which pass 10s to 100s of liters of seawater through the filter, creating a much larger sample relative to the filter area. Turnewitsch et al. [2007] found in their study of the Northeast Atlantic and Baltic Sea that the sorption of DOC to filters seems to be enhanced in the surface ocean compared to the deep ocean. For conservative POC concentration quantification, subtracting the amount of OC in a blank filter from amounts found in natural samples has been suggested [Moran et al., 1999].

The vacuum pressure used to filter large volumes of seawater through in-situ pumps may also 'force' POM that would otherwise be retained through the microquartz filter through, resulting in an erroneously low particle concentration. Particle wash-out of larger POM captured in the 70-μm Nitex mesh under higher energy hydrodynamic conditions can also result in the undercollection of POM. For samples taken in oligotrophic regions, pumps may underestimate POM concentrations because the average size of primary producers are often less than 1-μm. The biomass of picophytoplankton has been argued to be better captured on the 0.7 μm GF/F filters used for Niskin bottle sample filtration [Sheridan, 2000]. Liu et al. [2005] found that Niskin bottle samples also tend to collect more zooplankton, further adding to the discrepancy in collected biomass.

2.1.2 The Benthic Nepheloid Layer and Sediments

Less than 1% of POM produced in the euphotic zone settles to the sediment-water interface of the deep sea. In some areas, this POM and other sediment particles can be resuspended by turbulent shear flow as a loose "cloud" or "floc" which forms a nepheloid layer hovering above the seafloor (Fig. 2). The water column just above the nepheloid layer, "the clear water minimum," separates the water column into two zones defined by the dominant particle source and particle flux mechanisms [Biscaye and Eittreim, 1977].

POM present in the water column above this minimum reflects the net downward flux and reactions of material from the euphotic zone, while POM present below reflects the downward flux of material from the euphotic zone, the upward flux from the seabed, vertical mixing, and horizontal advection. The average particle size of POM within the sediment floc is several times larger than POM in the water column directly above it, suggesting POM entering the nepheloid layer is aggregated. Aggregation likely occurs while the particulate pigments sit on the seafloor before resuspension, where particles in direct contact are more likely to flocculate, and ingestion by benthos can contribute larger fecal pellets to the POM pool [Gardner et al., 1985]. Alternatively, aggregates with fresh material from the upper water column can be disaggregated at the seafloor and resuspended as floc, providing a source of labile material to the deep water column [Gardner et al., 1985]. The residence time of particles in the nepheloid layer documented in the western North Atlantic range from days to months 15-500 m above the seafloor. Smaller particles with a slower settling velocity may be resuspended just once over the course of their residence time, while larger particles may rapidly be exchanged with the sediment-water interface several times [Gardner et al., 1985].

Studies of POM in the deep western North Atlantic nepheloid layer indicate the nepheloid floc is compositionally distinct from sinking particulate pigments directly above it in the water column [Gardner et al., 1985]. The floc has a higher C/N ratio and a lower OC concentration relative to sinking particulate pigments directly above. There is also evidence for the repeated weakening of protective calcium carbonate of sinking organisms before burial [Gardner et al., 1985]. The exposure of labile organic matter protected in rapidly sinking calcareous ballast material [Armstrong et al., 2002, 2009, Wakeham et al., 2009] could provide a source of undegraded material, including pigments, to the seafloor.

2.1.3 Particle Aggregation-Disaggregation

The discovery that suspended particulate pigments collected in the mesopelagic zone are compositionally distinct from sinking particulate pigments is not consistent with theories of particle aggregation-disaggregation originating from radioisotope work [Bacon and Anderson, 1982]. Instead, Wakeham and Canuel [1988] postulated the existence of two distinct sinking particulate pigments pools, one pool consisting of zooplankton fecal pellets and other relatively degraded material, and the other pool consisting of labile particulate organic compounds that are incorporated into algal aggregates. Later studies suggested that the aggregated particulate pigments are bound by an organic "glue',' which is a combination of mucus, marine snow, or transparent exopolymers (TEP) [Alldredge et al., 1990, Passow, 2002].

2.2 Particulate Chloropigments

Pigments are useful indicators of diagenetic processes acting on POM because they have a unique source in surface waters and follow fairly well understood pathways of degradation as they sink. Among the pigments, chlorophyll is most commonly used to trace the alteration pathways of primary production [Lee et al., 2000].

Chl-a is an ester of phytol, an acyclic isoprenoid alcohol. It consists of a porphyrin ring containing a central Mg^{2+} ion with a phytol side chain [Bianchi and Canuel, 2011]. The chloropigments include the chlorophylls and their immediate early diagenetic products, the pheopigments; these degradation products have lost the phytol side chain and/or the central Mg^{2+}, but still retain the porphyrin structure. Pheopigments are usually formed biotically in marine systems, but can also be formed abiotically. Abiotic pheopigment-producing processes include photooxidation and hydrolysis. Biotic pheopigment-producing processes include grazing, phytoplankton cell senescence, and microbial degradation [Chen et al., 2003, Sun et al., 1991, Bianchi et al., 1988a].

2.2.1 Degradation of Chl-a

Chl-a is the major plant pigment, although other chlorophylls are common and can also be abundant. They all follow similar degradation pathways. Although some chlorophylls may be degraded directly to CO_2, most biological degradation of Chl-a in the marine environment proceeds mostly through the successive removal of one or more structural substituents (Fig. 3). Products include pyropheophorbide-a, pheophytin-a, or pheophorbide-a. These pheopigments are formed from the removal of -$COOCH_3$, -Mg^{2+}, and the phytol tail, respectively [Satoh and Hama, 2013]. $COOCH_3$-retaining pheopigments such as pheophorbide-a are favored under oxidative conditions over pheopigments retaining phytol side chains. Eventually, pyropheophorbide-a will be formed after losing all three substituents [Szymczak-Zyła et al., 2008]. Many of these compounds have very short lifespans, so that major degradation products found in the marine environment are pheophorbide-a , pheophytin-a, and pyropheophorbide-a. The degradation pathway depends on how the chlorophyll is present in the environment. For example, the chlorophyll in picoplankton such as prochlorophytes and cyanobacteria tends to degrade into

pheophorbide-a through the chlorophyllide pathway, while the Chl-a of green algae tends to degrade into pheophytin-a [Steinman et al., 1998, Szymczak-Zyła et al., 2008].

2.2.2 Chloropigment Distribution in the Water Column

The distribution of chlorophyll in the water column is dependent on light and nutrient conditions; the distribution of the different types of chlorophyll is dependent on phytoplankton community composition [Hoek, 1995]. In this thesis, I will analyze and discuss only Chl-a and Chl-b. All phytoplankton produce Chl-a and Chl-b, the major light harvesting pigment and accessory pigment, respectively, of Photosynthetically Active Radiation (PAR). The ratio of Chl-a to accessory pigments typically decreases with depth for each species of phytoplankton and varies among the phytoplankton depending on environmental factors. For example, organisms like prochlorophytes and cyanobacteria, which inhabit the Deep Chlorophyll Maximum Layer (DCML) rather than the surface euphotic zone have a lower Chl-a to accessory pigment ratio to better collect the small amount of light. As cyanobacteria do not produce Chl-b, very low Chl-a to Chl-b ratios indicate the presence of prochlorophytes [Hoek, 1995].

In the open ocean, particulate pigment concentrations decrease rapidly and are present in only very low concentrations at depth. Once chlorophyll is produced in surface waters by phytoplankton, various chemical reactions can alter its structure while it is sinking through the water column. The sequence of chemical reactions for each chlorophyll molecule is determined by the path it takes through the marine OM cycle. These pathways include: undisturbed descent through the water column in aggregates, particle exchange during aggregation-disaggregation, cell senescence, ingestion and egestion by zooplankton, microbial colonization and decomposition of particles, and decomposition in the sediments by benthic organisms including microbes (Fig. 1).

2.2.3 Undisturbed Descent Through the Water Column in Aggregates / Particle Exchange During Aggregation-Disaggregation

Undegraded POM can descend through the water column by evading heterotrophic grazing pressure. The "escape" from grazers is possible in two ways: sinking quickly enough to evade grazers that are present, or settling through the water column when grazers are absent [Steinman et al., 1998]. POM can sink more rapidly by forming aggregates with a greater effective particle size and density. More slowly sinking particulate pigments can escape grazing pressure simply by being present in the water column when grazers are not yet present, e.g., directly after a phytoplankton bloom before grazing and primary production are once again coupled.

Sinking particulate pigments can either descend quickly through the water column undisturbed or exchange material with surrounding particles through aggregation-disaggregation. The extent and mechanisms of POM exchange are important to understand because the degradation of POM during its transit to the seafloor will determine the quality and quantity of organic material eventually deposited at depth. In a biomarker study of aggregation-disaggregation in the Mediterranean Sea, [Abramson et al., 2010] found that

the extent of particle exchange was dependent on seasonal changes in primary production. During bloom periods, the composition of suspended and sinking particulate pigments remained distinct, suggesting little to no exchange. Sinking material was mostly fecal pellets with some aggregated fresh phytodetritus, while suspended material contained mostly fresh phytodetritus. By contrast, during periods of low primary production, suspended and sinking particulate pigments composition became more similar, suggesting more exchange between particles. Both sinking and suspended particles contained more biomarkers indicative of microbial decomposition and fewer fecal pellets relative to POM collected during blooms.

2.2.4 Cell Senescence

Phytoplankton senescence refers to the collective functional and morphological changes in a phytoplankton cell after growth stops [Daley and Brown, 1973, Eckardt et al., 1991]. The pheopigments produced during phytoplankton cell senescence can be more quantitatively important than the typically dominant fecal pellet pheopigments under several circumstances: the deposition of phytoplankton cells without heterotrophic pressure, the rapid sinking of algal mats and other aggregates, "sloppy feeding" (e.g., [Head and Harris, 1996]), and the senescence of cells that have remained intact within decomposing fecal pellets [Steinman et al., 1998].

As phytoplankton senesce, the Chl-a and carbohydrate content of the cell rapidly decreases [Carpenter et al., 1986], while the carotenoid pigments and certain lipids increases [Daley and Brown, 1973]. Laboratory studies that simulated "predator free" conditions Steinman et al. [1998] found senescing phytoplankton could be divided into two distinct groups by their Chl-a degradation sequence (Fig. 3). Phytoplankton exhibiting a high activity of the enzyme chlorophyllase tended to first produce chlorophyllide-a from Chl-a by de-esterification. This unstable chlorophyllide would then be demetallated, producing pheophorbide-a or pyropheophorbide-a. Phytoplankton with low chlorophyllase active, by contrast, produced pheophytin-a. Cyanobacteria are capable of producing the pheopigments from both pathways, but leave behind only the "signature" of pheophytin-a after a few months because it is more resistant to enzymatic degradation [Steinman et al., 1998].

2.2.5 Ingestion and Egestion by Zooplankton

Zooplankton ingest phytoplankton, take up essential organic compounds they are unable to synthesize, and egest the remaining organic matter as dense fecal pellets [Wakeham and Canuel, 1988]. The initial breakdown of chlorophyll during zooplankton grazing is rapid, occurring mostly during maceration and foregut chemical activity, which results in both enzymatic degradation and hydrolysis. These fecal pellets retain small amounts of Chl-a and Chl-b. Chl-a tends to decay more rapidly than Chl-b, suggesting different processes may be responsible for Chl-a and Chl-b degradation [Bustillos-Guzman et al., 2002]. Even after fecal pellets have been egested, they can still continue to be degraded microbially [Wakeham and Canuel, 1988]. External chemical alteration is partially buffered by the pellets' protective proteinaceous coating. The extent of zooplankton alteration is

also dependent on food abundance. A larger quantity of available food results in quicker feeding rates, and therefore shorter particle gut retention times. If there is a large food supply, the material passed through is expected to be less.

The alteration of Chl-a into pheophytin-a, pheophorbide-a and pyropheophorbide-a by zooplankton is well known, and these decomposition products have long been used as biomarkers of herbivorous zooplankton grazing and fecal pellet production. For example, pheophorbide-a was the dominant pheopigment observed in sediment traps deployed overnight, when zooplankton feed [Vernet and Lorenzen, 1987], although pyropheophorbide-a had not been characterized at the time of that study. Pheophorbide-a and pyropheophorbide-a are major products of macrozooplankton grazing and enzymatic degradation through the chlorophyllide pathway [Shuman and Lorenzen, 1975, Ziegler et al., 1988], so most of the Chl-a in the upper water column is first altered into pheophorbide-a, and subsequently to pyropheophorbide-a (Figs. 4, 3). The alteration of Chl-a into pheophorbide-a from pheophytin-a due to loss of phytol appears to be less important. Pheophytin-a is a major product of Chl-a degradation by marine protozoa [Klein et al., 1986, Strom, 1993], salps and some copepods [Hallegraeff, 1981]; these biologically mediated degradation processes may account for its presence and slow increase with increasing depth in the water column [Lee et al., 2000]. Significant amounts of pyropheophorbide-a, however, have also been found in fresh algae cultures of phagotrophic genera [Steinman et al., 1998], so clearly not all the sources and degradation pathways of Chl-a are known.

2.2.6 Microbial Colonization and Decomposition of Particles

In the oligotrophic open ocean, primary production is tightly coupled to decomposition in a microbial food web, with nearly 86% of primary production being respired by heterotrophic bacteria and protozoans [Hagström et al., 1988]. Because bacteria are osmotrophs, particulate "hot spots" of labile OM, such as phytoplankton cells, must enter the dissolved phase before the bacteria can consume it [Azam and Malfatti, 2007]. The egestion of DOM in vacuoles by the phagotrophic protists that consume picophytoplankton is one way OM can be transferred from the particulate to dissolved phased. Additionally, the enzymatic degradation of the outer protective mucus layer, or phycosphere, of live phytoplankton by protists "primes" the cell for bacterial colonization [Azam and Malfatti, 2007].

Dead phytoplankton cells can be directly colonized by bacteria with high cell-specific enzyme activity to form a "detritosphere" on sinking particulate pigments, which can either enhance aggregation through mucus production or disrupt aggregation through enzyme activity [Azam and Malfatti, 2007]. Studies have confirmed that aggregates are disrupted by intense bacterial hydrolytic enzyme activity capable of solubilizing Particulate Combined Amino Acids (PCAA) within 0.2-2.1 days [Smith et al., 1992]. The solubilized PCAA are present in the dissolved phase as combined rather than free, suggesting that aggregation-disaggregation may be an important source of labile 'biogenic sub-micron particles.'

The initial settling velocity of POM in the upper water column also determines the extent to which bacteria colonize POM, with bacteria having less time to colonize more

quickly sinking particles.

2.2.7 Decomposition in the Sediments by Benthic Organisms

Within the sediment, any pigments that reach the sediment-water interface are typically degraded within the upper two centimeters [Sun et al., 1991] (Fig. 4) . Bianchi et al. [1988b] and Cartaxana et al. [2003] found that benthic macrofauna converted Chl-a to pheophorbide-a, but microorganisms were responsible for the degradation of Chl-a to pheophytin-a. Sun et al. [1991] observed the formation of radiolabeled pheophytin-a directly from radiolabeled Chl-a in laboratory sediment decomposition experiments that excluded macrofauna with no significant degradation to pheophorbide-a. Extensive analyses of Long Island Sound sediments suggested no net production of pheophorbide-a from Chl-a in these sediments; the demetallation of Chl-a to pheophytin-a seemed to be the preferred pathway of degradation [Sun et al., 1991]. The preferential accumulation of pheophytin-a has also been observed in sediments of the Black Sea [King, 1993].

2.3 Description of Bermuda Rise Sampling Site

2.3.1 Physical setting

The Bermuda Rise is located in the Sargasso Sea, a subtropical gyre of the North Atlantic Ocean. The Bermuda Rise is an approximately 1500 x 1000 km area, with shallower bathymetry than the surrounding Sargasso Sea. The water column is 4000-4500 m deep. The seafloor of the Bermuda Rise is blanketed by sedimentary deposits 200-1300 m in thickness. Currently, sediment is being deposited by the Gulf Stream [Vogt and Jung, 2007]. The sedimentation rate at the BaRFlux site is approximately 4.5 cm kyr^{-1} (Cochran and Fitzgerald, personal communication). Sediment is also delivered to the subtropical North Atlantic Ocean by the transport of 20-30 m thick nepheloid layers formed due to enhanced seabed turbulence from strong current flow on the Scotian Shelf. This transported sediment cloud is enriched in aggregates and organic matter and has accelerated rates of geochemical reactions relative to the water above. [Pilskaln et al., 2014].

The Bermuda Rise is further north than the well-studied Hydrostation S and BATS sites, and is located more closely to an oceanographic transition zone. Between 25 and 32 degrees N, the seawater transitions from an oligotrophic subtropical convergence zone to the south to a eutrophic, Subtropical Mode Water (STMW) forming area to the north. In the oligotrophic subtropical convergence zone, the euphotic zone is permanently stratified and overlies high nutrient mode water. In the STMW forming area, passing cold fronts destroy the thermocline in the winter, mixing the water column deeply. This well-mixed, nutrient-rich water then slowly spreads south, separating the seasonal and permanent thermoclines [Steinberg et al., 2001]. In the summer, by contrast, a high pressure system blocks fronts from passing. This blockage in combination with summer and early autumn storms results in the formation of a shallow, low salinity, warm mixed layer.

2.3.2 Biological Oceanography

Although few publications specifically address the biological oceanography of the Bermuda Rise, the nearby Bermuda Atlantic Time Series (BATS) and Hydrostation S stations have been extensively characterized. These locations have been sampled since 1988 and 1954, respectively. Primary production is approximately 8-20 mg C m^{-2} d^{-1} [Steinberg et al., 2001]. There is a great deal of seasonal and internal variability in the phytoplankton and zooplankton community structure and biomass at these stations [Steinberg et al., 2001]. The prymnesiophytes and pelagophytes dominate the flux of POM in the spring. Aggregates of these eukaryotes are responsible for over half of the total POM flux in the region. During the rest of the year, the phytoplankton community is dominated by the prokaryotic picoplankton (Fig. 5). These picoplankton are present at their highest concentration from late spring through early winter. A smaller bloom of bacterioplankton also takes place in the summer. This summer bloom forms in highly stratified, nutrient depleted water and results in a Deep Chlorophyll Maximum Layer (DCML) from 60 to 120 m (Fig. 6). Within the DCML, the Chl-a maximum occurs above 100 m, while the Chl-b maximum occurs at about 100 m (Fig. 6). The deeper Chl-b maximum indicates the presence of prochlorophyte picoplankton below most of the phytoplankton community [Steinberg et al., 2001].

Cyanobacteria in the BATS study area are the most abundant from late spring through summer after the onset of seasonal stratification between 40 and 120 m and consist mostly of *Prochlorococcus* and *Synechococcus*. The cyanobacteria community resides between the shallower eukaryotic community and the deeper prochlorophyte community. Within the cyanobacteria community, *Prochlorococcus* is found deeper than *Synechococcus*; *Prochlorococcus* is more sensitive to N limiting conditions and remains close to the nitricline [Steinberg et al., 2001].

Bacterioplankton at BATS are an important part of the microbial food web and account for the majority of the biomass between 20-80 m and are at least equally abundant as the rest of the phytoplankton biomass (Fig. 7). The bacterioplankton and protozoans together are 70% of heterotrophic biomass found in the euphotic zone [Steinberg et al., 2001]. The bacterioplankton are the most abundant from late spring through autumn, when a combination of advection, winter mixing, and grazing destroys the subsurface bacteria maximum [Steinberg et al., 2001]. During the later stages of the spring bloom, the bacterioplankton become abundant deeper in the water column between 100 and 250 m and are present until late June or July. This bacterioplankton maximum contains lower concentrations of oxygen and DOC because the bacterioplankton remineralize DOM.

The protozoan assemblage at BATS is predominantly planktonic mixotrophic sarcodines, including foraminifera, radiolaria, and acantharia. These mixotrophs contribute most to primary production in the >70-μm sized POM pool, and also contribute a significant amount, about 15%, to the sinking POC flux [Michaels et al., 1995, Steinberg et al., 2001].

On average, macroscopic zooplankton at the BATS study area contribute to about 9% of sinking POC flux in the form of rapidly sinking fecal pellets. The peak in zooplankton biomass coincides with the spring and summer phytoplankton blooms after a one month

lag is applied. The spring zooplankton biomass peak is three times larger than the summer zooplankton biomass peak because the zooplankton are less efficient at grazing on the smaller phytoplankton and protozoans present during the summer [Steinberg et al., 2001]. During the spring bloom period, macroscopic zooplankton fecal pellets can contribute to as much as 65% of POC flux at the base of the euphotic zone [Deevey and Brooks, 1977]. In addition to contributing to the POC flux by egestion, macroscopic zooplankton impact the carbon cycle by diel migration. The contribution of diel migrating zooplankton to the POC flux at the base of the euphotic zone can be up to 70% at times.

3 Methods

3.1 Sample Collection

All samples were collected during the Bermuda Rise Flux project (BaRFlux) cruises aboard R/V Endeavor and R/V Atlantic Explorer. Six successive cruises to the Bermuda Rise (33.68°N, 57.6°W) in the Sargasso Sea commenced in October 2011 and ended in June 2013 (Table 1). Particle samples were collected using Niskin bottles, in-situ pumps, and sediment traps. Deposited sediment was also collected using box cores.

Table 1: Cruise dates for BaRFlux cruises and types of samples collected.

Cruise	Start	End	Samples
1	Oct. 26, 2011	Nov. 7, 2011	pump, Niskin
2	Feb. 8, 2012	Feb. 20, 2012	pump, Niskin, trap
3	May 7, 2012	May 15, 2012	pump, Niskin, trap
4	Aug. 15, 2012	Aug. 27, 2012	pump, Niskin, core
5	Nov. 9, 2012	Nov. 19, 2012	pump, Niskin
6	June, 2013	June, 2013	pump, Niskin

Water column particle samples were collected at depths from the euphotic zone down to a few hundred meters above the sediment-water interface using both in-situ pumps and Niskin bottles. The depths of samples for each cruise are shown in Tables 2, 3. Niskin bottles brought sealed water samples to the surface, where they were transferred into smaller containers through a spigot and filtered onto 25-mm 0.7-μm GF/F filters. All filters were frozen until analysis. Challenger Oceanic battery-operated in-situ pumps were outfitted with a filter stack consisting of a 142-mm diameter Teflon mesh (70-μm) followed by a 142-mm diameter quartz microfiber filter (QMA; 1μm). Seawater (usually >1000L) was pressure-filtered at depth over a period of several hours, and one quarter of the filter was frozen for organic analyses.

Table 2: In-situ pump log of depths sampled (in m).

BF1	BF2	BF3	BF 4	BF5	BF6	BF6 contd.
		100	100	2000	60	2490
300	300	300	300	4200	80	2510
1000	1000	1000	1000		90	2990
1500	1500	1500	1500		140	3010
2000	2000	2000	2000		160	3500
3500	3500	3500	3500		500	3990
4000	4000	4000	4000		1000	4010
4200	4200	4200	4200		1500	4190
					2000	4210

Table 3: Depths (m) sampled by Niskin bottles. $^{+}$ indicates sample depth of Chl-a fluorescence maximum

BF2	BF3	BF4	BF5	BF6
50	50	50	50	10
100	100-107^{+}	68^{+}	75^{+}	25
150	200	75	100	50
300	500	100	100	68^{+}
	800	200	200	70
	1250	300	300	75
	1750	500	500	80
	2500	800	1000	100
	3000	1000	2000	150
	3500	1500	4200	200
	4000	1750		300
	4300	2000		500
	4430	2500		800
		3000		1000
		3500		1500
		4000		2000
		4200		2500
				3000
				3500
				4000
				4200
				4573

Water column sinking particle samples were collected by moored sediment trap arrays that were deployed during BaRFlux 2 and recovered during BaRFlux 3 to quantify and characterize the chemical composition of the sinking flux of POM at selected depths as a function of time (in days) and settling velocity. No other samples were recovered from sediment traps deployed during BaRFlux. Standard sediment traps have been used to collect time-series samples of sinking particulate pigments [Dymond et al., 1981, Gardner et al., 1985, Honjo et al., 1980, Wakeham et al., 2009]. Sediment trap arrays used during BaRFlux contained Indented Rotating Sphere sediment traps (IRS) [Peterson et al., 1993, 2005] that can collect in either time series (TS) or settling velocity (SV) mode. The former remains opened for a fixed period of time, while the latter collects sinking particulate pigments with different ranges of settling velocities. POM was collected in TS mode to determine bulk pigment composition and pigment concentration changes as a function of time, while POM was collected in SV mode to examine the changes in pigment composition and concentration as a function of settling velocity (Table 4). POM sinking at specific settling velocities was collected by rotating the carousel within the IRS for a duration of time determined by the relationship between trap collection time and settling velocity as

per Armstrong et al. [2009]. All IRS traps were rotated daily to minimize in-situ alteration by zooplankton. Recovered samples were split ten ways and one fraction was filtered onto 25-mm Whatman GF/F glass fiber filters and frozen until pigment analysis.

Box cores were taken during BaRFlux 4, and a 5-cm sediment sub-core was removed with a 30-mL sterile syringe and frozen within a few hours of deck recovery. The sub-core was divided into 0.5-cm subsections near the sediment-water interface and into centimeter subsections from 1 to 5 cm. All subsections were frozen until analysis.

3.2 Pigment Analysis

Pigments were extracted from filters and sediments with 100% acetone in the dark to avoid laboratory-induced chlorophyllase activity following the method of Sun et al. [1991]. All samples were stored in amber vials on ice in the dark until HPLC analysis (usually less than 2 hours). Pigments were separated by polarity with reverse-phase High Performance Liquid Chromatography using a 5-μm C-18 Alltech column (250 mm x 4.6 mm). The mobile phase, a 1:4 solution of acetone and methanol (MeOH) was ramped from 0 to 100% over 20 minutes and held at 100% from 20 to 65 minutes. Buffer solution was prepared as in Sun et al. [1991]. Pigments were detected by fluorescence using an excitation wavelength (λ) of 440 nm and emission λ of 660 nm as per Jeffrey et al. [1999]. All samples were run in duplicate. If the percent error between duplicates exceeded 10%, additional replicates were run.

Standard solutions were prepared from Sigma-Aldridge authentic standards diluted to the desired concentrations with the exception of pheophytin-a; pheophytin-a was prepared by acidifying the Chl-a standard. All calculations were made using Python v2.7. Effective sample volumes were used to determine concentrations (μg L^{-1} and μmol L^{-1}) for water column samples, and sediment trap area and deployment time was used to determine flux (μg $m^{-2}d^{-1}$ and μmol $m^{-2}d^{-1}$) for sediment trap samples.

Table 4: Settling Velocity 1500 m Sediment Trap IRS schedules and calculated settling velocities for cruise 3. Each tube number refers to a specific sediment collection tube within the IRS. ▲ Indicates samples analyzed for pigments.

Trap tube	time (min)	Theoretical SV (m d^{-1})
2	1	979.20
3	1	979.20
4	1	979.20
5	1	979.20
6▲	2	489.60
7▲	4	244.80
8▲	8	122.40
9	16	61.20
10▲	64	15.30
11▲	96	10.20
12	166	5.90

Table 5: Time Series 300 m sediment trap schedule for traps deployed during BF2. ♦ indicates samples analyzed for pigments.

Tube	Duration (days)	start date (in 2012)
2♦	7	18-Feb
3♦	7	25-Feb
4	7	3-Mar
5	7	10-Mar
6	7	17-Mar
7♦	7	24-Mar
8	7	31-Mar
9♦	7	7-Apr
10♦	7	14-Apr
11♦	7	21-Apr
12	7	28-Apr

4 Results

4.1 Niskin Bottle Suspended Particulate Chloropigments

The total concentration of suspended particulate chloropigments collected using Niskin bottles ranged between 0.2 to 12.3 μg/L in the euphotic zone and undetectable below the mesopelagic zone (Table 6, Fig. 9). Typically, concentrations were between 0.01 and 6 μg/L. In general, total pigment concentrations in the euphotic zone were lowest in samples collected during the February cruise (BF2), were about 25 times higher in May (BF3), returned to lower values in June (BF6) and August (BF4), and then were about 10 times higher again in November (BF5), although some of the months were sampled in different years (Table 6, Figs. 8, 9). The large difference in the maximum pigment concentration between some of the cruises is partly due to the coarser sampling resolution of certain profiles (e.g., BF2, BF3), that did not include a sample from the chlorophyll maximum (Table 6), which is typically between 60 and 100 m (Fig. 8).

Chl-a concentrations at the BaRFlux site were much higher than at the nearby BATS station. Concentrations of Chl-a can reach levels of 700 ng/L at the Chl maximum, but more common values are 200-400 ng/L there; values decrease to below detection levels below 300 m [Monk and Johnson, 2014]. The highest BaRFlux Niskin bottle Chl-a concentration during the spring bloom at 100 m of 9000 ng/L was more than 10 times higher than at BATS, but also decreased to below detection level at the same depth.

The pigment composition was predominantly Chl-a with smaller mole percentages of pheophorbide-a and Chl-b in the shallower water, and was all Chl-a and Chl-b in deeper water (Fig. 10). The dominance of chlorophylls in the deeper samples does not necessarily mean the suspended particulate pigments at depth is more "fresh,"but simply that pheopigments are below the detection limit of the HPLC fluorescence detector at such low concentrations. Only the February and November cruises (BF2 and BF5) contained pheophytin-a, which was present in the upper water column only (Fig. 10). Only the February (BF2) and the August (BF4) cruises contained pyropheophorbide-a. In the August cruise, pyropheophorbide-a was present only in the upper to mid water column. Because Niskin bottle samples were only taken in the upper 300 m during the February cruise, the distribution of pyropheophorbide below 300 m is not known.

4.2 In-situ Pump Suspended Particulate Pigments (>1-μm, <70-μm)

The general seasonal pattern of particulate pigment concentration agreed with the seasonal pattern seen in Niskin bottle particulate pigment samples: higher pigment concentrations in February (BF2) through June (BF3, BF6) and lower pigment concentrations in August (BF4) and November (BF1). The particulate pigment concentrations in in-situ pump samples and Niskin bottle samples did not agree as to the month of the greatest particulate pigment concentration. The Niskin bottle particulate pigment profiles show higher particulate pigment concentrations in November (BF5) than in February (BF2) and peak concentrations in May (BF3), while the in-situ pump pigment profiles show

Table 6: Total particulate pigment concentrations collected with Niskin bottles over depth (m) and reported as g/L.

BF2		BF3		BF4		BF5		BF6	
Depth	total	depth	total	depth	total	depth	total	depth	total
50	0.684±0.018	50	0.306 ±0.063	50	0.260±0.050	50	0.536	10	0.263±0.015
100	0.455±0.071	100	12.36±0.91	68	1.330±0.216	75	2.108±3.720	25	1.117
150	0.227±0.019	107	1.645±0.201	75	1.749±0.284	100	5.388±1.999	50	0.542±0.049
300	0.120±0.014	200	0.0452±0.024	100	0489±0.084	200	0.005	68	1.111
		500	0.000	200	0.001±0.001	300	0.001	70	2.513
		800	0.006±0.002	300	0.023±0.005	500	0.000	75	2.256±0.043
		1250	0.000	500	0.020±0.009	1000	0.000	80	1.818±0.025
		1750	0.000	800	0.019±0.008	2000	0.000	100	0.526±0.159
		2500	0.000	1000	0.056±0.025	4200	0.000	150	0.000
		3000	0.000	1500	0.001		0.00	200	0.016
		3500	0.000	1750	0.001			300	0.002±0.001
		4000	0.000	2000	0.001			500	0.000
		4300	0.000	2500	0.000			800	0.001
		4430	0.001	3000	0.000			1000	0.002±0.001
				3500	0.000			1500	0.000
				4000	0.000			2000	0.000
				4200	0.000			2500	0.003
								3000	0.000
								3500	0.000

higher particulate pigment concentrations in February (BF2).

Total pigment concentrations in small (1-mole%) suspended particulate pigments collected by in-situ pumps ranged from approximately 200-350 ng/L in the euphotic zone and decreased rapidly in the upper mesopelagic zone to concentrations of 1-5 ng/L (Table 7). Suspended particulate pigments pigments decreased with depth in August (BF4), while pigment profiles in November (BF1) and February (BF2) showed a mid-depth maximum near the seafloor in the total pigment concentration in the bathypelagic zone (Fig. 9). Suspended particulate pigment samples collected by in-situ pumps in the euphotic zone generally had pigment concentrations 3 orders of magnitude less than Niskin bottle samples at comparable depths, while concentrations below the euphotic zone collected by both methods were low or below detection levels. The higher pigment concentrations in November and February in the deep water were not seen in February Niskin bottle pigment profiles; however, November samples were not taken below 300 m. (Table 6).

Table 7: Average total particulate (>1-μm, < mole%) pigment concentrations collected over depth (m) by in-situ pumps. Concentrations reported in ng/L.

Depth	BF1	BF2	BF3	BF4	BF6
100	–	–	204.05±47.54	–	351.23±74.70
300	8.82±1.40	236.47±119.72	13.75±2.57	68.71±22.71	18.97±6.52
1000	1.46±0.18	4.28±1.23	14.48±4.03	5.12±1.18	4.32±1.90
1500	1.47±0.27	6.71±1.67	1.62±0.21	5.87±1.61	11.09±4.94
2000	3.17±0.90	11.35±3.19	1.79±0.47	5.39±1.98	5.62±2.33
3500	6.33±1.08	0.42±0.07	0.98±0.29	6.63±2.06	4.38±2.25
4000	2.28±0.59	224.12±104.96	0.29±0.05	2.35±0.85	11.33±4.25
4200	2.54±0.51	307.54±109.42	0.47±0.11	4.26±1.84	0.00

The mole% Chl-b, pyropheophorbide-a, and pheophorbide-a in small suspended particulate pigments collected by in-situ pumps decreased with depth, while the mole% of pheophytin-a and Chl-a increased with depth through around 3500-4000 m, after which the mole% of Chl-b, pyropheophorbide-a, and pheophorbide-a once again increased and the mole% of pheophytin-a and Chl-a once again decreased. This reversal in the mole% pigment trend at depth is always present, but is seen most strongly in samples from the February cruise (B2) and the June cruise (B6). Interestingly, particulate pigment samples from the same two cruises also had a much less marked increase in the mole% of pheophytin-a over depth (Fig. 11).

The mole% composition of suspended particulate pigments pigments collected with in-situ pumps was different than that collected with Niskin bottles. In-situ pump data clearly indicated that pheophorbide-a and pyropheophorbide-a were major constituents of the total chloropigments at most depths, and that pheophytin-a accounted for a greater mole% of the total pheopigments with increasing depth. Only Niskin bottle samples from the February (BF2) and August cruises (BF4) contained detectable pyropheophorbide-a or pheophytin-a (Figs. 10, 13).

4.3 In-situ Pump Suspended Particulate Pigments (>70-μm)

The concentrations of >70-μm particulate pigments were quite variable, but generally lower than small suspended particulate pigments by several orders of magnitude (Tables 7, 8). The concentrations were lowest in February (BF2), which coincides with when small particle concentrations were highest (Table 7). Concentrations were also relatively low in November (BF1) and February (BF2). The highest concentrations were present in surface waters, particularly during BF3 and 4, although there was also a high concentration at 3500 m during BF3.

The pigment composition changed greatly over season (Fig. 14). Because pigment concentrations were so low in deeper waters, mole% data is not as reliable below the surface waters. The composition of >mole% particulate pigments collected during November (BF1), February (BF2), and August (BF4) was almost uniformly Chl-a across all depths (Fig. 14). In samples collected during May (BF3) and June (BF6), the compositional patterns were more similar to the patterns seen in the smaller suspended particulate pigments: pyropheophorbide-a and pheophorbide-a accounted for most of the pheopigments at each depth and mole% pheophytin-a increased with depth (Figs. 13, 14).

Table 8: Total particulate (>70-μm) pigment concentrations collected by in-situ pumps over depth (m). Concentrations reported in ng/L.

Depth	BF1	BF2	BF3	BF4	BF6
100	–	0	14.206	21.363±0.164	3.447±0.036
300	0.016±0.000	0.005±0.002	0.149±0.023	23.890±10.074	–
1000	–	0	0.119±0.016	0.346±0.001	0.192±0.005
1500	0.224±0.051	0	0.12	0.005±0.000	0.292±0.033
2000	0.066±0.010	0.025	0.121±0.018	0.049±0.003	0.162±0.011
3500	0.023±0.001	0	22.574±7.435	0.136±0.049	0.1015±0.002
4000	0.009±0.00	0.027	0.163	0.027±0.004	–
4200	0.102±0.044	0.142	0.151	0	–

4.4 Sinking Particulate Pigments

The total flux of sinking particulate pigments collected from February through April from a time-series IRS trap at 300 m ranged from approximately 300 to 3100 μg m^{-2} d^{-1} and peaked in late March and early April (Table 9). Sinking particulate pigments collected from the time series IRS trap at 300 m and a settling velocity IRS trap at 1500 m had nearly identical bulk pigment compositions (Figs. 15, 16), indicating very little compositional change in sinking particulate pigments with depth. Pyropheophorbide-a consistently dominated the composition of sinking particulate pigments collected at all times and settling velocities.

The IRS sediment trap may not have collected at the appropriate times and settling rates due to software failure (Black, personal communication), so a definitive time or

Table 9: Average flux of sinking particulate pigments collected at 300 m during BF3 by an IRS Time Series sediment trap. All fluxes are in μg pigment $m^{-2}d^{-1}$. All dates reported are for 2012.

Date	Total
Feb-18	346.16±3.70
Feb-25	736.52±15.70
Mar-24	1143.81±66.23
Apr-07	3100.82±10.40
Apr-14	1072.53±22.72
Apr-21	397.26±7.82

settling velocity cannot be assigned to each sample. The calculated times and settling velocities are therefore presented as "assumed" (Tables 4, 5).

As estimated setting velocity increased, the composition of the sinking particulate pigments collected at 1500 m showed several interesting patterns (Fig. 16). The mole% pyropheophorbide-a increased, mol% pheophorbide-a decreased, total mole% chlorophyll increased, and the Chl-a to Chl-b ratio decreased. No pheophytin-a was detected.

4.5 Sedimentary Particulate Pigments

The μmol total pigments/g sediment decreased with increasing depth below the sediment-water interface from approximately 1.6 x 10^{-4} (0-0.5 cm) to about 0.3 x 10^{-4} (4-5 cm)in the syringe sub-core taken during the summer cruise (BF4). The mole percent composition was consistently almost 100 percent pheophorbide-a. In the centimeter of sediment directly below the sediment-water interface, there was a small mole percent (<0.5 percent) of Chl-a (Fig. 17).

4.6 The Nepheloid Layer

Percent beam transmissivity profiles taken with onboard CTD sensor arrays illustrate that the nepheloid layer was an extensive and permanent feature of the deep water column in the BaRFlux area during our study (Fig. 18). The characteristic "tail"of lower transmissivity directly above the sediment-water interface remains fairly small during November (BF5) and August (BF4) and was the most pronounced in profiles taken during February (BF2) and May (BF3) (Fig. 18).

4.7 Comparison of BaRFlux with EqPac and MedFlux data

The early biologically mediated POM degradation processes that occur between its production in the euphotic zone and burial at the seafloor have been the focus of several multi-year research projects. The BaRFlux pigment data will be compared with two of these previous studies: EqPac [Lee et al., 2000] and Medflux [Wakeham et al., 2009], which were performed in the open Equatorial Pacific Ocean and the Northwest Mediterranean

Sea, respectively. EqPac was conducted to determine the change in POM quantity and composition with latitude, while the Medflux cruises were taken to determine the change in POM quality and quantity with time and particle settling velocity. Similar methods were used in these studies to collect POM, e.g., in-situ pumps and sediment traps. However, the Nitex mesh screen in the pumps used during EqPac and MedFlux had a pore size of 53 μm, and therefore collected finer material than the 70-μm mesh screen used during the BaRFlux cruises. The particles were also collected with filters made of different material: EqPac filters were glass fiber, while BaRFlux were quartz fiber.

4.7.1 Comparison with EqPac

Suspended particulate pigment samples collected with MULVS in-situ pumps during EqPac had similar total small particulate pigment concentrations to BarFlux, 100s of ng/L. Small particulate pigments collected during EqPac had a greater proportion of Chl-a ($\sim$90 mole%) than comparable BaRFlux samples ($\sim$60 mole%) in the euphotic zone. This difference may be due to the higher productivity in the upwelling region, and more reprocessing in the oligotrophic North Atlantic. In both areas, pheophorbide-a and pyropheophorbide-a were produced between the euphotic zone and mesopelagic zone. The increase in mole% pheophytin with depth seen in BaRFlux small particles was not seen in EqPac pigments, in which mole% pheophytin-a was always <10%. The large particulate pigments collected during BaRFlux and EqPac had similar compositions, typically >90% Chl-a.

Sinking particulate pigment samples collected by BaRFlux sediment traps had similar pigment compositions to sediment trap samples collected during EqPac. Pheopigments accounted for nearly 90 mole% of the total pigments in both studies. The BaRFlux sediment trap samples typically contained pyropheophorbide-a and pheophorbide-a in a 2 to 1 ratio, while EqPac sediment trap samples at similar depths contained nearly equal amounts of pyropheophorbide-a and pheophorbide-a. Additionally, EqPac samples also contained about 20 mole% pheophytin-a while BaRFlux samples did not contain detectable pheophytin-a. The maximum EqPac sinking particle pigment flux out of the euphotic zone was 51 μg/m^2/d just north of the equator [Lee et al., 2000], compared to 2700 μg/m^2/d at BaRFlux (Table 9).

Sediment directly below the sediment-water interface collected during the BaRFlux summer cruise (Fig. 15) had a different composition than EqPac sediment. EqPac sediment collected over the first 0.5 cm below the sediment-water interface contained, from least to greatest mole%: Chl-a, pheophorbide-a, pyropheophorbide-a, and pheophytin-a. BaRFlux sedimentary POM collected over the same depths contained nearly 100 mole% pheophorbide-a at all depths and less than 1 mole% Chl-a, which was present only in the centimeter immediately below the sediment-water interface.

4.7.2 Comparison with MedFlux

The SV and TS sediment traps recovered in May (BF3) were deployed at a similar time of year as the Medflux 2003, Period 1 traps (Table 10), although they collected

material in different years [Wakeham et al., 2009]. The traps deployed during the Medflux cruises collected sinking particulate pigments at similar depths to the BaRFlux cruises; the recovered BaRFlux TS and SV sediment traps collected material from 300 m and 1500 m, respectively. The MedFlux Time Series traps collected material from 238 and 771 m in Period 1 and 117 and 1918 during Period 2.

Table 10: Time Series sediment trap collection dates for BaRFlux and MedFlux.*Wakeham et al., 2009; **Lee et al., 2000

Cruise Name	TS Period start	TS Period End	Trap depths (m)	Max. pigment flux (μg/m^2/d)
BaRFlux 3	02/17/2012	05/8/2012	300	2700
MedFlux 2003, Period 1	03/06/2003	05/06/2003	238, 771	600, 450*
MedFlux 2003, Period 2	05/14/2003	06/30/2003	117, 1918	200, 50*
EqPac 1992, Survey I	02/1992	03/1992	313, 924	51**

The phytoplankton bloom in the MedFlux study area occurred in March in 2003 [Wakeham et al., 1997] during Period 1. At BATS, relatively near BaRFlux, a short spring bloom occurs between January and March [Steinberg et al., 2001], so that traps deployed in February would have collected during part of the bloom period. In any case, the sinking flux of particulate pigments was much higher at the BaRFlux study area than at MedFlux (Table 10).

The bulk pigment composition of sinking particulate pigments in BaRFlux samples was different than samples collected during the MedFlux cruises. BaRFlux sinking particulate pigments collected at 300 m contained nearly 90 mole% pyropheophorbide-a (Fig. 15), while MedFlux samples around the same depth contained only 40-50 mole% pyropheophorbide-a during Period 1 and 20-30 mole% during Period 2. Part of this lower mole% at MedFlux is from the inclusion of the fucoxanthin in the mole% pigment calculations. Pheophytin-a increased from 10-20 mole% during MedFlux Period 1 to 50-70 mole% during Period 2. Medflux samples also contained a significantly more Chl-a (about 20 mole%) than BaRFlux samples.

The pigment composition of sinking particulate pigments in the BaRFlux samples did not vary significantly between 300 and 1500 m (Figs. 15, 16), while MedFlux samples exhibited significant compositional changes. The BaRFlux sinking particulate pigments collected in the mesopelagic zone consistently contained nearly 90 mole% pyropheophorbide-a, whereas at MedFlux pheophytin-a steadily increased to 60 mole% of the total pigments while pheophorbide-a decreased. Unlike the BaRFlux 300 m sediment trap (Figs. 15, 16), the Medflux sample data also shows temporal variation in pigment composition. TS trap samples from MedFlux contained more pheopigments and less labile material from early to late spring, consistent with the presence of more highly grazed material during the later part of the spring bloom. By contrast, BaRFlux time series trap samples had a relatively constant composition from February through May, suggesting that the sinking particulate pigments are consistently heavily grazed material over that period.

Sinking particulate pigment samples from the SV traps recovered during BF3, which

collected particles from February through May, did not exhibit the same changes in composition with settling velocity as MedFlux samples collected during a similar time span. Both BaRFlux and MedFlux samples decreased in zooplankton pheopigments (pyropheophorbide-a) with increasing settling velocity. However, sinking particulate pigments collected during BaRFlux became more enriched in Chl-a and Chl-b relative to pyropheophorbide-a as settling velocity increased (Fig. 16), while during Medflux sinking particulate pigments became more enriched in pheophytin-a as settling velocity increased.

5 Discussion

5.1 How Collecting with Pumps vs. Bottles Influences Composition and Concentration

The disparity between Niskin bottle and in-situ pump particle OM concentrations documented by many previous studies [Bishop et al., 1978, Gardner et al., 2003, Turnewitsch et al., 2007] was seen in BaRFlux data. Both the concentration and composition data of pigments in bottles and pump samples were markedly different. Niskin bottle POC and PN measurements have been reported as 5-200 times higher than in-situ pump values for the same water depth. The 2-3 orders of magnitude disagreement in the total particulate pigment concentrations between bottles and pumps from the BaRFlux area are much greater. The composition of both sample types is also very different. The particulate pigments collected by in-situ pumps had a larger mole percentage of pheopigments, specifically pyropheophorbide-a and pheophytin-a, compared to Niskin bottle samples.

One of the factors these discrepancies have been attributed to is error from adsorbed DOC on GF/F filters due to small sample size [Moran et al., 1999, Turnewitsch et al., 2007]. The sorption of DOC to filters is not relevant for comparing the retention efficiency of particulate pigments because there are no dissolved pigments in seawater. The lack of detectable pigments on filter blanks taken during BaRFlux confirms that adsorbed material does not contain quantifiable pigments. It has also been argued that in-situ pump samples have lower apparent POC concentrations because the vacuum pressure can force particles through the filter[Gardner et al., 2003, Liu et al., 2005]. This might explain why the pump and bottle disagreement was so large at the BaRFlux site since picophytoplankton, which are 0.2-2 μm in size, make up a large portion of the phytoplankton community at the nearby BATS study area [Steinberg et al., 2001]. The relatively high Chl-b:Chl-a measured at BarFlux stations supports this hypothesized community composition. Because picophytoplankton typically inhabit the DCML, their Chl-a:Chl-b ratio will be lower relative to phytoplankton in the shallow euphotic zone to increase the collection efficiency of PAR.

Liu et al. (2005) attributed POC concentration differences between bottles and pumps to Niskin bottles capturing zooplankton that can evade pumps but not bottles. They found higher numbers of zooplankton in bottle than in pump samples. However, the higher mole% of Chl-a and Chl-b in BaRFlux bottle samples indicates that the higher concentration of particles in bottles is due to the presence of more primary producers Fig. 10). Because the concentration of total pigments in oligotrophic regions is generally low (on the order of 10^{-3} g/L), bottle samples ranging in volume from 0.5-2 L may be an inaccurate representation of the pigment distribution due to probability alone (Fig. 19). Most previous studies on the efficiency of bottle and pump samples were conducted in more productive coastal waters, where the concentration and the size of larger phytoplankton and grazing zooplankton are much greater, and therefore have a higher probability of retrieving representative bottle samples.

5.2 How POM Composition is Influenced by Particle Size

There are several interesting differences in the pigment composition of large and small particles. Because bottle and pump data are so different, we chose to consider only the pump data size fractions in considering the question of how particle size influences pigment composition. The pigment composition of POM collected by the smaller (1-μm) and larger (>70-μm) in-situ pump filters reflects the net balance of labile organic matter produced by phytoplankton and its transport and degradation by different biologically mediated processes (Fig. 3)for each size pool spatially, temporally, and over depth.

In the more productive equatorial Pacific, Lee et al. [2000] reported a general pattern of a shallow water maximum of Chl-a, with pheophorbide-a and pyropheophorbide-a both peaking in the mid-water column, and pheophytin-a slowly increasing with depth. A similar composition pattern was seen in the BaRFlux small suspended POM, but with pyropheophorbide-a and pheophorbide-a having a more shallow maximum (Figs. 13, 20).This shallower maximum in zooplankton alteration indicators was not surprising, because oligotrophic regions typically produce POM of a smaller mean size that is recycled efficiently in the euphotic zone and is more tightly coupled to grazing [Lomas and Moran, 2011]. The compositional change in pheopigments suggests that microbial degradation replaces zooplankton degradation as the dominant mode of pigment degradation with depth (Fig. 4). The small amount of pheophytin-a at more shallow depths was unexpected (Fig. 13), because bacteria are known to be an important component of the euphotic zone biomass (Fig. 7)in the subtropical North Atlantic [Steinberg et al., 2001, Rivkin and Anderson, 1997].

The pigment composition of large suspended POM (>70-μm) collected from most of the cruises was predominantly labile, Chl-a enriched material, likely from a combination of larger phytoplankton and aggregates [Lomas and Moran, 2011, Armstrong et al., 2002, Klaas and Archer, 2002] and sometimes a small percentage of degraded pyropheophorbide-a enriched material indicative of larger zooplankton fecal pellets(Fig. 14). The conservation of the larger particles' pigment composition over depth implies that: 1. the labile, Chl-a enriched material is evading degradation during its transit to the seafloor; 2. the larger particles are not exchanging material with the smaller particles.

However, in samples taken during May(BF3) and June(BF6), the pigment composition patterns over depth more closely resembled the patterns seen in the smaller suspended POM (Figs. 13, 14). The similar composition of the two differently sized particles that are normally so different suggests particle exchange occurs in May and June. It is possible that as the water column begins to stratify around the temporal middle of the spring bloom, the higher concentration of POM in a smaller, density restricted mixed layer increases the likelihood of particle-to-particle collisions, and therefore particle exchange. The presence of sticky materials like mucus or Transparent Exopolymers (TEP) are capable of binding aggregated material [Alldredge et al., 1990, Passow, 2002].These substances are produced during times of elevated nutrient stress or predation pressure. Both of these conditions are expected in May(BF3) and June(BF6), when phytoplankton have drawn down nutrient levels and zooplankton grazing pressure is greater. Alternatively, zooplankton grazing [Behrenfeld and Boss, 2014] or bacteria colonization [Cho and Azam, 1988] could have

been recoupled with phytoplankton growth, resulting in similar composition patterns without particle exchange.

It is interesting that the ratio of Chl-b to Chl-a, which is typically 1:10, is much higher in June relative to other months (Fig. 14). For the >70-μm POM to be so enriched in Chl-b, there must either be an additional source of Chl-b unique to the month of June, or Chl-b is less susceptible to degradation than Chl-a. If the second case were true, the same Chl-b to Chl-a ratio should be seen during all months in all POM containing Chl-a and Chl-b. The first case is more likely, especially because recent studies report evidence that picoplankton aggregates are exported from the euphotic zone in the Sargasso Sea [Lomas and Moran, 2011].

5.3 What Does the Difference in Pigment Quality in Sinking and Suspended Particulate Pigments Suggest About the Role of Settling Velocity in the OM Cycle?

Samples collected by different instruments during the BaRFlux cruises represent very different temporal scales and, potentially, different pools of material. Pumps and bottles (minutes to hours), sediment traps (days-months), and cores (hundreds to thousands of years) are frequently compared, however, because of their connections within the marine POM cycle [Wakeham et al., 1997, Lee et al., 2000]. The pigment quantity and composition of suspended POM provides a "snapshot" of the net degradation processes acting on slowly settling POM in the water column. Using the same reasoning, the data from sinking POM collected by sediment traps reflects the degradation of the sinking POM pool as it moves towards the seafloor (Fig. 1, Fig. 4). By comparing the pigments of these two pools of POM, we can better understand the relationship between particle size and early degradation processes.

Although sediment traps were recovered only during BF3 at 300 and 1500 m, it is instructive to compare the pigment composition of sinking OM in the upper and lower mesopelagic zone because it is an area of significant OM early degradation. Sinking particulate pigments from both depths had a bulk composition rich in zooplankton feeding indicating pheopigments and poor in Chl-a and Chl-b (Figs. 15, 16). This was the expected pigment composition because zooplankton are consuming OM and no new labile OM is being produced . Repackaging ingested labile organic matter into larger, highly degraded, dense fecal pellets is an important "connecting" process that links the suspended and sinking pools.The nearly identical bulk relative mole percent pigment composition of 300 m and 1500 m sediment traps suggests that sinking POM is little altered between the upper and lower mesopelagic zone (Figs. 15, 16). Furthermore, while the flux of sinking particulate pigments collected at 300 m changed over time, the composition remained fairly constant(Fig. 15). Therefore, on the time scale of one month and the mesopelagic spatial scale (100s of meters), the relative importance of the different degradation processes remain constant.

The settling velocity mode of sediment traps measures flux in settling velocity classes that collect over the entire deployment time (Fig. 16). Assuming the settling velocities

calculated for the trap is correct, as settling velocity increases, the relative mole percent of labile, Chl-a and Chl-b rich material increases. Interestingly, as in the $>70-\mu$m suspended POM, the Chl-a:Chl-b ratio was significantly lower than the 1:10 typically seen in phytoplankton. The ratio departed further from 1:10 with increasing settling velocity, which suggests that picophytoplankton aggregates are an important source of labile rapidly sinking material. At all settling velocities, larger zooplankton egestion is still dominant- the mole percentage of total labile material does not exceed 10%. The net composition can be seen as a balance between the competing processes of zooplankton grazing and rapid sinking. Aggregation can make labile POM once too small to be detected by larger zooplankton suddenly "available." As aggregation continues, the largest, most rapidly sinking material can evade ingestion, while the material that is large enough to be detected by larger zooplankton but not sinking rapidly enough to "escape" is altered and egested as pyropheophorbide-a rich fecal matter.

5.4 How the Nepheloid Layer Influences Composition of Particles

The nepheloid layer was detected in the BaRFlux study area with transmissivity instruments, which measure the percentage of light passing through seawater to a detector. The very regular decrease in a transmissivity profile with depth directly above the sediment-water interface approximates the shape of the benthic boundary layer. In Biscaye and Eittreim [1977] , (Fig. 2), the shape of the particle profile in the nepheloid layer reflects the downward flux of material from the euphotic zone, vertical mixing, and horizontal advection [Gardner et al., 1985]. Because mixing and advection at the bottom of the water column are stronger in the northern hemisphere winter, a more pronounced nepheloid layer was present in February and May than in August.

The C shape of the transmissivity profiles is best reflected in the shapes and magnitudes of the small suspended particulate pigment concentration profiles (Figs. 12, 18). Several observations of the quality and quantity of particulate pigments near the seabed suggest that POM in the nepheloid layer is highly degraded. First, the Chl-a fluoresence profiles(Fig. 8) are not inverse images of the beam transmissivity profile (Fig. 18) near the sediment-water interface as they are in the euphotic zone. This pattern indicates that the resuspended particles scattering light at depth do not contain labile pigments. Secondly, the pigment composition of small suspended POM near the sediment-water interface (Figs. 12, 13) indicates the presence of highly degraded POM. The resuspended material is probably also degraded. The >70-μm particles are probably not being resuspended as much as the smaller particles (Fig. 12) because there is a size fractionation within the nepheloid layer towards finer material away from the seabed. If some larger particulate pigments do make it to the sediment-water interface, they are therefore more likely to be buried than resuspended.

The in-situ pump data for May(BF3) and June(BF6) suggests that these months have a significant amount of particle exchange (Figs. 13, 14). It is also apparent by comparing the total particulate pigment profiles of the >70-μm particulate pigments from these

months that C profile shape is more marked than the >70-μm profiles from other cruises (Fig. 12). If particle exchange is occurring during the time periods with the most extensive nepheloid layers, the nepheloid layer could be functioning at depth in a way similar to the higher concentrations of POM in the euphotic zone by enhancing particle exchange through increasing the possibility of particle-to-particle collisions.

5.5 Comparison of POM Composition at the Sediment-Water Interface and in Deep Water Column Samples

The typically observed pigment pattern in sediment is the net result of the seasonally variable deposition of fresh POM "rain" to the sediment-water interface and its rapid consumption relative to the temporal scale of mixing by benthos and redox reactions [Aller, 1982]. The low abundance of available POM for benthos and low sedimentation rates in the deep open ocean result in a very tight coupling between POM delivery and consumption, and the total quantity of pigments in sediment is therefore low. Fresh pigments in the BaRFlux August (BF4) sub-core were just a small mole percent (<1%) of the total pigments and were most abundant directly below the sediment-water interface(Fig. 17). More than 99 mole percent of the pigments at all depths in the August(BF4)sub-core was pheophorbide-a. These results are consistent with previous studies, which found that Chl-a rapidly decreased with increasing depth below the sediment-water interface, and became depleted within a centimeter [Sun et al., 1991]. The pheopigments, which make up the majority of pigments in sediment, are typically compositionally uniform, and are either composed entirely of pheophytin-a or pheophorbide-a. These pheopigments indicate degradation by benthic microbes [Sun et al., 1991] or macrofauna [Bianchi et al., 1988b], respectively. Typically, pheophytin-a is the most abundant pigment in the sediment of the open ocean [Sun et al., 1991, Lee et al., 2000], whereas pheophorbide-a tends to be more characteristic of coastal sediment [Bianchi et al., 1988b]. Although it was surprising to have a more "coastal" signature, it is consistent with the bioturbation that was documented at the BaRFlux study area [Cochran, personal communication]. The possible association of the observed chloropigment heterogeneity with biogenic structures as seen on the Scotian Rise [Aller and Aller, 1986] and in the equatorial Pacific [Smith et al., 1996] is consistent with pulse delivery of POM to the deep seabed.

The pigment composition of small (>1 and <70-μm) and large (>70-μm) in-situ pump water column samples and sediment trap samples was compared to the sub-core sample to determine which particle size pool(s) is(are) being deposited. The smaller suspended POM is an unlikely source, because the mole percent of pheophytin-a in that material increases with increasing depth (Fig. 13). Sinking particles are an unlikely source because their pigment composition is almost all pyropheophorbide-a. The larger suspended POM is a likely candidate. The total pigment concentrations are low, but consistently Chl-a rich over all depths in August (BF4), and do not appear to be strongly coupled to the nepheloid layer processes (Figs. 12, 14). The small quantity of larger suspended POM is likely the source of the labile pigments found directly below the sediment-water interface.

6 Conclusions

Because chloropigments have a unique source in the surface ocean and undergo structural changes in response to biologically mediated degradation processes, they are a useful biomarker to trace the marine POM cycle. The application of chloropigment biomarker analysis to POM samples taken during the NSF BaRFlux cruises offers significant insight into the early cycling of POM in the North Atlantic subtropical gyre. The cycling of OM in subtropical gyres is important to understand for several reasons: 1. subtropical gyres are areas of Ekman suction, and therefore particle transport to deep water; The remineralization of downwelling POM determines the carbon budget of deep ocean water; 2. The expansion of subtropical gyres is one of the projected effects of global warming. If this type of setting will be the largest in the marine POM cycle, its biogeochemistry should be well understood.

The collection methods used for sampling - Niskin bottles/in-situ pumps (suspended POM), sediment traps (sinking POM), and box cores (deposited POM)- subdivided the POM into pools of distinct composition. The natural variable causing their distinct compositions seemed to be time- both the time of year (seasonal) and the time it took particles to settle through the water column (settling velocity). The former is related to particle abundance and the latter is related to particle size and density. Because the quantity and the composition of pigments are a net balance between the supply of labile organic matter and various degradation processes, both the seasonal variability in supply and the variability in degradation over time at different depths will determine the patterns seen in the data.

The POM cycle at BaRFlux can be thought of in terms of the differential production and degradation of each particle size pool during non-bloom (most of the year) and bloom (BF3 and BF6) seasons. The following description should be read while following Fig. 21. During non-bloom seasons, the small suspended POM becomes rapidly altered below the euphotic zone, and is increasingly altered by microbes and less altered by zooplankton as depth increases. Some of the smaller suspended POM is transferred into the sinking POM pool by being ingested by larger zooplankton and egested as highly degraded, more quickly sinking fecal pellets. The large suspended POM is much less abundant and remains unaltered during its transit to the seafloor. The smaller suspended POM is resuspended in a benthic nepheloid layer while the larger suspended POM is deposited at the sediment water interface and is rapidly consumed by macrobenthos. During bloom seasons, the small suspended POM partially follows the same degradation sequence of the non-bloom period, but part of the pool is exchanged with the larger suspended POM because both the stratification of the water column and higher supply of POM from primary production enhance particle-to-particle collisions. Some of the small suspended POM is also aggregated and therefore made available to larger zooplankton, which transfer the material from the small suspended to the sinking POM pool.

The pigment data from suspended particles collected by Niskin bottles and in-situ pumps can result in significantly different interpretations of the POM cycle. The complete absence of pheophytin-a and pyropheophorbide-a in most bottle samples would suggest to the incautious reader that zooplankton excretion and microbial degradation are not

important processes in the BaRFlux POM cycle. Of the many reasons proposed for the disparity between bottle and pump data by myriad studies, two are relevant to the biases seen in the BaRFlux data: 1. The small volume of collected water sample relative to the filter area; 2. The different retention efficiency of picophytoplankton by GF/F (0.7 μm pore) and in-situ pump microquartz filters (1-μm pore). For areas like the BaRFlux site, using in-situ pumps with a GF/F filter is recommended. The smaller pore size would increase the retention efficiency of picophytoplankton, while the large volume of seawater pumped will minimize biases from the low probability of capturing a representative pigment distribution in a dilute particle area.

Although the nepheloid layer is known to be a region of dynamic particle cycling in the deep ocean, it is much understudied. It is apparent from previous work [Gardner et al., 1985] and this study that nepheloid layers are an extensive and constant feature in the open Atlantic Ocean and should be included in POM models. Although equipment failure prevented the analysis of the actual floc taken with the box corer, several observations suggest that the POM resuspended in the nepheloid layer is highly degraded: 1. The C shape of the nepheloid layer is reflected in the profile shapes of the small suspended particulate pigments, which are highly degraded by microbial processes at depth; 2. The Chl-a fluorescence profiles do not reflect the C shape of the nepheloid layer. The analysis of the floc material is desirable in the future to have a truly complete picture of the POM cycle of the study area because the nepheloid layer connects the actively cycled material and the material that is removed from the POM cycle by burial. Higher resolution profiling near the seabed would be important, particularly given the known size fractionation vertically away from the seabed.

A Figures

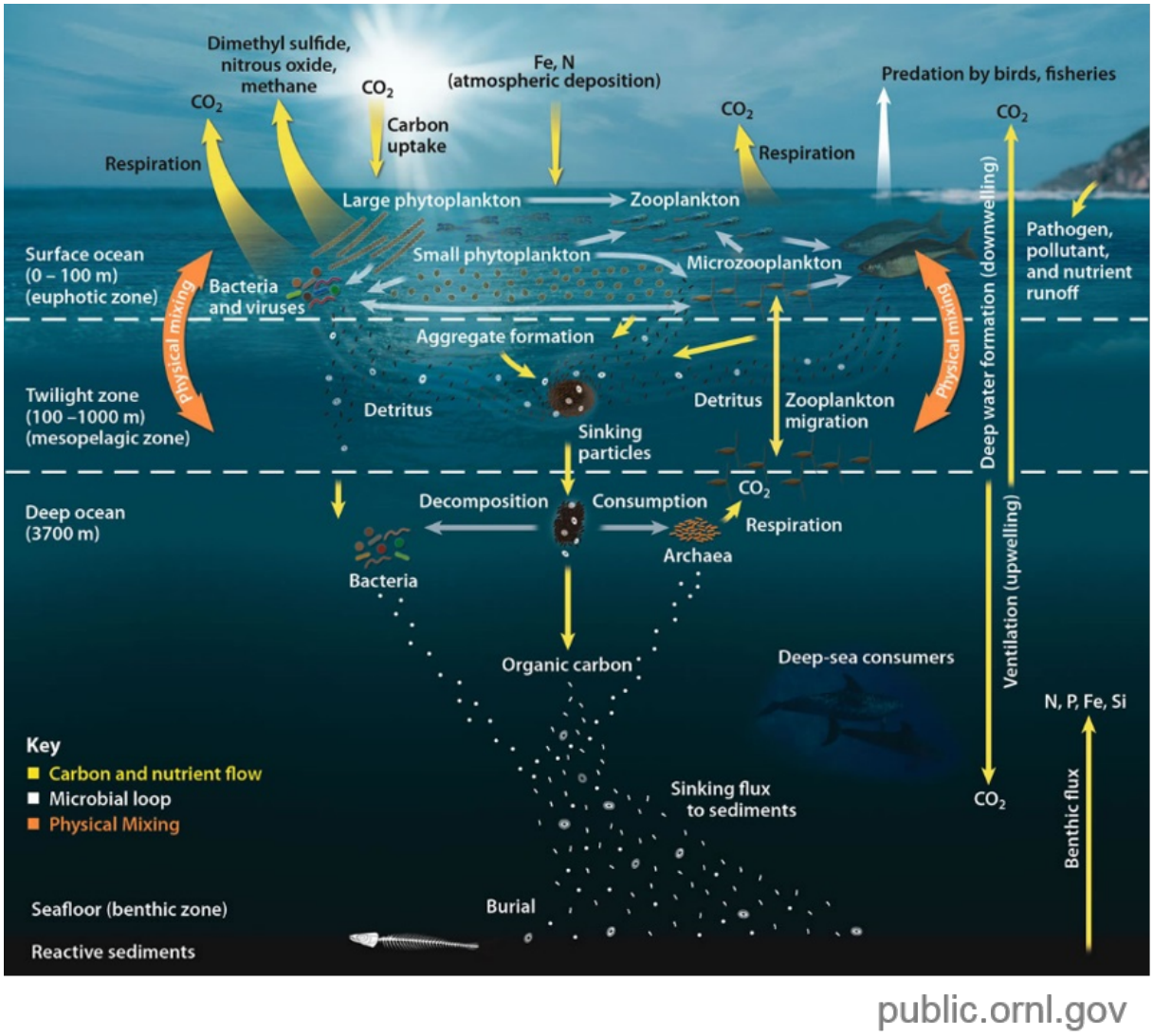

Figure 1: The marine POM cycle. POM is produced in the euphotic zone and degraded by various processes during its descent through the water column. Only a small fraction is eventually buried in sediment.

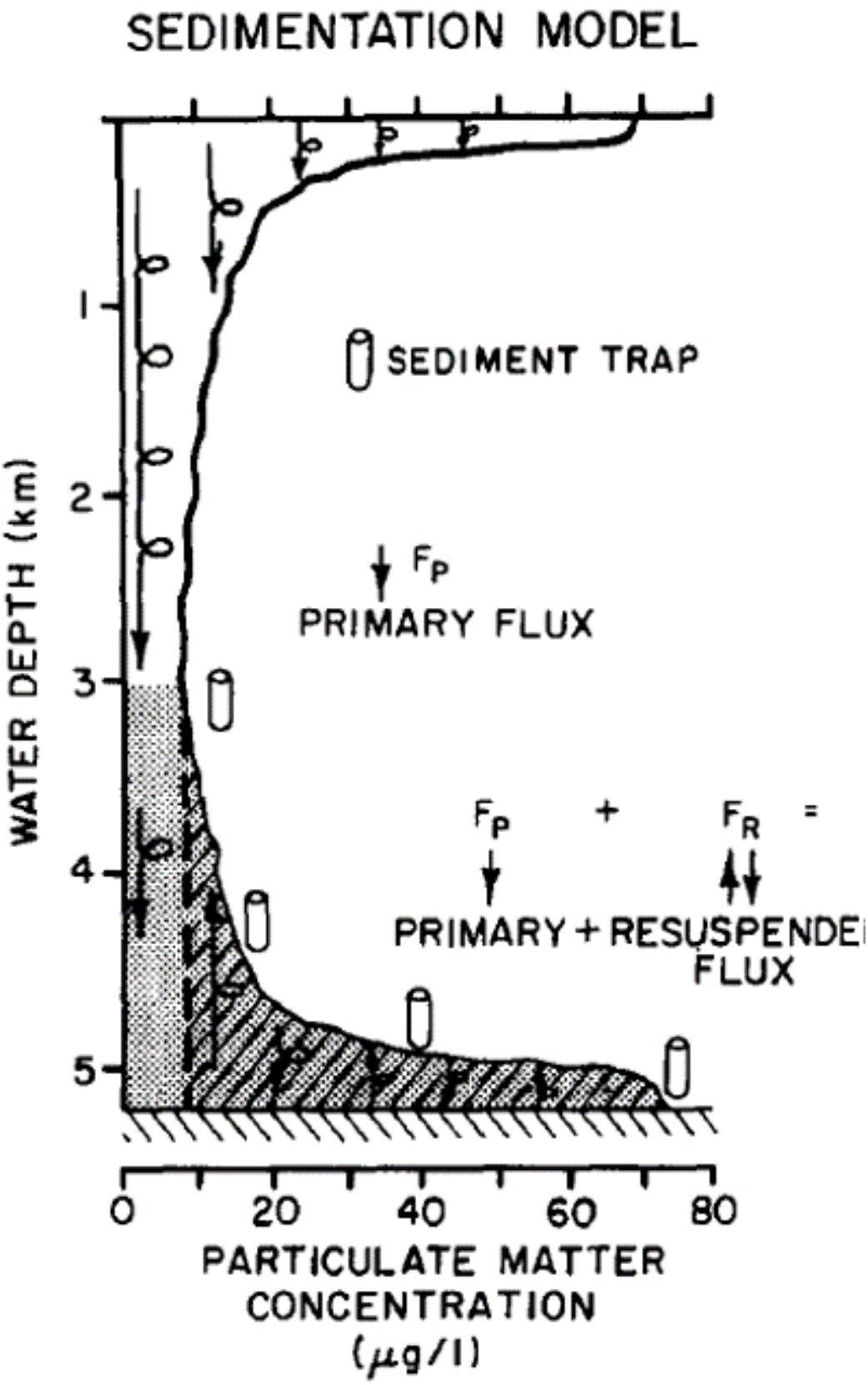

Figure 2: Biscaye and Eittreim's model for sedimentation of POM in the open ocean (figure from Gardner et al., 1985).

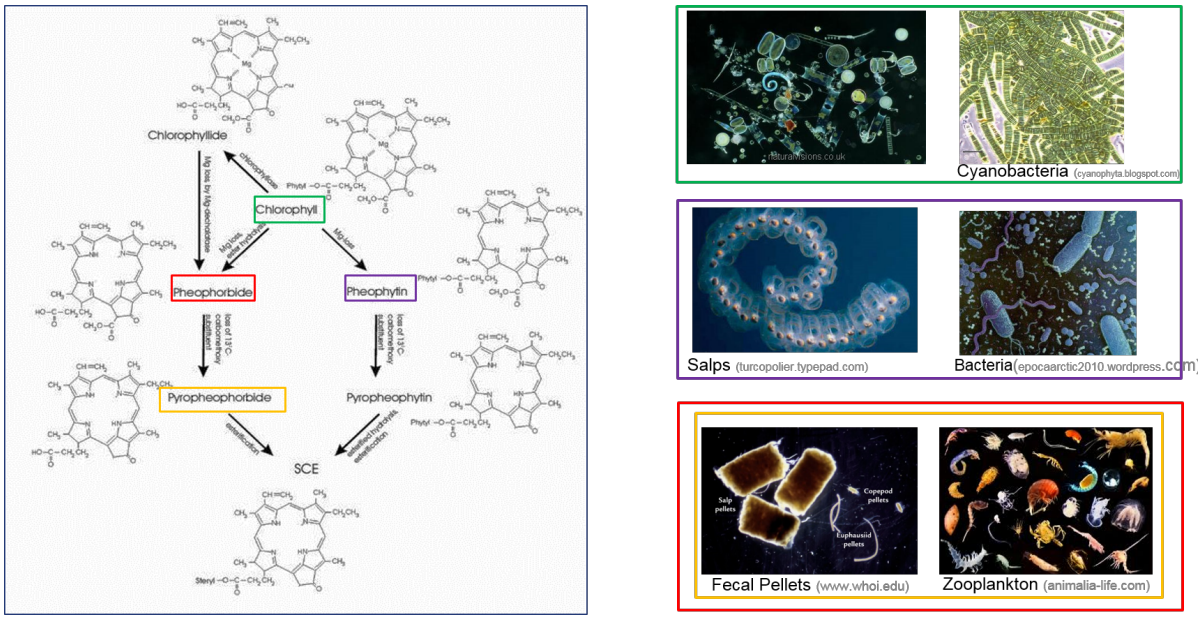

Figure 3: The degradation pathways of chlorophyll-a and the organisms associated with each chemical change.

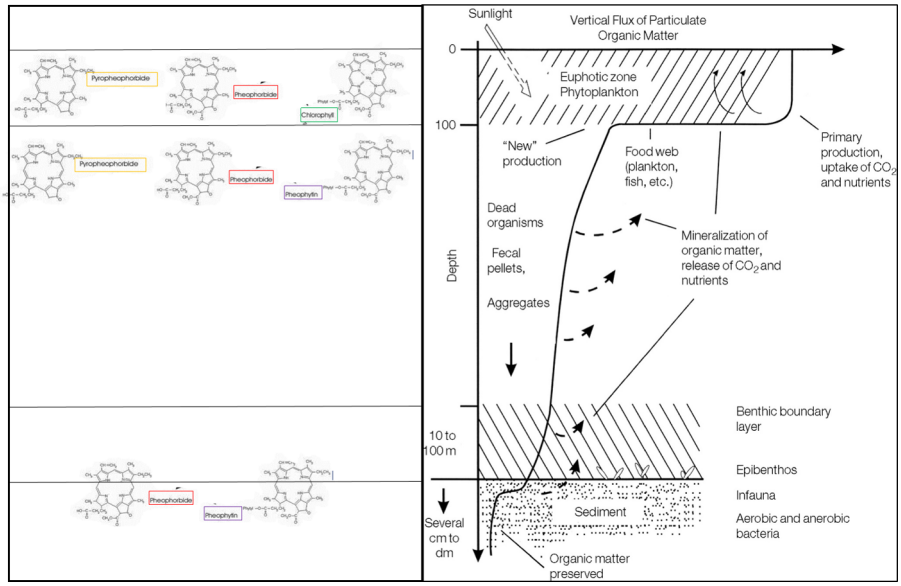

Figure 4: The comparison of POM degradation pathways in the water column, the nepheloid layer, and sediment and their associated pigments. Figure modified from Libes(2012)

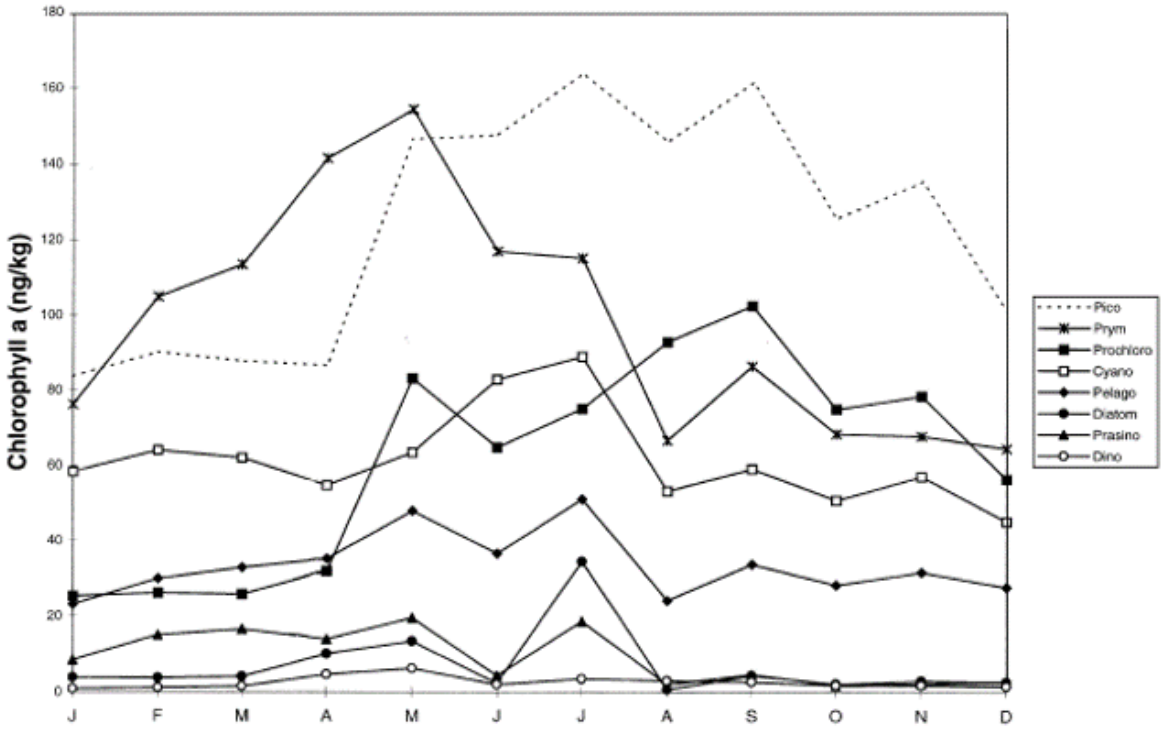

Figure 5: Concentrations of chlorophyll-a from various phytoplankton groups with month at BATS (Steinberg, 2001)

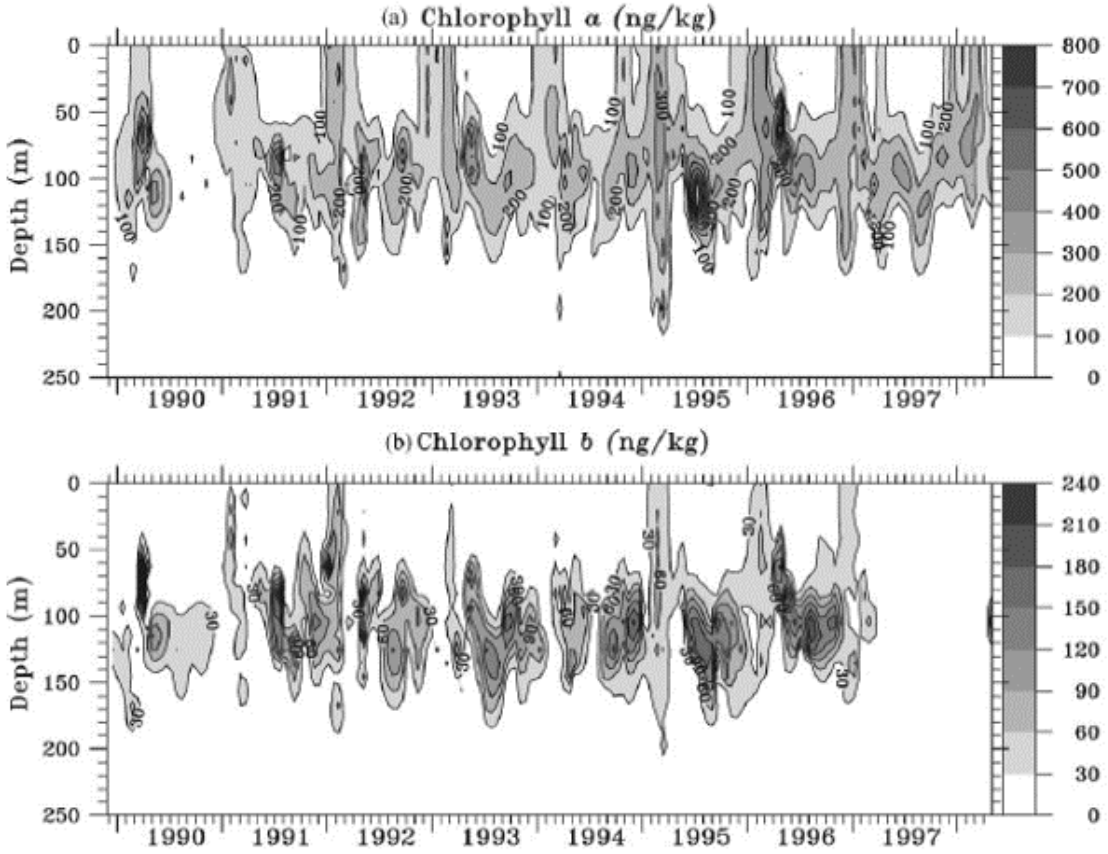

Figure 6: Concentration of chlorophylls a and b over depth and time at BATS (Steinberg et al., 2001)

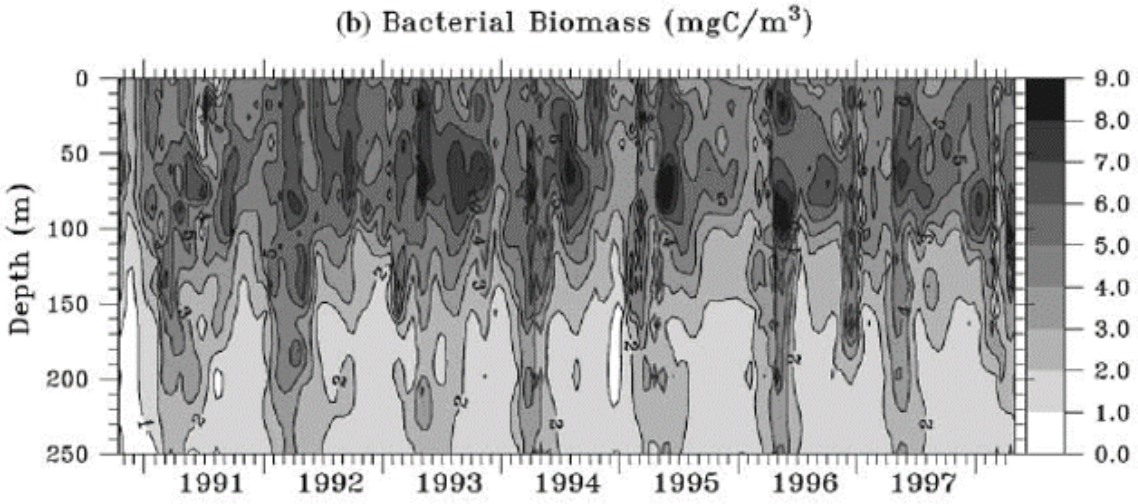

Figure 7: Concentration of bacterial biomass over depth and time at BATS (figure from Steinberg et al., 2001)

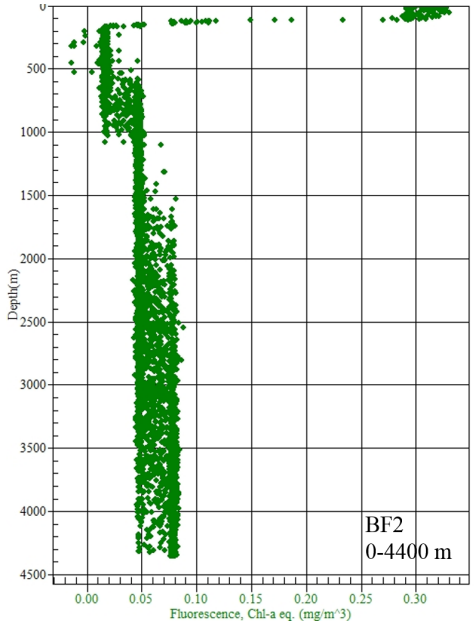

(a) BF2 , full profile

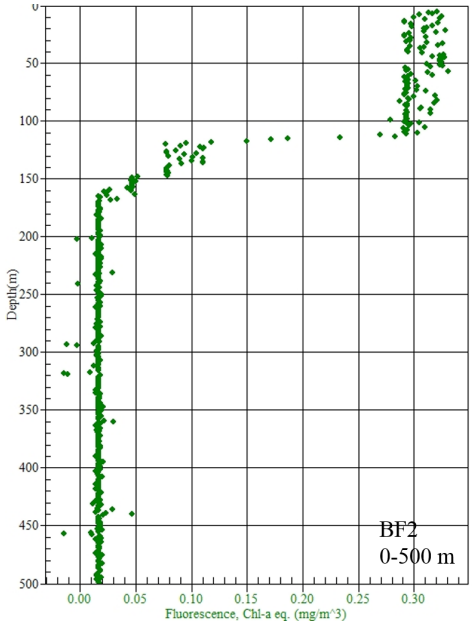

(b) BF2, 0-500 m

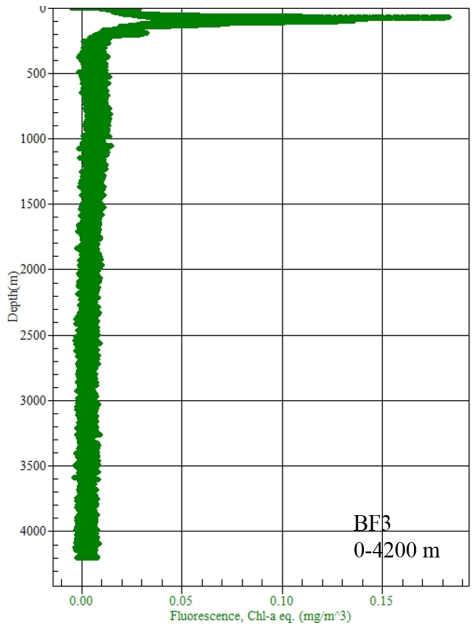

(c) BF3, full profile

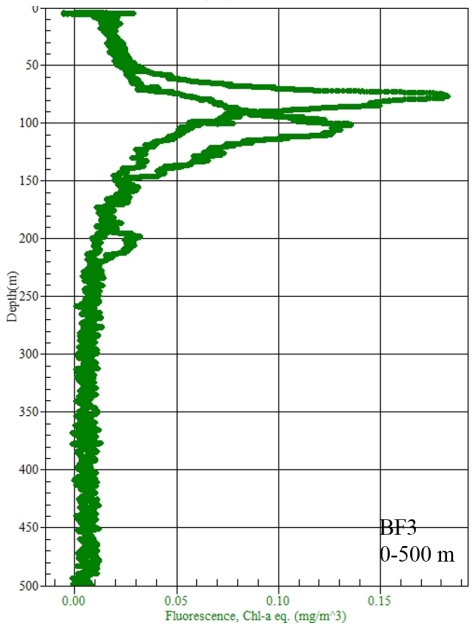

(d) BF3, 0-500 m

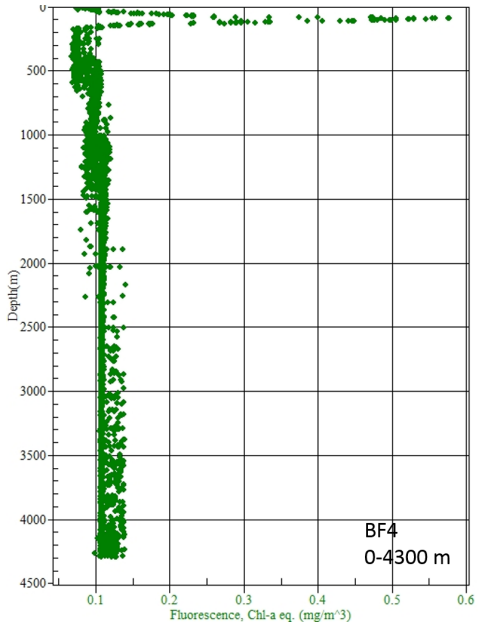

(e) BF4, full profile

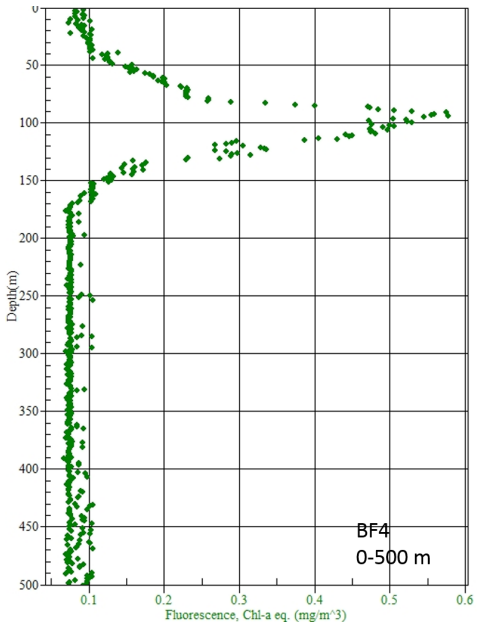

(f) BF4, 0-500 m

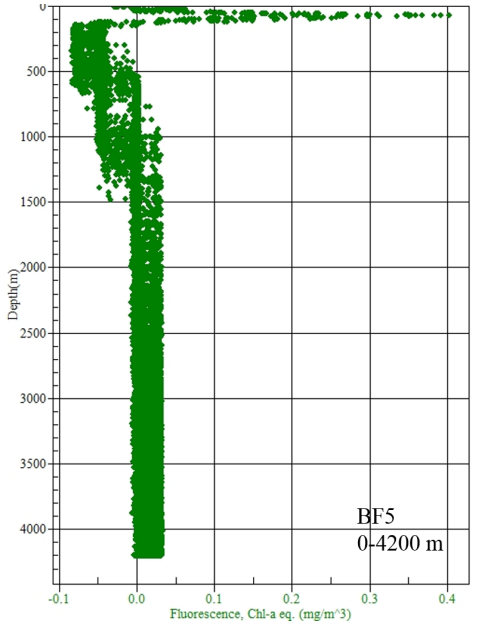

(g) BF5, full profile

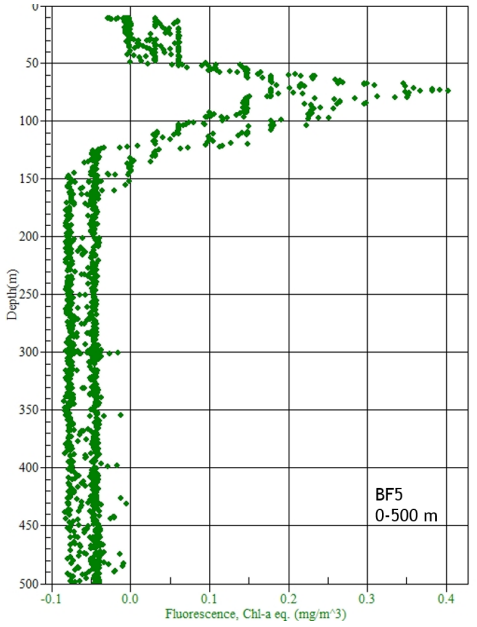

(h) BF5, 0-500 m

Figure 8: Fluorescence-Depth profiles collected with onboard SeaBird CTD arrays and processed with SeaBird/SeaPlot software. Fluorescence is reported in wet lab chlorophyll-a equivalent concentrations in μg/L

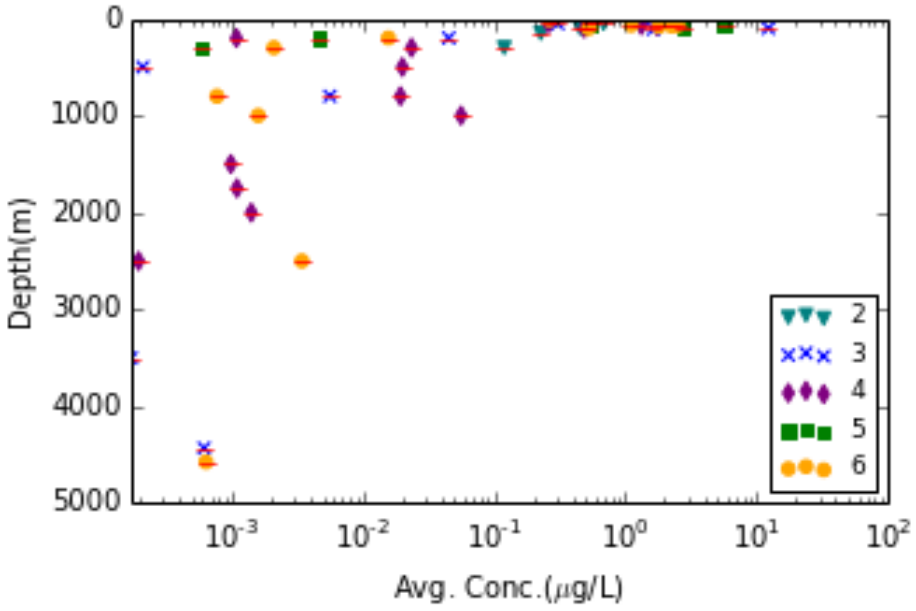

Figure 9: Total particulate pigment concentration collected by Niskin bottles. Numbers in legend correspond to cruise number. Red bars proportional to errors.

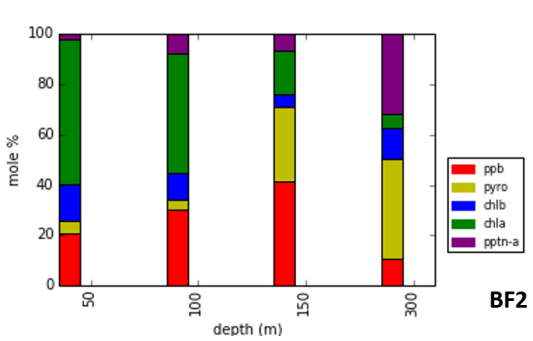

(a) BF2

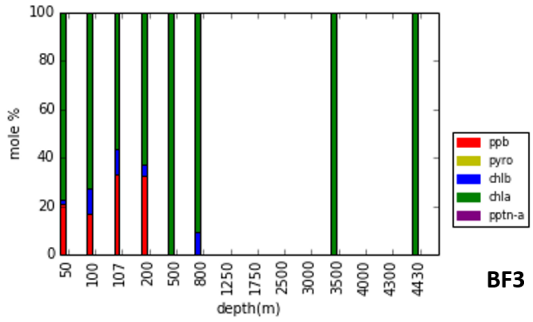

(b) BF3

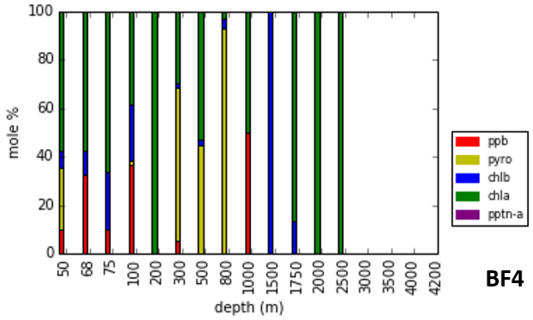

(c) BF4

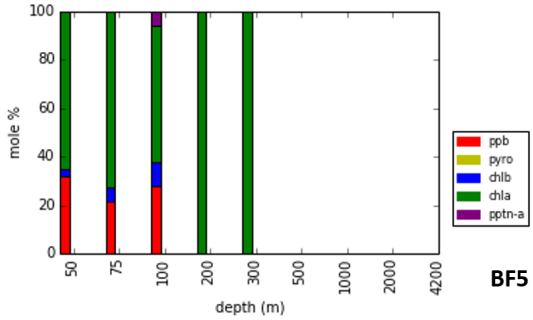

(d) BF5

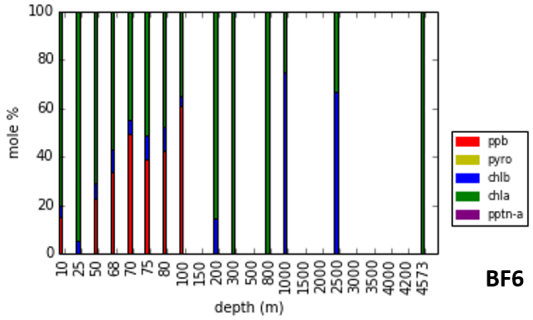

(e) BF6

Figure 10: Pigment composition of suspended particles collected over depth by Niskin bottle and filtered through 0.7 μm filters

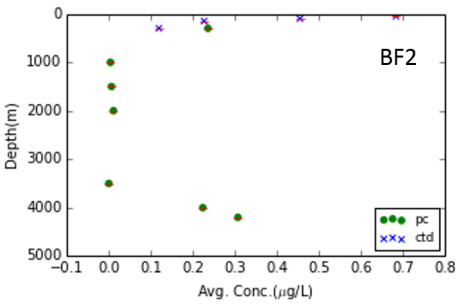

(a) BF2

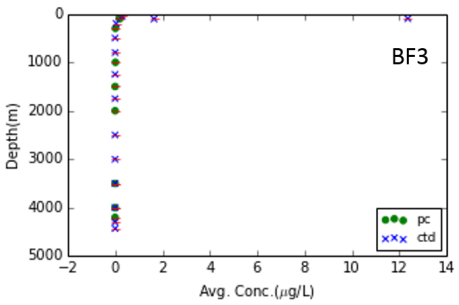

(b) BF3

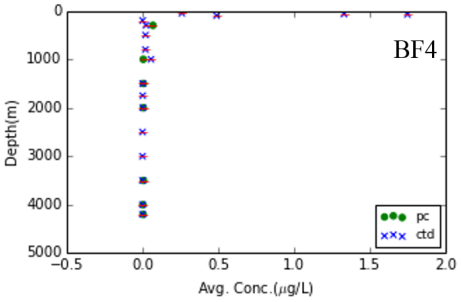

(c) BF4

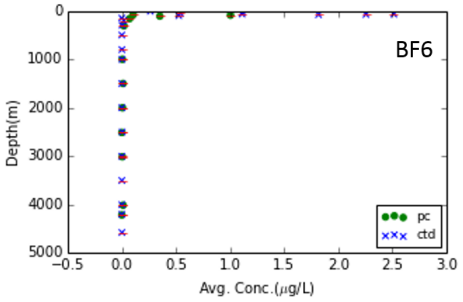

(d) BF5

Figure 11: Average total pigment concentrations reported in μg/L for Niskin bottles (x) and in-situ pumps (o). Red bars are proportional to error.

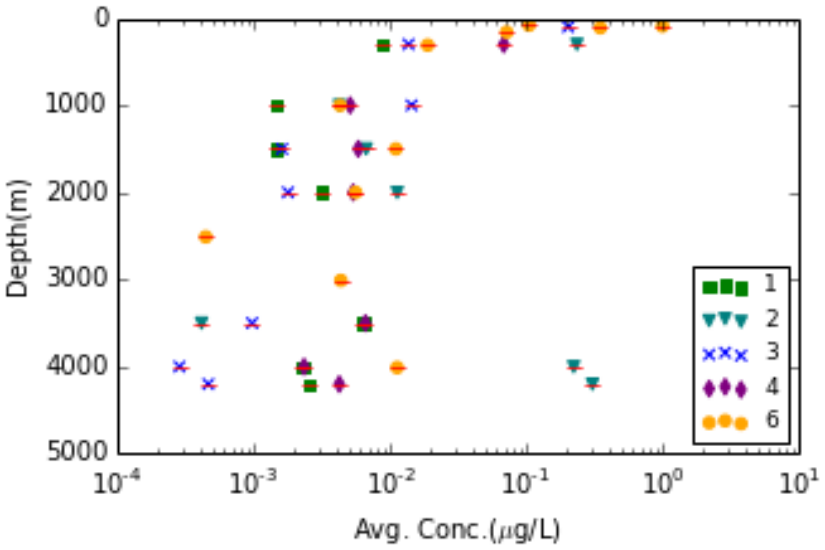

(a) >1 <70-μm particles

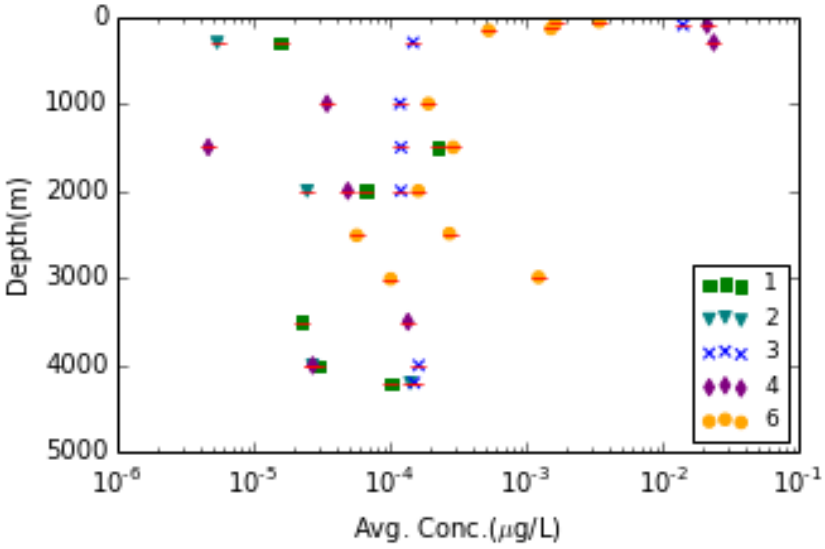

(b) > 70-μm particles

Figure 12: Total particulate pigment concentration collected by in-situ pumps. Numbers in legend correspond to cruise number. Red bars proportional to errors.

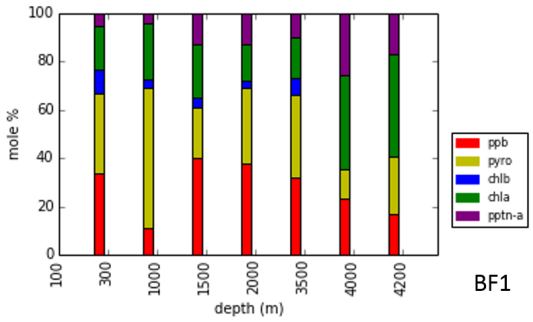

(a) BF1

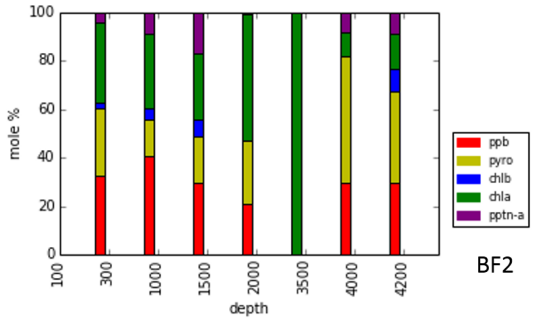

(b) BF2

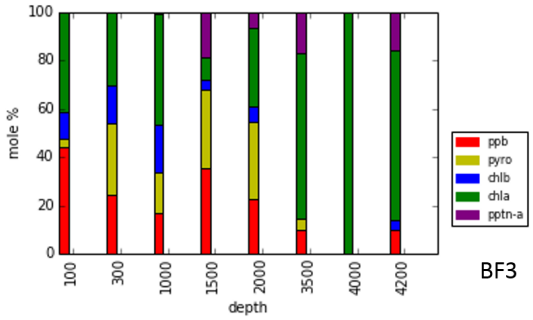

(c) BF3

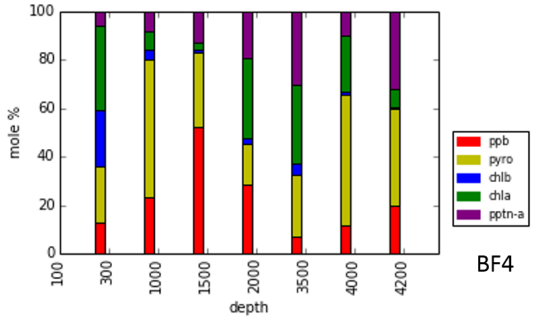

(d) BF4

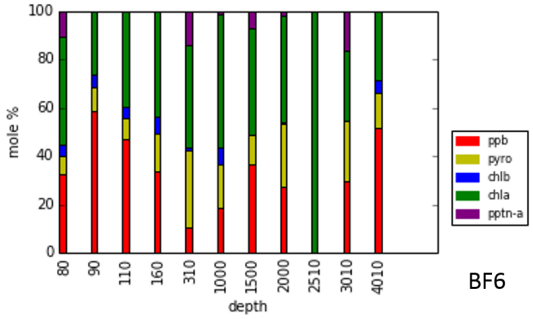

(e) BF6

Figure 13: Particulate (>1μm, <70-μm) pigment compositions collected by in-situ pumps over depth. Depth reported in meters.

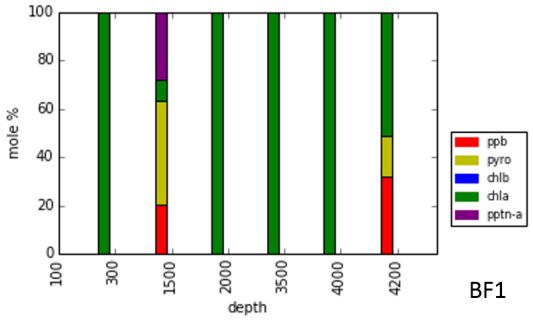

(a) BF1

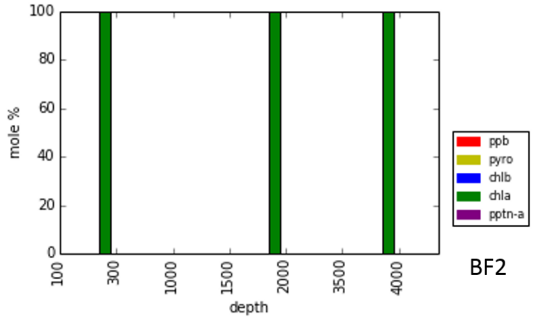

(b) BF2

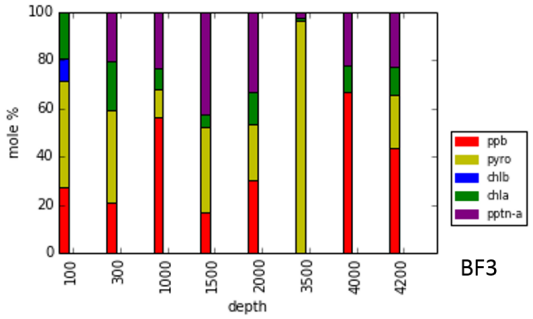

(c) BF3

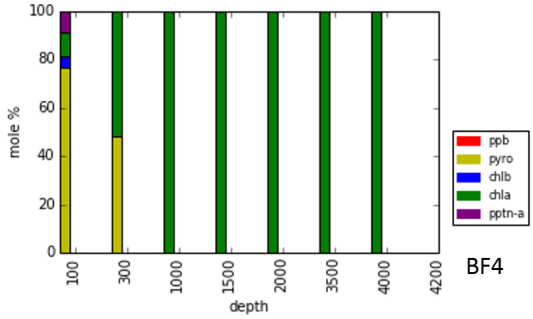

(d) BF4

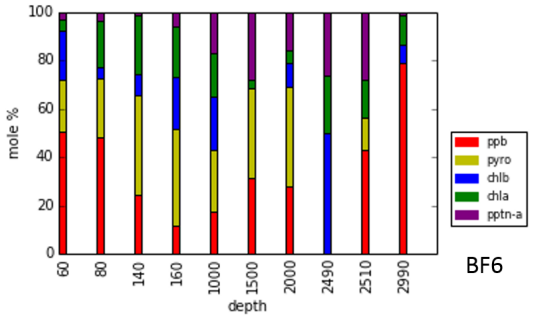

(e) BF6

Figure 14: Particulate ($> 70\mu$m) pigment compositions collected by in-situ pumps over depth. Depth reported in meters.

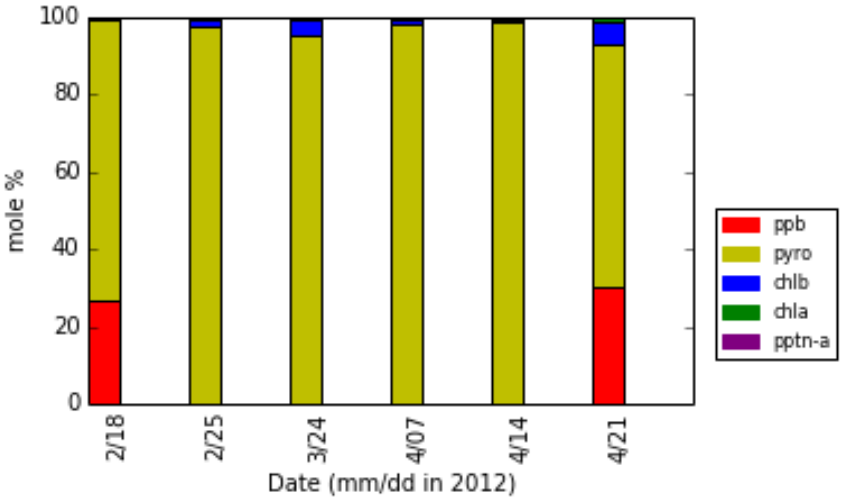

(a) Mole% pigment composition vs. time

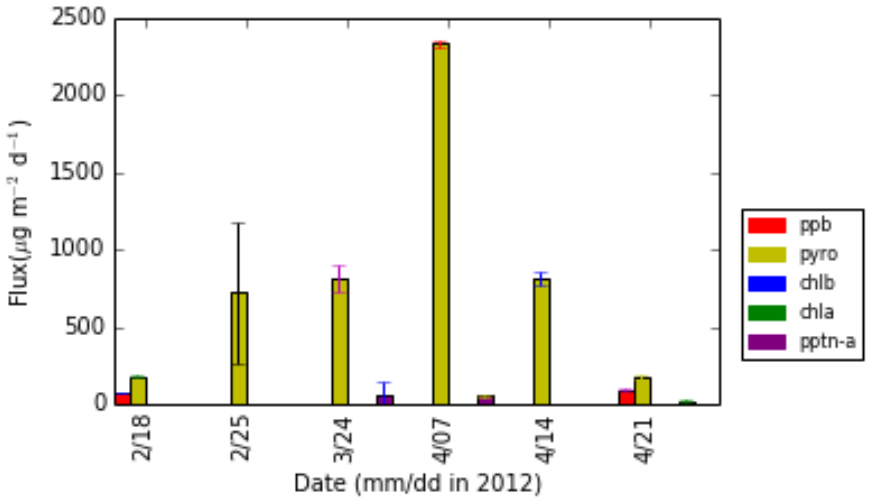

(b) Pigment flux v. time

Figure 15: BF3, 300 m TS Trap

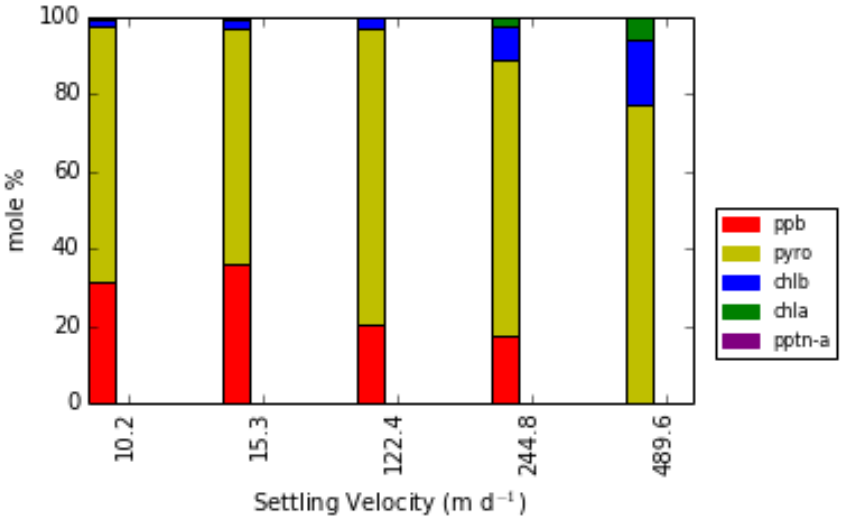

(a) Mole% pigment composition vs. settling velocity.

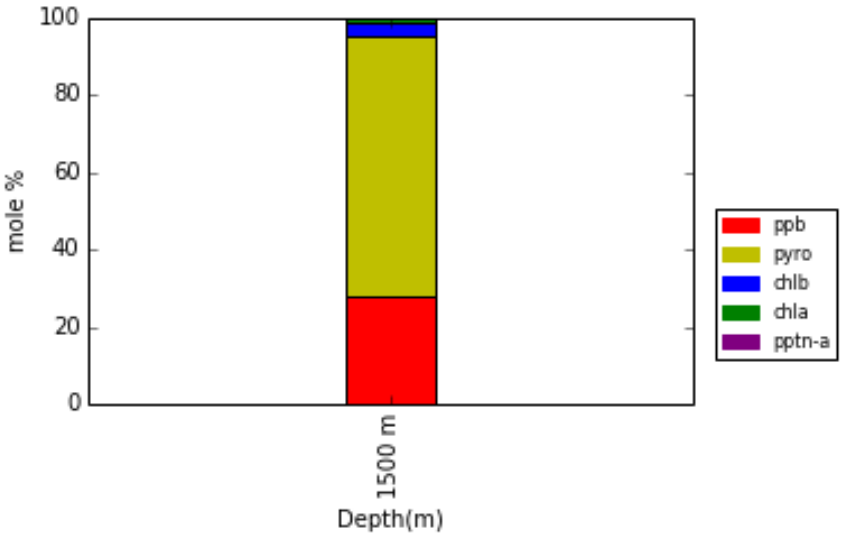

(b) Bulk SV trap composition determined by summing moles of each pigment over all settling velocities and normalizing to total moles pigment. Total error $\leq 3.5\%$ for all pigments.

Figure 16: BaRFlux 3, 1500 m SV Trap

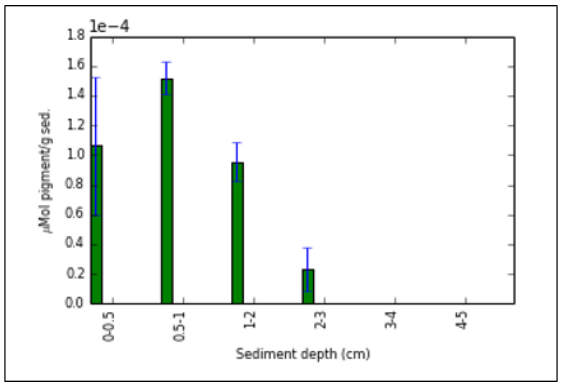

(a) Total μg pigment/g sediment

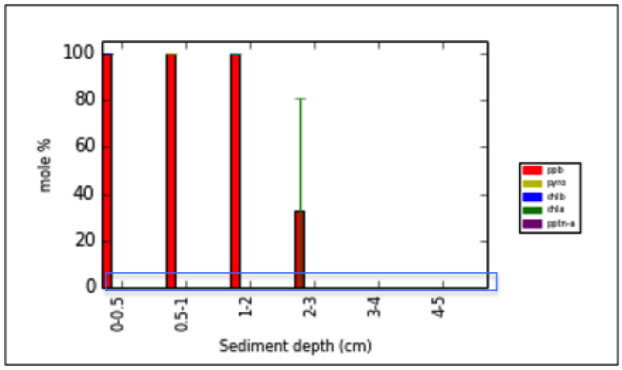

(b) Mole% of individual pigments from 0-5 cm below the sediment-water interface. Blue box (bottom) blows up 0-0.2 mole% area of graph shown in (c)

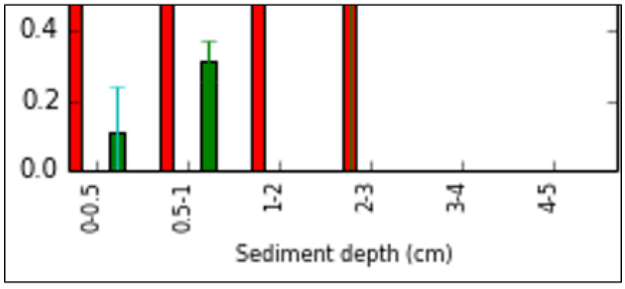

(c) Zoomed in area of (b) in blue box

Figure 17: Cruise 4 Syringe Core

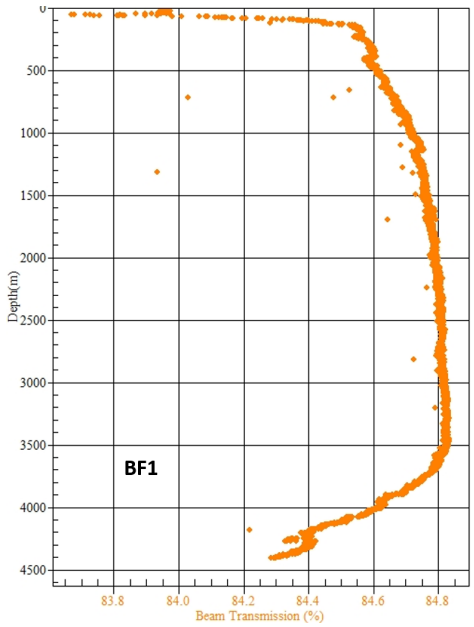

(a) BF1

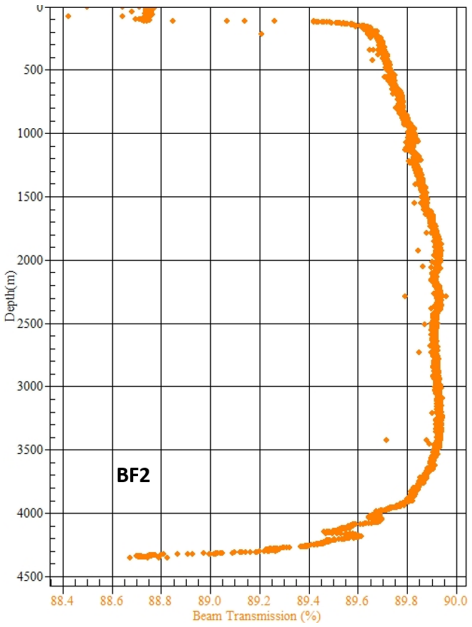

(b) BF2

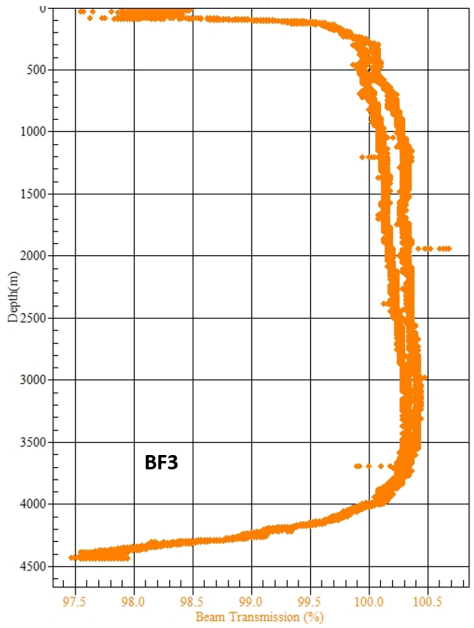

(c) BF3

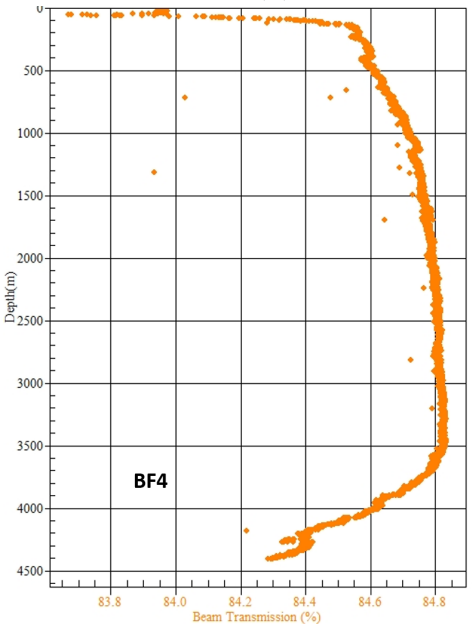

(d) BF4

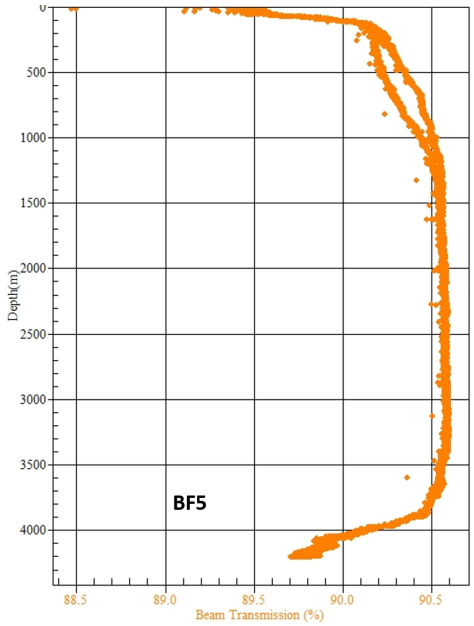

(e) BF5

Figure 18: Percent beam transmission profiles taken with onboard SeaBird CTD arrays.

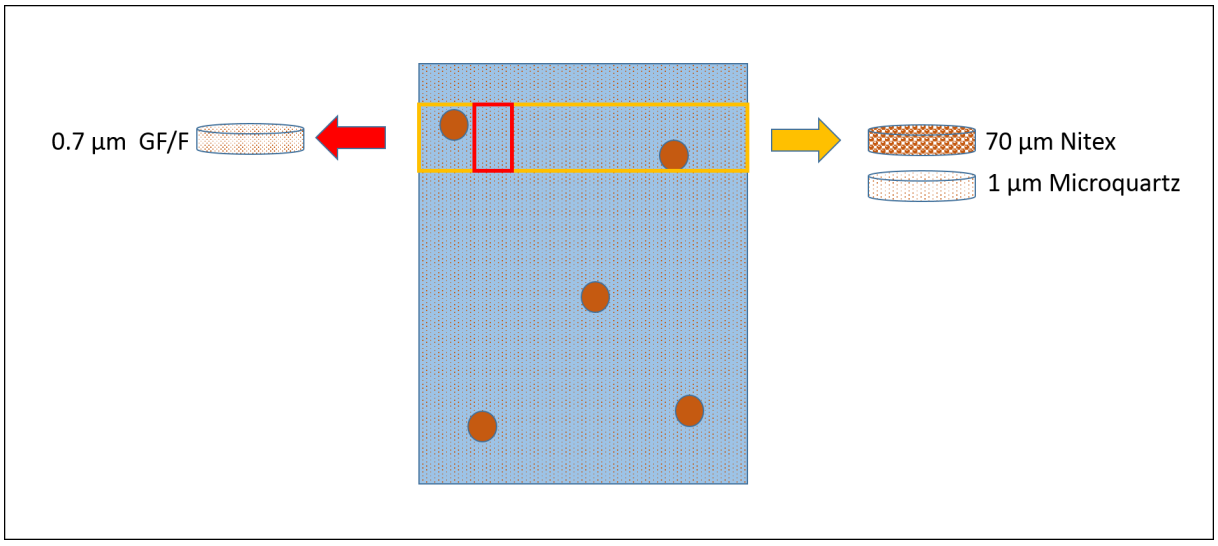

Figure 19: The differences in Niskin bottle and in-situ pump particle data due to probability. The Niskin bottle sampling volume (red box/arrow) is much smaller than the sampling volume of an in-situ pump. Rare larger particles can be missed by the bottle, creating a sampling bias towards a finer particle size and finer particle composition. The in-situ pump (yellow box/arrow) will retrieve a more representative water sample, but the slightly larger pore size of the filter will create a sampling bias towards a slightly coarser particle size and coarser particle composition.

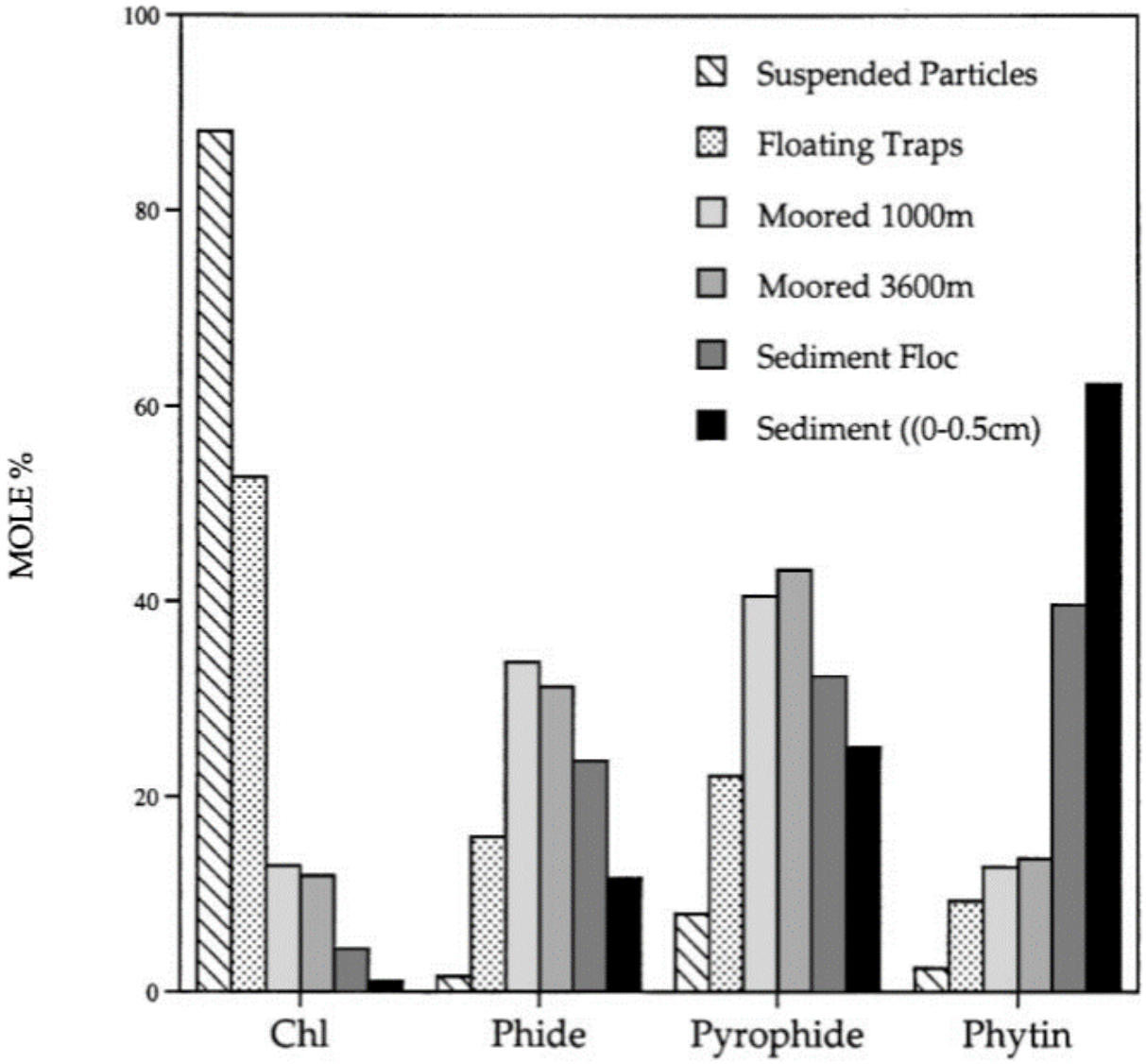

Figure 20: In Lee et al. [2000], pigment data from the Equatorial Pacific shows the mole percent pigment with increasing depth pattern as: a shallow Chl-a max, a mid-water pyropheophorbide-a and pheophorbide-a max, and gradually increasing pheophytin-a with increasing depth.

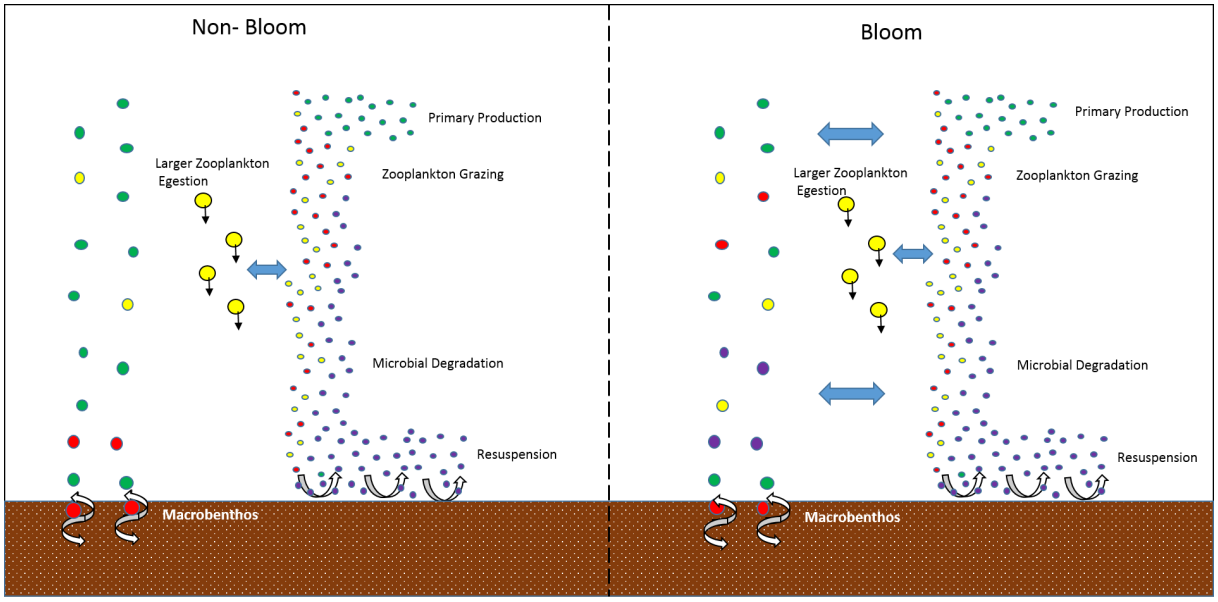

Figure 21: POM cycling in the BaRFlux study area during non-bloom and bloom (BF3 and BF6) periods. Pigment color coding is the same as in all plots. Double headed arrows indicate particle exchange.

B Data Tables

- ND (not detected) indicates pigment amount below detection limit.

B.1 Cruise 1 Samples

B.1.1 In-situ Pump Samples

Table 11: Mole percent pigment compositions of in-situ pump samples collected on 1-μm filters during BaRFlux cruise 1. Depth is in meters.

1-μm filters

depth	ppb-a	stdev	pyro-a	stdev	chl-b	stdev	chl-a	stdev	pptn-a	stdev
300	33.61	24.41	32.91	5.54	9.84	7.48	18.23	17.66	5.41	0.70
1000	10.97	7.77	58.22	10.46	3.45	4.88	23.23	16.23	4.13	2.92
1500	40.34	28.59	20.45	2.95	4.47	6.31	21.66	11.79	13.10	11.79
2000	37.97	21.08	31.20	10.03	2.83	5.66	14.75	12.70	13.25	12.05
3500	32.30	23.08	33.84	2.58	6.84	9.67	16.81	17.96	10.22	7.66
4000	17.73	17.79	8.82	8.82	ND	ND	29.23	41.04	19.22	19.23
4200	17.19	19.49	23.79	20.67	ND	ND	41.98	41.05	17.05	12.82

Table 12: Pigment concentrations of in-situ pump samples collected during BaRFlux cruise 1 in ng/L. Depth is in meters.

ng/L

depth	ppb-a	stdev	pyro-a	stdev	chl-b	stdev	chl-a	stdev	pptn-a	stdev
300	3.66	2.59	2.59	1.67	0.77	0.12	1.19	0.37	0.61	0.28
1000	0.19	0.14	0.77	0.37	0.04	0.05	0.36	0.07	0.11	0.08
1500	0.69	0.58	0.26	0.17	0.04	0.06	0.32	0.01	0.16	0.07
2000	1.50	1.72	0.99	0.99	0.05	0.09	0.41	0.27	0.22	0.11
3500	2.73	1.93	1.73	1.06	0.08	0.11	0.51	0.03	1.29	1.00
4000	0.66	0.68	0.30	0.30	ND	ND	0.27	0.21	1.05	1.07
4200	0.49	0.52	0.74	0.71	ND	ND	0.48	0.20	0.84	0.69

Table 13: Pigment to POC ratios of in-situ pump samples collected on 1-μm filters during BaRFlux 1 cruise. Depth is in meters.

pigment/POC

depth	ppb-a	stdev	pyro-a	stdev
300	1.13 x 10^{-3}	7.98 x 10^{-4}	7.96 x 10^{-4}	5.15 x 10^{-4}
1000	1.13 x 10^{-4}	8.04 x 10^{-5}	4.60 x 10^{-4}	2.20 x 10^{-4}
1500	7.94 x 10^{-4}	6.67 x 10^{-4}	2.98 x 10^{-4}	1.97 x 10^{-4}
2000	1.42 x 10^{-4}	7.08 x 10^{-5}	5.55 x 10^{-4}	2.18 x 10^{-4}
3500	2.73 x 10^{-3}	1.94 x 10^{-3}	1.73 x 10^{-3}	1.06 x 10^{-3}
4000	1.01 x 10^{-4}	1.01 x 10^{-4}	8.13 x 10^{-5}	3.72 x 10^{-5}
4200	1.35 x 10^{-4}	9.51 x 10^{-5}	1.14 x 10^{-4}	9.93 x 10^{-5}

Table 14: Pigment to POC ratios of in-situ pump samples collected on 1-μm filters during BaRFlux 1 cruise. Depth is in meters.

pigment/POC contd.

depth	chl-b	stdev	chl-a	stdev	pptn-a	stdev
300	2.38 x 10^{-4}	3.58 x 10^{-5}	3.66 x 10^{-4}	1.14 x 10^{-4}	1.88 x 10^{-4}	8.56 x 10^{-5}
1000	2.08 x 10^{-5}	2.94 x 10^{-5}	2.13 x 10^{-4}	4.30 x 10^{-5}	6.28 x 10^{-5}	4.45 x 10^{-5}
1500	4.62 x 10^{-5}	6.54 x 10^{-5}	3.66 x 10^{-4}	1.15 x 10^{-5}	1.82 x 10^{-4}	8.08 x 10^{-5}
2000	2.77 x 10^{-5}	5.55 x 10^{-5}	2.29 x 10^{-4}	7.67 x 10^{-5}	1.37 x 10^{-4}	7.89 x 10^{-5}
3500	7.92 x 10^{-5}	1.12 x 10^{-4}	5.12 x 10^{-4}	2.65 x 10^{-5}	1.29 x 10^{-3}	9.99 x 10^{-4}
4000	7.95 x 10^{-5}	5.92 x 10^{-5}	2.79 x 10^{-4}	1.03 x 10^{-4}	1.82 x 10^{-4}	1.13 x 10^{-4}
4200	9.27 x 10^{-5}	1.02 x 10^{-4}	2.78 x 10^{-4}	1.44 x 10^{-4}	4.59 x 10^{-5}	3.24 x 10^{-5}

Table 15: Mole percent pigment compositions of in-situ pump samples collected on 70-μm filters during BaRFlux cruise 1. Depth is in meters.

70-μm filters

depth	ppb-a	stdev	pyro-a	stdev	chl-b	stdev	chl-a	stdev	pptn-a	stdev
300	ND	ND	ND	ND	ND	ND	100	ND	ND	ND
1500	20.31	16.07	42.93	17.32	ND	ND	8.90	10.03	27.86	13.05
2000	ND	ND	ND	ND	ND	ND	100	ND	ND	ND
3500	ND	ND	ND	ND	ND	ND	100	ND	ND	ND
4000	ND	ND	ND	ND	ND	ND	100	ND	ND	ND
4200	ND	ND	ND	ND	ND	ND	50.81	49.19	49.19	49.19

Table 16: Pigment concentrations of in-situ pump samples collected on 70-μm filters during BaRFlux cruise 1 in pg/L.

pg/L

depth	ppb-a	stdev	pyro-a	stdev	chl-b	stdev	chl-a	stdev	pptn-a	stdev
300	ND	ND	ND	ND	ND	ND	1.58	0.06	ND	ND
1500	6.46	5.82	7.64	5.76	ND	ND	0.66	0.26	7.61	7.89
2000	ND	ND	ND	ND	ND	ND	6.61	2.15	ND	ND
3500	ND	ND	ND	ND	ND	ND	2.26	0.11	ND	ND
4000	ND	ND	ND	ND	ND	ND	0.87	0.06	ND	ND
4200	ND	ND	ND	ND	ND	ND	0.29	0.05	9.93	9.93

Table 17: Pigment to POC ratios of in-situ pump samples collected during BaRFlux 1 cruise on 70-μm filters.

pigment/POC

depth	ppb-a	stdev	pyro-a	stdev
300	ND	ND	ND	ND
1500	1.46×10^{-2}	2.03×10^{-2}	1.65×10^{-2}	2.30×10^{-2}
2000	ND	ND	ND	ND
3500	ND	ND	ND	ND
4000	ND	ND	ND	ND
4200	ND	ND	ND	ND

Table 18: Pigment to POC ratios of in-situ pump samples collected during BaRFlux 1 cruise on 70-μm filters.

pigment/POC contd.

depth	chl-b	stdev	chl-a	stdev	pptn-a	stdev
300	ND	ND	2.74×10^{-5}	1.06×10^{-6}	ND	ND
1500	ND	ND	1.03×10^{-1}	1.46×10^{-1}	1.43×10^{-3}	1.75×10^{-3}
2000	ND	ND	1.63×10^{-4}	5.30×10^{-5}	ND	ND
3500	ND	ND	6.59×10^{-5}	3.15×10^{-6}	ND	ND
4000	ND	ND	8.50×10^{-5}	5.83×10^{-6}	ND	ND
4200	ND	ND	1.34×10^{-5}	2.20×10^{-6}	4.64×10^{-4}	4.64×10^{-4}

B.2 Cruise 2 Samples

B.2.1 In-situ Pump Samples

Table 19: Mole percent pigment compositions of in-situ pump samples collected on 1-μm filters during BaRFlux cruise 2. Depth is in meters.

1-μm filters

depth	ppb-a	stdev	pyro-a	stdev	chl-b	stdev	chl-a	stdev	pptn-a	stdev
300	32.49	22.13	27.91	19.85	2.45	3.10	33.05	33.60	4.09	4.94
1000	40.84	28.02	15.22	15.08	4.42	4.21	30.45	35.75	9.07	9.96
1500	29.67	22.26	19.38	15.76	6.78	5.87	27.30	31.90	16.87	20.68
2000	20.91	21.16	26.31	26.54	ND	ND	51.94	48.06	0.85	0.87
3500	ND	ND	ND	ND	ND	ND	100	ND	ND	ND
4000	29.48	21.19	52.26	19.52	ND	ND	10.11	7.13	8.14	7.76
4200	29.48	22.34	37.97	28.43	9.05	15.67	14.73	12.17	8.77	6.07

Table 20: Pigment concentrations of in-situ pump samples collected on 1-μm filters during BaRFlux cruise 2 reported in ng/L. Depth is in meters.

ng/L

depth	ppb-a	stdev	pyro-a	stdev	chl-b	stdev	chl-a	stdev	pptn-a	stdev
300	128.58	234.28	55.72	94.42	0.28	0.55	51.77	88.67	0.11	0.11
1000	2.34	2.59	0.48	0.45	0.40	0.49	0.61	0.37	0.45	0.51
1500	2.73	2.98	1.64	1.76	0.98	1.17	0.75	0.40	0.62	0.66
2000	4.65	4.70	5.29	5.35	ND	ND	1.13	0.17	0.28	0.29
3500	ND	ND	ND	ND	ND	ND	0.42	0.15	ND	ND
4000	2.28	1.62	155.54	216.12	ND	ND	65.27	91.47	1.02	1.07
4200	17.22	25.79	116.41	199.05	54.25	93.97	96.21	95.88	23.44	39.47

B.2.2 Niskin Bottle

Table 21: Pigment to POC ratios of in-situ pump samples collected during BaRFlux 2 cruise on 1-μm filters. Depth is in meters.

pigment/POC

depth	ppb-a	stdev	pyro-a	stdev
300	7.89 x 10^{-4}	9.05 x 10^{-4}	4.74 x 10^{-4}	3.89 x 10^{-4}
1000	1.21 x 10^{-3}	1.34 x 10^{-3}	2.48 x 10^{-4}	2.32 x 10^{-4}
1500	1.24 x 10^{-3}	1.36 x 10^{-3}	7.47 x 10^{-4}	8.01 x 10^{-4}
2000	1.86 x 10^{-3}	1.88 x 10^{-3}	2.12 x 10^{-3}	2.14 x 10^{-3}
3500	ND	ND	ND	ND
4000	1.35 x 10^{-3}	9.62 x 10^{-4}	1.69 x 10^{-3}	2.14 x 10^{-4}
4200	1.08 x 10^{-3}	9.64 x 10^{-4}	1.11 x 10^{-3}	6.83 x 10^{-4}

Table 22: Pigment to POC ratios of in-situ pump samples collected during BaRFlux 2 cruise on 1-μm filters. Depth is in meters.

pigment/POC contd.

depth	chl-b	stdev	chl-a	stdev	pptn-a	stdev
300	7.23 x 10^{-5}	1.43 x 10^{-4}	3.48 x 10^{-4}	2.86 x 10^{-4}	2.83 x 10^{-5}	2.91 x 10^{-5}
1000	2.08 x 10^{-4}	2.52 x 10^{-4}	3.16 x 10^{-4}	1.89 x 10^{-4}	2.30 x 10^{-4}	2.62 x 10^{-4}
1500	4.44 x 10^{-4}	5.32 x 10^{-4}	3.40 x 10^{-4}	1.81 x 10^{-4}	2.82 x 10^{-4}	3.01 x 10^{-4}
2000	ND	ND	4.52 x 10^{-4}	6.98 x 10^{-5}	1.11 x 10^{-4}	1.14 x 10^{-4}
3500	ND	ND	2.54 x 10^{-4}	9.19 x 10^{-5}	ND	ND
4000	ND	ND	4.94 x 10^{-4}	2.03 x 10^{-4}	6.07 x 10^{-4}	6.36 x 10^{-4}
4200	2.18 x 10^{-4}	3.77 x 10^{-4}	4.85 x 10^{-4}	2.88 x 10^{-4}	3.74 x 10^{-4}	2.67 x 10^{-4}

Table 23: Mole percent pigment compositions of in-situ pump samples collected on 70-μm filters during BaRFlux cruise 2. Depth is in meters.

70-μm filters

depth	ppb-a	stdev	pyro-a	stdev	chl-b	stdev	chl-a	stdev	pptn-a	stdev
100	ND	ND	ND	ND	ND	ND	ND	ND	ND	ND
300	ND	ND	ND	ND	ND	ND	50	50	ND	ND
1000	ND	ND	ND	ND	ND	ND	ND	ND	ND	ND
1500	ND	ND	ND	ND	ND	ND	ND	ND	ND	ND
2000	ND	ND	ND	ND	ND	ND	100	ND	ND	ND
3500	ND	ND	ND	ND	ND	ND	ND	ND	ND	ND
4000	ND	ND	ND	ND	ND	ND	100	ND	ND	ND
4200	ND	ND	ND	ND	ND	ND	100	ND	ND	ND

Table 24: Pigment concentrations of in-situ pump samples collected on 70-μm filters during BaRFlux cruise 2 reported in ng/L. Depth is in meters.

ng/L

depth	ppb-a	stdev	pyro-a	stdev	chl-b	stdev	chl-a	stdev	pptn-a	stdev
100	ND	ND	ND	ND	ND	ND	ND	ND	ND	ND
300	ND	ND	ND	ND	ND	ND	05	05	ND	ND
1000	ND	ND	ND	ND	ND	ND	ND	ND	ND	ND
1500	ND	ND	ND	ND	ND	ND	ND	ND	ND	ND
2000	ND	ND	ND	ND	ND	ND	0.025	ND	ND	ND
3500	ND	ND	ND	ND	ND	ND	ND	ND	ND	ND
4000	ND	ND	ND	ND	ND	ND	0.027	ND	ND	ND
4200	ND	ND	ND	ND	ND	ND	0.142	ND	ND	ND

Table 25: Pigment to POC ratios of in-situ pump samples collected during BaRFlux 2 cruise on 70-μm filters. Depth is in meters.

pigment/POC

depth	ppb-a	stdev	pyro-a	stdev
100	4.33×10^{-2}	ND	4.91×10^{-2}	ND
300	ND	ND	ND	ND
1000	ND	ND	ND	ND
1500	ND	ND	ND	ND
2000	ND	ND	ND	ND
3500	ND	ND	ND	ND
4000	ND	ND	ND	ND
4200	ND	ND	ND	ND

Table 26: Pigment to POC ratios of in-situ pump samples collected during BaRFlux 2 cruise on 70-μm filters. Depth is in meters.

pigment/POC contd.

depth	chl-b	stdev	chl-a	stdev	pptn-a	stdev
100	ND	ND	3.10×10^{-1}	ND	3.90×10^{-3}	ND
300	ND	ND	2.33×10^{-5}	2.33×10^{-5}	ND	ND
1000	ND	ND	ND	ND	ND	ND
1500	ND	ND	ND	ND	ND	ND
2000	ND	ND	4.80×10^{-5}	ND	ND	ND
3500	ND	ND	ND	ND	ND	ND
4000	ND	ND	1.31×10^{-4}	ND	ND	ND
4200	ND	ND	6.20×10^{-4}	ND	ND	ND

Table 27: Mole percent pigment compositions of Niskin bottle samples collected during BaRFlux cruise 2. Depth is in meters.
*Indicates Chlorophyll maximum

depth	ppb-a	stdev	pyro-a	stdev	chl-b	stdev	chl-a	stdev	pptn-a	stdev
50	20.61	2.34	5.31	3.79	14.33	0.29	57.69	6.84	2.06	0.43
100*	30.34	16.88	3.98	2.92	10.61	1.93	47.71	16.88	7.36	4.44
150	41.70	8.29	29.37	16.75	5.25	2.10	17.43	4.40	6.25	1.96
300	10.85	2.25	39.53	17.59	12.51	1.76	5.61	2.36	31.50	19.46

Table 28: Pigment concentrations of Niskin bottle samples collected during BaRFlux cruise 2 in ng/L. Depth is in meters.
*Indicates Chlorophyll maximum

ng/L

depth	ppb-a	stdev	pyro-a	stdev	chl-b	stdev	chl-a	stdev	pptn-a	stdev
50	103.22	16.13	24.63	18.06	109.47	6.98	431.19	32.55	15.21	3.79
100*	87.68	25.07	13.63	9.67	57.12	24.09	266.15	153.93	30.60	10.60
150	82.41	0.22	60.59	41.76	15.23	3.36	51.37	3.05	17.72	2.23
300	10.66	1.40	36.85	18.62	19.33	4.18	8.72	4.22	44.02	24.95

Table 29: Pigment to POC ratios of Niskin bottle samples collected during BaRFlux 2 cruise.
*Indicates Chlorophyll maximum

pigment/POC

depth	ppb-a	stdev	pyro-a	stdev
50	4.70×10^{-4}	7.35×10^{-5}	1.12×10^{-4}	8.23×10^{-5}
100*	4.17×10^{-4}	1.19×10^{-4}	6.48×10^{-5}	4.59×10^{-5}
150	–	–	–	–
300	–	–	–	–

Table 30: Pigment to POC ratios of Niskin bottle samples collected during BaRFlux 2 cruise.
*Indicates Chlorophyll maximum

pigment/POC contd.

depth	chl-b	stdev	chl-a	stdev	pptn-a	stdev
50	4.99×10^{-4}	3.18×10^{-5}	1.96×10^{-3}	1.48×10^{-4}	6.94×10^{-5}	1.73×10^{-5}
100*	2.71×10^{-4}	1.14×10^{-4}	1.26×10^{-3}	7.31×10^{-4}	1.45×10^{-4}	5.03×10^{-5}
150	–	–	–	–	–	–
300	–	–	–	–	–	–

B.3 Cruise 3 Samples

B.3.1 In-situ Pump Samples

Table 31: Mole percent pigment compositions of in-situ pump samples collected on 1-μm filters during BaRFlux cruise 3. Depth is in meters.

1-μm filters

depth	ppb-a	stdev	pyro-a	stdev	chl-b	stdev	chl-a	stdev	pptn-a	stdev
100	44.31	13.24	3.64	6.21	10.44	4.10	41.59	14.03	0.01	0.03
300	24.43	19.97	29.84	14.46	15.17	12.68	30.56	20.67	ND	ND
1000	16.85	20.66	16.77	20.56	19.77	32.57	45.52	44.52	1.09	1.03
1500	35.67	11.34	32.48	10.93	3.56	2.12	9.76	9.44	18.53	5.61
2000	22.91	16.73	31.99	22.24	6.07	6.63	32.31	36.94	6.72	8.40
3500	9.88	13.97	4.81	6.81	ND	ND	68.02	45.22	17.28	24.44
4000	ND	ND	ND	ND	ND	ND	100	ND	ND	ND
4200	9.96	14.09	ND	ND	4.07	5.75	70.29	42.02	15.69	22.18

Table 32: Pigment concentrations of in-situ pump samples collected on 1-μm filters during BaRFlux cruise 3 in ng/L. Depth is in meters.

ng/L

depth	ppb-a	stdev	pyro-a	stdev	chl-b	stdev	chl-a	stdev	pptn-a	stdev
100	73.02	69.50	14.49	25.01	34.50	43.11	82.03	63.15	0.02	0.05
300	4.34	4.46	4.12	3.28	1.62	1.00	3.67	1.19	ND	ND
1000	5.16	6.41	4.61	5.66	2.64	2.46	1.78	1.38	0.28	0.27
1500	0.57	0.40	0.46	0.25	0.09	0.06	0.15	0.07	0.35	0.06
2000	0.58	0.79	0.59	0.61	0.19	0.28	0.27	0.11	0.15	0.18
3500	0.16	0.22	0.07	0.10	ND	ND	0.34	0.17	0.41	0.58
4000	ND	ND	ND	ND	ND	ND	0.29	0.12	ND	ND
4200	0.06	0.08	ND	ND	0.04	0.05	0.24	0.11	0.13	0.19

B.3.2 Niskin Bottle

Table 33: Pigment to POC ratios of in-situ pump samples collected during BaRFlux 3 cruise on 1-μm filters. Depth is in meters

pigment/POC

depth	ppb-a	stdev	pyro-a	stdev
100	6.99×10^{-3}	6.65×10^{-3}	1.39×10^{-3}	2.39×10^{-3}
300	8.31×10^{-3}	8.18×10^{-3}	2.16×10^{-3}	2.61×10^{-3}
1000	2.77×10^{-3}	3.44×10^{-3}	2.47×10^{-3}	3.04×10^{-3}
1500	3.95×10^{-4}	2.74×10^{-4}	3.14×10^{-4}	1.69×10^{-4}
2000	5.09×10^{-4}	6.93×10^{-4}	5.18×10^{-4}	5.29×10^{-4}
3500	1.43×10^{-4}	2.03×10^{-4}	6.30×10^{-5}	8.92×10^{-5}
4000	ND	ND	ND	ND
4200	6.23×10^{-5}	8.81×10^{-5}	ND	ND

Table 34: Pigment to POC ratios of in-situ pump samples collected during BaRFlux 3 cruise on 1-μm filters. Depth is in meters

pigment/POC contd.

depth	chl-b	stdev	chl-a	stdev	pptn-a	stdev
100	3.30×10^{-3}	4.13×10^{-3}	7.85×10^{-3}	6.04×10^{-3}	1.97×10^{-6}	5.20×10^{-6}
300	4.06×10^{-3}	4.60×10^{-3}	7.76×10^{-3}	7.50×10^{-3}	3.46×10^{-5}	6.91×10^{-5}
1000	1.42×10^{-3}	1.32×10^{-3}	9.57×10^{-4}	7.39×10^{-4}	1.52×10^{-4}	1.47×10^{-4}
1500	6.37×10^{-5}	3.89×10^{-5}	1.02×10^{-4}	4.91×10^{-5}	2.43×10^{-4}	4.14×10^{-5}
2000	1.66×10^{-4}	2.42×10^{-4}	2.40×10^{-4}	9.98×10^{-5}	1.33×10^{-4}	1.56×10^{-4}
3500	ND	ND	3.10×10^{-4}	1.56×10^{-4}	3.69×10^{-4}	5.22×10^{-4}
4000	ND	ND	1.90×10^{-4}	7.75×10^{-5}	ND	ND
4200	3.90×10^{-5}	5.51×10^{-5}	2.70×10^{-4}	1.23×10^{-4}	1.44×10^{-4}	2.04×10^{-4}

Table 35: Mole percent pigment compositions of in-situ pump samples collected on 70-μm filters during BaRFlux cruise 3. Depth is in meters.

70-μm filters

depth	ppb-a	stdev	pyro-a	stdev	chl-b	stdev	chl-a	stdev	pptn-a	stdev
100	27.58	ND	44.11	ND	9.17	ND	19.14	ND	ND	ND
300	20.81	5.91	38.57	29.27	ND	ND	20.19	18.90	20.43	4.47
1000	56.14	6.83	12.08	12.08	ND	ND	8.33	2.83	23.45	8.09
1500	16.79	ND	35.50	ND	ND	ND	4.96	ND	42.75	ND
2000	30.11	19.20	23.17	3.27	ND	ND	13.65	7.78	33.07	14.69
3500	ND	ND	96.17	2.66	ND	ND	1.15	0.78	2.67	1.88
4000	66.82	ND	ND	ND	ND	ND	10.79	ND	22.40	ND
4200	43.77	ND	21.91	ND	ND	ND	11.69	ND	22.63	ND

Table 36: Pigment concentrations of in-situ pump samples collected on 70-μm filters during BaRFlux cruise 3 in ng/L. Depth is in meters.

ng/L

depth	ppb-a	stdev	pyro-a	stdev	chl-b	stdev	chl-a	stdev	pptn-a	stdev
100	3.55	ND	5.13	ND	1.81	ND	3.72	ND	ND	ND
300	0.03	0.01	0.05	0.04	ND	ND	0.04	0.03	0.04	0.01
1000	0.06	0.03	0.02	0.02	ND	ND	0.02	0.01	0.03	0.01
1500	0.02	ND	0.03	ND	ND	ND	0.01	ND	0.06	ND
2000	0.04	0.04	0.02	0.02	ND	ND	0.02	0.00	0.04	0.00
3500	ND	ND	20.43	16.55	ND	ND	0.65	0.63	1.49	1.44
4000	0.09	ND	ND	ND	ND	ND	0.02	ND	0.05	ND
4200	0.06	ND	0.03	ND	ND	ND	0.02	ND	0.04	ND

Table 37: Pigment to POC ratios of in-situ pump samples collected during BaRFlux 3 cruise on 70-μm filters. Depth is in meters

pigment/POC

depth	ppb-a	stdev	pyro-a	stdev
100	4.12×10^{-3}	ND	5.95×10^{-3}	ND
300	1.42×10^{-4}	2.89×10^{-5}	2.58×10^{-4}	2.05×10^{-4}
1000	2.32×10^{-4}	1.10×10^{-4}	7.55×10^{-5}	7.55×10^{-5}
1500	1.23×10^{-4}	ND	2.34×10^{-4}	ND
2000	2.84×10^{-4}	2.48×10^{-4}	1.59×10^{-4}	9.85×10^{-5}
3500	ND	ND	3.55×10^{-2}	ND
4000	6.00×10^{-4}	ND	ND	ND
4200	1.86×10^{-4}	ND	8.41×10^{-5}	ND

Table 38: Pigment to POC ratios of in-situ pump samples collected during BaRFlux 3 cruise on 70-μm filters. Depth is in meters

pigment/POC contd.

depth	chl-b	stdev	chl-a	stdev	pptn-a	stdev
100	2.10×10^{-3}	ND	4.32×10^{-3}	ND	ND	ND
300	ND	ND	1.96×10^{-4}	1.81×10^{-4}	2.06×10^{-4}	2.81×10^{-5}
1000	ND	ND	6.62×10^{-5}	5.02×10^{-5}	1.23×10^{-4}	3.33×10^{-5}
1500	ND	ND	5.46×10^{-5}	ND	4.59×10^{-4}	ND
2000	ND	ND	1.02×10^{-4}	6.47×10^{-6}	2.63×10^{-4}	2.79×10^{-5}
3500	ND	ND	2.27×10^{-4}	ND	4.65×10^{-4}	ND
4000	ND	ND	1.46×10^{-4}	ND	2.96×10^{-4}	ND
4200	ND	ND	7.50×10^{-5}	ND	1.42×10^{-4}	ND

Table 39: Mole percent pigment compositions of Niskin bottle samples collected during BaRFlux cruise 3. Depth is in meters.
*Indicates Chlorophyll maximum

depth	ppb-a	stdev	pyro-a	stdev	chl-b	stdev	chl-a	stdev	pptn-a	stdev
50	20.81	26.39	0	ND	2.17	2.01	77.02	26.93	ND	0
100	17.29	17.29	0	ND	10.25	0.63	72.46	17.92	ND	0
107*	33.01	26.97	0	ND	10.53	4.36	56.46	22.68	ND	0
200	32.92	46.56	0	ND	4.49	6.13	62.58	43.94	ND	0
500	ND	ND	0	ND	0	ND	33.33	47.14	ND	0
800	ND	ND	0	ND	9.63	9.63	90.37	9.63	ND	0
1250	ND	ND	0	ND	0	ND	0	ND	ND	0
1750	ND	ND	0	ND	0	ND	0	ND	ND	0
2500	ND	ND	0	ND	0	ND	0	ND	ND	0
3000	ND	ND	0	ND	0	ND	0	ND	ND	0
3500	ND	ND	0	ND	0	ND	100	ND	ND	0
4000	ND	ND	0	ND	0	ND	0	ND	ND	0
4300	ND	ND	0	ND	0	ND	0	ND	ND	0
4430	ND	ND	0	ND	0	ND	100	ND	ND	0

Table 40: Pigment concentrations of Niskin bottle samples collected during BaRFlux cruise 3 in ng/L. Depth is in meters.
*Indicates Chlorophyll maximum

ng/L

depth	ppb-a	stdev	pyro-a	stdev	chl-b	stdev	chl-a	stdev	pptn-a	stdev
50	90.85	131.12	ND	ND	8.95	7.58	206.67	51.46	ND	ND
100	1950.73	1950.73	ND	ND	1412.36	468.18	9003.80	274.54	ND	ND
107*	520.38	425.63	ND	ND	177.63	17.63	947.31	146.22	ND	ND
200	37.72	53.34	ND	ND	0.93	0.95	6.53	5.68	ND	ND
500	ND	ND	ND	ND	ND	ND	0.21	0.30	ND	ND
800	ND	ND	ND	ND	1.06	1.06	4.54	4.20	ND	ND
1250	ND	ND	ND	ND	ND	ND	ND	ND	ND	ND
1750	ND	ND	ND	ND	ND	ND	ND	ND	ND	ND
2500	ND	ND	ND	ND	ND	ND	ND	ND	ND	ND
3000	ND	ND	ND	ND	ND	ND	ND	ND	ND	ND
3500	ND	ND	ND	ND	ND	ND	0.17	ND	ND	ND
4000	ND	ND	ND	ND	ND	ND	ND	ND	ND	ND
4300	ND	ND	ND	ND	ND	ND	ND	ND	ND	ND
4430	ND	ND	ND	ND	ND	ND	0.62	ND	ND	ND

Table 41: Pigment to POC ratios of Niskin bottle samples collected during BaRFlux 3 cruise. Depth is in meters
*Indicates Chlorophyll maximum

pigment/POC

depth	ppb-a	stdev	pyro-a	stdev
50	8.72×10^{-4}	1.23×10^{-3}	ND	ND
100	–	–	–	–
107	–	–	–	–
200	1.53×10^{-3}	2.16×10^{-3}	ND	ND
500	ND	ND	ND	ND
800	ND	ND	ND	ND
1250	ND	ND	ND	ND
1750	ND	ND	ND	ND
2500	–	–	–	–
3000	ND	ND	ND	ND
3500	ND	ND	ND	ND
4000	ND	ND	ND	ND
4300	ND	ND	ND	ND
4430	ND	ND	ND	ND

Table 42: Pigment to POC ratios of Niskin bottle samples collected during BaRFlux 3 cruise. Depth is in meters.
*Indicates Chlorophyll maximum

pigment/POC contd.

depth	chl-b	stdev	chl-a	stdev	pptn-a	stdev
50	8.69×10^{-5}	7.47×10^{-5}	2.01×10^{-3}	4.86×10^{-4}	ND	ND
100	–	–	–	–	–	–
107	–	–	–	–	–	–
200	3.40×10^{-5}	3.32×10^{-5}	2.41×10^{-4}	1.96×10^{-4}	ND	ND
500	ND	ND	8.77×10^{-6}	1.24×10^{-5}	ND	ND
800	4.83×10^{-5}	4.83×10^{-5}	2.06×10^{-4}	1.92×10^{-4}	ND	ND
1250	ND	ND	ND	ND	ND	ND
1750	ND	ND	ND	ND	ND	ND
2500	–	–	–	–	–	–
3000	ND	ND	ND	ND	ND	ND
3500	ND	ND	8.49×10^{-6}	ND	ND	ND
4000	ND	ND	ND	ND	ND	ND
4300	ND	ND	ND	ND	ND	ND
4430	ND	ND	2.43×10^{-5}	ND	ND	ND

B.3.3 Sediment Traps

Table 43: Pigment mole percentages from settling velocity 1500 m IRS sediment trap recovered during BaRFlux 3 cruise. Depth is in meters. SV is settling velocity in m d^{-1}.

Settling Velocity Trap, 1500 m

sv	ppb-a	stdev	pyro-a	stdev	chl-b	stdev	chl-a	stdev	pptn-a	stdev
10.20	31.77	ND	65.64	ND	1.79	ND	0.80	ND	ND	ND
15.30	36.20	ND	60.62	ND	2.16	ND	1.02	ND	ND	ND
122.40	20.69	20.69	75.97	19.67	2.85	1.12	0.48	0.44	ND	ND
244.80	17.37	12.28	71.52	4.44	8.33	5.89	2.50	2.15	0.29	0.21
489.60	ND	ND	77.42	6.36	16.34	5.34	6.25	1.03	ND	ND

Table 44: Pigment(μg) to POC(μg) ratios from settling velocity 1500 m IRS sediment trap recovered during BaRFlux 3 cruise. Depth is in meters. SV is settling velocity in m d^{-1}.

pigment/POC

sv	ppb-a	stdev	pyro-a	stdev
10.20	9.69×10^{-4}	ND	1.81×10^{-3}	ND
15.30	1.09×10^{-3}	ND	1.65×10^{-3}	ND
122.40	4.96×10^{-4}	4.96×10^{-4}	1.49×10^{-3}	2.74×10^{-4}
244.80	6.02×10^{-4}	4.25×10^{-4}	1.61×10^{-3}	7.45×10^{-4}
489.60	ND	ND	6.06×10^{-4}	1.50×10^{-4}

Table 45: Pigment(μg) to POC(μg) ratios from settling velocity 1500 m IRS sediment trap recovered during BaRFlux 3 cruise. Depth is in meters. SV is settling velocity in m d^{-1}.

pigment/POC contd.

sv	chl-b	stdev	chl-a	stdev	pptn-a	stdev
10.20	8.35 x 10^{-5}	ND	3.70 x 10^{-5}	ND	ND	ND
15.30	9.94 x 10^{-5}	ND	4.65 x 10^{-5}	ND	ND	ND
122.40	9.64 x 10^{-5}	3.65 x 10^{-5}	1.49 x 10^{-5}	1.34 x 10^{-5}	ND	ND
244.80	2.14 x 10^{-4}	8.70 x 10^{-6}	5.60 x 10^{-5}	7.21 x 10^{-6}	1.50 x 10^{-5}	1.06 x 10^{-5}
489.60	2.02 x 10^{-4}	3.38 x 10^{-5}	7.84 x 10^{-5}	3.50 x 10^{-7}	ND	ND

Table 46: Pigment mole percentages from time series 300 m IRS sediment trap recovered during BaRFlux 3 cruise. Depth is in meters. Dates are for 2012.

Time Series Trap, 300 m

date	ppb-a	stdev	pyro-a	stdev	chl-b	stdev	chl-a	stdev	pptn-a	stdev
18-Feb	28.20	0.62	71.04	0.65	0.32	0.01	0.44	0.02	ND	ND
25-Feb	ND	ND	96.68	0.91	2.58	0.93	0.75	0.26	ND	ND
24-Mar	ND	ND	95.90	4.54	3.33	4.24	0.77	0.30	ND	ND
7-Apr	ND	ND	98.12	0.20	1.30	0.20	0.58	ND	ND	ND
14-Apr	ND	ND	98.95	0.07	0.54	0.08	0.52	0.01	ND	ND
21-Apr	31.98	2.70	61.98	3.63	4.71	0.69	1.07	0.02	0.25	0.25

Table 47: Pigment fluxes from time series 300 m IRS sediment trap recovered during BaRFlux 3 cruise. Depth is in meters. Dates are for 2012. Fluxes measured in μg m^{-2} d^{-1}.

date	ppb-a	stdev	pyro-a	stdev	chl-b	stdev	chl-a	stdev	pptn-a	stdev
18-Feb	104.98	0.36	0.18	0.01	238.72	8.27	0.45	0.02	1.84	0.02
25-Feb	ND	ND	ND	ND	729.84	34.59	1.37	0.07	5.31	3.08
24-Mar	ND	ND	ND	ND	1066.63	110.46	2.00	0.21	75.18	98.64
7-Apr	ND	ND	ND	ND	3026.99	20.98	5.66	0.04	68.17	9.99
14-Apr	ND	ND	ND	ND	1060.84	50.80	1.98	0.10	9.71	1.02
21-Apr	133.50	12.92	0.23	0.02	232.97	10.79	0.44	0.02	30.13	4.78

Table 48: Pigment to POC ratios from time series 300 m IRS sediment trap recovered during BaRFlux 3 cruise. Depth is in meters. Dates are for 2012.

pigment/POC

date	ppb-a	stdev	pyro-a	stdev
18-Feb	2.25×10^{-4}	7.66×10^{-7}	5.13×10^{-4}	1.78×10^{-5}
25-Feb	ND	ND	6.53×10^{-4}	3.04×10^{-5}
24-Mar	ND	ND	2.89×10^{-4}	3.00×10^{-5}
7-Apr	–	–	–	–
14-Apr	ND	ND	2.21×10^{-4}	1.06×10^{-5}
21-Apr	6.84×10^{-5}	6.60×10^{-6}	1.19×10^{-4}	5.53×10^{-6}

Table 49: Pigment to POC ratios from time series 300 m IRS sediment trap recovered during BaRFlux 3 cruise. Depth is in meters. Dates are for 2012.

pigment/POC contd.

date	chl-b	stdev	chl-a	stdev	pptn-a	stdev
18-Feb	3.96×10^{-6}	5.50×10^{-8}	5.25×10^{-6}	1.00×10^{-7}	ND	ND
25-Feb	4.07×10^{-6}	2.44×10^{-6}	5.44×10^{-6}	2.71×10^{-6}	ND	ND
24-Mar	2.04×10^{-5}	2.68×10^{-5}	4.14×10^{-6}	2.27×10^{-6}	ND	ND
7-Apr	–	–	–	–	–	–
14-Apr	2.03×10^{-6}	2.15×10^{-7}	1.94×10^{-6}	1.35×10^{-7}	ND	ND
21-Apr	1.55×10^{-5}	2.45×10^{-6}	3.45×10^{-6}	1.00×10^{-8}	8.10×10^{-7}	8.10×10^{-7}

B.4 Cruise 4 Samples

B.4.1 In-situ Pump Samples

Table 50: Mole percent pigment compositions of in-situ pump samples collected on 1-μm filters during BaRFlux cruise 4. Depth is in meters.

1-μm filters

depth	ppb-a	stdev	pyro-a	stdev	chl-b	stdev	chl-a	stdev	pptn-a	stdev
300	12.97	14.84	23.10	26.39	23.16	24.65	34.61	29.28	6.17	8.11
1000	23.25	18.57	57.02	29.60	3.64	5.98	7.69	4.30	8.39	10.86
1500	52.09	31.81	30.71	20.57	1.25	1.98	3.14	1.21	12.82	15.69
2000	28.74	30.48	16.61	20.19	2.24	5.06	33.16	38.91	19.25	28.01
3500	7.38	10.50	25.50	33.45	4.29	8.24	32.76	42.62	30.08	35.59
4000	11.60	16.76	53.94	36.75	1.46	4.08	23.22	32.04	9.78	12.01
4200	19.85	20.04	39.82	30.17	0.58	1.73	7.48	4.29	32.27	36.21

Table 51: Pigment oncentrations of in-situ pump samples collected on 1-μm filters during BaRFlux cruise 4 in ng/L. Depth is in meters.

ng/L

depth	ppb-a	stdev	pyro-a	stdev	chl-b	stdev	chl-a	stdev	pptn-a	stdev
300	12.62	16.99	26.11	44.47	10.80	14.21	13.21	8.53	5.97	6.28
1000	1.33	1.81	2.89	1.89	0.21	0.22	0.41	0.10	0.28	0.22
1500	3.44	2.81	1.75	2.20	0.04	0.06	0.28	0.20	0.36	0.46
2000	2.22	2.99	1.56	2.99	0.13	0.29	0.64	0.26	0.84	1.28
3500	0.74	1.47	1.63	2.15	0.73	1.71	1.68	1.97	1.86	2.75
4000	0.14	0.24	1.74	1.88	0.04	0.11	0.29	0.11	0.15	0.19
4200	0.95	1.73	1.20	1.29	0.08	0.03	0.24	0.06	1.87	3.51

B.4.2 Niskin Bottle

B.4.3 Syringe sub-core

Table 52: Pigment to POC ratios of in-situ pump samples collected during BaRFlux 4 cruise on 1-μm filters. Depth is in meters.

pigment/POC

depth	ppb-a	stdev	pyro-a	stdev
300	3.70×10^{-3}	2.83×10^{-3}	2.05×10^{-2}	3.03×10^{-2}
1000	4.01×10^{-2}	5.47×10^{-2}	8.71×10^{-2}	5.70×10^{-2}
1500	1.26×10^{-1}	1.03×10^{-1}	6.38×10^{-2}	8.01×10^{-2}
2000	4.80×10^{-2}	6.58×10^{-2}	3.36×10^{-2}	6.56×10^{-2}
3500	3.64×10^{-2}	4.83×10^{-2}	3.77×10^{-2}	7.38×10^{-2}
4000	5.09×10^{-3}	8.47×10^{-3}	6.38×10^{-2}	6.93×10^{-2}
4200	2.42×10^{-2}	4.37×10^{-2}	3.21×10^{-2}	3.41×10^{-2}

Table 53: Pigment to POC ratios of in-situ pump samples collected during BaRFlux 4 cruise on 1-μm filters. Depth is in meters.

pigment/POC contd.

depth	chl-b	stdev	chl-a	stdev	pptn-a	stdev
300	3.58×10^{-4}	3.83×10^{-4}	6.65×10^{-3}	5.59×10^{-3}	4.62×10^{-3}	9.59×10^{-3}
1000	6.31×10^{-3}	6.68×10^{-3}	1.25×10^{-2}	3.05×10^{-3}	8.41×10^{-3}	6.56×10^{-3}
1500	1.41×10^{-3}	2.23×10^{-3}	1.04×10^{-2}	7.16×10^{-3}	1.32×10^{-2}	1.68×10^{-2}
2000	2.35×10^{-3}	5.31×10^{-3}	1.25×10^{-2}	6.93×10^{-3}	1.35×10^{-2}	1.93×10^{-2}
3500	4.18×10^{-3}	7.29×10^{-3}	1.06×10^{-2}	7.44×10^{-3}	2.87×10^{-2}	4.54×10^{-2}
4000	1.34×10^{-3}	4.11×10^{-3}	1.07×10^{-2}	4.22×10^{-3}	5.47×10^{-3}	7.24×10^{-3}
4200	2.10×10^{-4}	6.29×10^{-4}	6.61×10^{-3}	1.61×10^{-3}	5.36×10^{-2}	1.02×10^{-1}

Table 54: Mole percent pigment compositions of in-situ pump samples collected on 70-μ filters during BaRFlux cruise 4. Depth is in meters.

70-μm filters

depth	ppb-a	stdev	pyro-a	stdev	chl-b	stdev	chl-a	stdev	pptn-a	stdev
100	ND	ND	76.35	0.74	4.68	0.66	9.85	0.12	9.12	0.04
300	ND	ND	48.12	48.12	ND	ND	51.88	48.12	ND	ND
1000	ND	ND	ND	ND	ND	ND	100	ND	ND	ND
1500	ND	ND	ND	ND	ND	ND	100	ND	ND	ND
2000	ND	ND	ND	ND	ND	ND	100	ND	ND	ND
3500	ND	ND	ND	ND	ND	ND	100	ND	ND	ND
4000	ND	ND	ND	ND	ND	ND	100	ND	ND	ND
4200	ND	ND	ND	ND	ND	ND	ND	ND	ND	ND

Table 55: Pigment oncentrations of in-situ pump samples collected on 70-μm filters during BaRFlux cruise 4 in ng/L. Depth is in meters.

ng/L

depth	ppb-a	stdev	pyro-a	stdev	chl-b	stdev	chl-a	stdev	pptn-a	stdev
100	ND	ND	14.11	0.31	1.46	0.19	3.04	ND	2.75	0.05
300	ND	ND	22.42	22.48	ND	ND	1.47	1.49	ND	ND
1000	ND	ND	ND	ND	ND	ND	0.04	0.03	ND	ND
1500	ND	ND	ND	ND	ND	ND	0.05	ND	ND	ND
2000	ND	ND	ND	ND	ND	ND	0.05	0.07	ND	ND
3500	ND	ND	ND	ND	ND	ND	0.14	0.11	ND	ND
4000	ND	ND	ND	ND	ND	ND	0.03	0.08	ND	ND
4200	ND	ND	ND	ND	ND	ND	ND	ND	ND	ND

Table 56: Pigment to POC ratios of in-situ pump samples collected during BaRFlux 4 cruise on 70-μm filters. Depth is in meters.

pigment/POC

depth	ppb-a	stdev	pyro-a	stdev
100	ND	ND	1.54×10^{-2}	3.39×10^{-4}
300	ND	ND	7.85×10^{-3}	7.85×10^{-3}
1000	ND	ND	ND	ND
1500	ND	ND	ND	ND
2000	ND	ND	ND	ND
3500	ND	ND	ND	ND
4000	ND	ND	ND	ND
4200	ND	ND	ND	ND

Table 57: Pigment to POC ratios of in-situ pump samples collected during BaRFlux 4 cruise on 70-μm filters. Depth is in meters.

pigment/POC contd.

depth	chl-b	stdev	chl-a	stdev	pptn-a	stdev
100	1.59×10^{-3}	2.06×10^{-4}	3.31×10^{-3}	4.99×10^{-7}	2.99×10^{-3}	5.18×10^{-5}
300	6.94×10^{-4}	6.94×10^{-4}	1.67×10^{-3}	1.65×10^{-3}	1.52×10^{-3}	1.52×10^{-3}
1000	ND	ND	8.31×10^{-5}	7.20×10^{-6}	ND	ND
1500	ND	ND	2.32×10^{-5}	1.69×10^{-6}	ND	ND
2000	ND	ND	6.45×10^{-5}	8.54×10^{-6}	ND	ND
3500	ND	ND	4.49×10^{-5}	1.33×10^{-5}	ND	ND
4000	ND	ND	1.28×10^{-4}	3.70×10^{-5}	ND	ND
4200	ND	ND	ND	ND	ND	ND

Table 58: Mole percent pigment compositions of Niskin bottle samples collected during BaRFlux cruise 4. Depth is in meters.
*Indicates Chlorophyll maximum

depth	ppb-a	stdev	pyro-a	stdev	chl-b	stdev	chl-a	stdev	pptn-a	stdev
50	10.25	11.05	25.25	25.83	6.90	1.91	57.59	36.96	ND	ND
68*	32.89	23.50	ND	ND	9.34	2.98	57.78	20.52	ND	ND
75	9.80	13.86	ND	ND	24.10	11.27	65.62	2.34	0.48	0.68
100	36.70	25.97	1.89	2.67	23.12	32.65	38.29	16.03	ND	ND
200	ND	ND	ND	ND	ND	ND	33.33	47.14	ND	ND
300	5.22	9.05	63.40	37.33	1.83	3.17	29.55	40.68	ND	ND
500	ND	ND	44.93	44.94	2.05	3.55	53.02	47.03	ND	ND
800	ND	ND	46.38	46.51	2.18	3.77	1.44	1.49	ND	ND
1000	49.81	49.81	ND	ND	ND	ND	50.19	49.81	ND	ND
1500	ND	ND	ND	ND	50	50	ND	ND	ND	ND
1750	ND	ND	ND	ND	13.54	19.16	86.46	19.16	ND	ND
2000	ND	ND	ND	ND	ND	ND	100	ND	ND	ND
2500	ND	ND	ND	ND	ND	ND	33.33	47.14	ND	ND
3000	ND	ND	ND	ND	ND	ND	ND	ND	ND	ND
3500	ND	ND	ND	ND	ND	ND	ND	ND	ND	ND
4000	ND	ND	ND	ND	ND	ND	ND	ND	ND	ND
4200	ND	ND	ND	ND	ND	ND	ND	ND	ND	ND

Table 59: Pigment concentrations of Niskin bottle samples collected during BaRFlux cruise 4 in ng/L. Depth is in meters.
*Indicates Chlorophyll maximum

ng/L

depth	ppb-a	stdev	pyro-a	stdev	chl-b	stdev	chl-a	stdev	pptn-a	stdev
50	22.43	22.55	54.77	61.25	22.89	12.17	159.80	89.94	ND	ND
68*	480.47	342.08	ND	ND	122.26	57.64	727.44	336.83	ND	ND
75	206.96	292.68	ND	ND	344.75	57.02	1191.45	561.79	5.56	7.87
100	197.15	143.33	10.22	14.46	45.70	31.31	236.02	117.92	ND	ND
200	ND	ND	ND	ND	ND	ND	1.09	1.54	ND	ND
300	2.14	3.71	17.93	10.54	0.77	1.33	2.65	0.71	ND	ND
500	ND	ND	16.14	19.65	1.89	3.27	1.98	0.77	ND	ND
800	ND	ND	17.34	18.13	1.14	1.98	0.87	0.87	ND	ND
1000	55.33	55.33	ND	ND	ND	ND	0.75	0.10	ND	ND
1500	ND	ND	ND	ND	0.99	0.99	ND	ND	ND	ND
1750	ND	ND	ND	ND	0.25	0.35	0.85	0.21	ND	ND
2000	ND	ND	ND	ND	ND	ND	1.41	ND	ND	ND
2500	ND	ND	ND	ND	ND	ND	0.19	0.28	ND	ND
3000	ND	ND	ND	ND	ND	ND	ND	ND	ND	ND
3500	ND	ND	ND	ND	ND	ND	ND	ND	ND	ND
4000	ND	ND	ND	ND	ND	ND	ND	ND	ND	ND
4200	ND	ND	ND	ND	ND	ND	ND	ND	ND	ND

Table 60: Pigment to POC ratios of Niskin bottle samples collected during BaRFlux 4 cruise. Depth is in meters.
*Indicates Chlorophyll maximum

pigment/POC

depth	ppb-a	stdev	pyro-a	stdev
50	4.54×10^{-4}	4.56×10^{-4}	1.11×10^{-3}	1.24×10^{-3}
68	3.62×10^{-5}	2.58×10^{-5}	ND	ND
75	3.36×10^{-3}	4.75×10^{-3}	ND	ND
100	4.93×10^{-3}	3.59×10^{-3}	2.56×10^{-4}	3.62×10^{-4}
200	–	–	–	–
300	6.45×10^{-5}	1.12×10^{-4}	5.39×10^{-4}	3.17×10^{-4}
500	ND	ND	3.88×10^{-4}	4.72×10^{-4}
800	ND	ND	4.67×10^{-4}	4.88×10^{-4}
1000	1.52×10^{-3}	1.52×10^{-3}	ND	ND
1500	–	–	–	–
1750	–	–	–	–
2000	–	–	–	–
2500	ND	ND	ND	ND
3000	ND	ND	ND	ND
3500	ND	ND	ND	ND
4000	ND	ND	ND	ND
4200	ND	ND	ND	ND

Table 61: Pigment to POC ratios of Niskin bottle samples collected during BaRFlux 4 cruise. Depth is in meters.
*Indicates Chlorophyll maximum.

pigment/POC contd.

depth	chl-b	stdev	chl-a	stdev	pptn-a	stdev
50	4.63×10^{-4}	2.46×10^{-4}	3.23×10^{-3}	1.82×10^{-3}	ND	ND
68	9.22×10^{-6}	4.35×10^{-6}	5.48×10^{-5}	2.54×10^{-5}	ND	ND
75	5.59×10^{-3}	9.25×10^{-4}	1.93×10^{-2}	9.11×10^{-3}	9.02×10^{-5}	1.28×10^{-4}
100	1.14×10^{-3}	7.83×10^{-4}	5.91×10^{-3}	2.95×10^{-3}	ND	ND
200	–	–	–	–	–	–
300	2.32×10^{-5}	4.01×10^{-5}	7.96×10^{-5}	2.12×10^{-5}	ND	ND
500	4.53×10^{-5}	7.85×10^{-5}	4.75×10^{-5}	1.86×10^{-5}	ND	ND
800	3.07×10^{-5}	5.33×10^{-5}	2.34×10^{-5}	2.34×10^{-5}	ND	ND
1000	ND	ND	2.07×10^{-5}	2.80×10^{-6}	ND	ND
1500	–	–	–	–	–	–
1750	–	–	–	–	–	–
2000	–	–	–	–	–	–
2500	ND	ND	5.53×10^{-6}	7.83×10^{-6}	ND	ND
3000	ND	ND	ND	ND	ND	ND
3500	ND	ND	ND	ND	ND	ND
4000	ND	ND	ND	ND	ND	ND
4200	ND	ND	ND	ND	ND	ND

Table 62: Pigment mole percentages from syringe box core collected during BaRFlux 4 cruise. Depth is in cm.

depth	ppb-a	stdev	pyro-a	stdev	chl-b	stdev	chl-a	stdev	pptn-a	stdev
0.0-0.5	99.89	0.13	ND	ND	ND	ND	0.11	0.13	ND	ND
0.5-1.0	99.69	0.06	ND	ND	ND	ND	0.31	0.06	ND	ND
1.0-2.0	100	ND	ND	ND	ND	ND	ND	ND	ND	ND
2.0-3.0	33.33	47.14	ND	ND	ND	ND	ND	ND	ND	ND
3.0-4.0	ND	ND	ND	ND	ND	ND	ND	ND	ND	ND
4.0-5.0	ND	ND	ND	ND	ND	ND	ND	ND	ND	ND

Table 63: Mass pigment to sediment ratio from syringe box core collected during BaRFlux 4 cruise. Depth is in cm.

ng pigment/g sediment

depth	ppb-a	stdev	pyro-a	stdev	chl-b	stdev	chl-a	stdev	pptn-a	stdev
0.0-0.5	68.57	66.86	ND	ND	ND	ND	0.08	0.06	ND	ND
0.5-1.0	86.74	14.17	ND	ND	ND	ND	0.40	0.03	ND	ND
1.0-2.0	54.37	16.07	ND	ND	ND	ND	ND	ND	ND	ND
2.0-3.0	14.26	20.17	ND	ND	ND	ND	ND	ND	ND	ND
3.0-4.0	ND	ND	ND	ND	ND	ND	ND	ND	ND	ND
4.0-5.0	ND	ND	ND	ND	ND	ND	ND	ND	ND	ND

B.5 Cruise 5 Samples

B.5.1 Niskin Bottle

Table 64: Mole percent pigment compositions of Niskin bottle samples collected during BaRFlux cruise 5. Depth is in meters.
*Indicates Chlorophyll maximum

depth	ppb-a	stdev	pyro-a	stdev	chl-b	stdev	chl-a	stdev	pptn-a	stdev
50	31.94	ND	ND	ND	2.81	ND	65.24	ND	ND	ND
75*	21.59	21.59	ND	ND	6.02	1.72	72.39	19.87	ND	ND
100	27.91	4.43	ND	ND	9.70	1.23	56.58	3.44	5.82	4.16
200	ND	ND	ND	ND	ND	ND	100	ND	ND	ND
300	ND	ND	ND	ND	ND	ND	100	ND	ND	ND
500	ND	ND	ND	ND	ND	ND	ND	ND	ND	ND
1000	ND	ND	ND	ND	ND	ND	ND	ND	ND	ND
2000	ND	ND	ND	ND	ND	ND	ND	ND	ND	ND
4200	ND	ND	ND	ND	ND	ND	ND	ND	ND	ND

Table 65: Piigment concentrations of Niskin bottle samples collected during BaRFlux cruise 5. Depth is in meters.
*Indicates Chlorophyll maximum

ng/L

depth	ppb-a	stdev	pyro-a	stdev	chl-b	stdev	chl-a	stdev	pptn-a	stdev
50	127.18	ND	ND	ND	17.16	ND	391.63	ND	ND	ND
75	1857.12	1857.12	ND	ND	292.17	274.09	3511.41	3299.20	ND	ND
100	471.35	410.94	ND	ND	260.50	235.28	1790.60	1853.42	247.52	300.88
200	ND	ND	ND	ND	ND	ND	4.62	ND	ND	ND
300	ND	ND	ND	ND	ND	ND	0.591	ND	ND	ND
500	ND	ND	ND	ND	ND	ND	ND	ND	ND	ND
1000	ND	ND	ND	ND	ND	ND	ND	ND	ND	ND
2000	ND	ND	ND	ND	ND	ND	ND	ND	ND	ND
4200	ND	ND	ND	ND	ND	ND	ND	ND	ND	ND

Table 66: Pigment to POC ratios of Niskin bottle samples collected during BaRFlux 5 cruise. Depth is in meters.
*Indicates Chlorophyll maximum

pigment/POC

depth	ppb-a	stdev	pyro-a	stdev
50	2.57×10^{-3}	ND	ND	ND
75	3.20×10^{-2}	3.20×10^{-2}	ND	ND
100	1.11×10^{-2}	9.71×10^{-3}	ND	ND
200	ND	ND	ND	ND
300	ND	ND	ND	ND
500	ND	ND	ND	ND
1000	ND	ND	ND	ND
2000	–	–	–	–
4200	ND	ND	ND	ND

Table 67: Pigment to POC ratios of Niskin bottle samples collected during BaRFlux 5 cruise. Depth is in meters.
*Indicates Chlorophyll maximum

pigment/POC contd.

depth	chl-b	stdev	chl-a	stdev	pptn-a	stdev
50	3.46×10^{-4}	ND	7.90×10^{-3}	ND	ND	ND
75	5.03×10^{-3}	4.72×10^{-3}	6.04×10^{-2}	5.68×10^{-2}	ND	ND
100	6.16×10^{-3}	5.56×10^{-3}	4.23×10^{-2}	4.38×10^{-2}	5.85×10^{-3}	7.11×10^{-3}
200	ND	ND	1.15×10^{-4}	ND	ND	ND
300	ND	ND	1.59×10^{-5}	ND	ND	ND
500	ND	ND	ND	ND	ND	ND
1000	ND	ND	ND	ND	ND	ND
2000	–	–	–	–	–	–
4200	ND	ND	ND	ND	ND	ND

B.6 Cruise 6 Samples

B.6.1 In-situ Pump Samples

Table 68: Mole percent pigment compositions of in-situ pump samples collected on 1-μm filters during BaRFlux cruise 6. Depth is in meters.

1-μm filters

depth	ppb-a	stdev	pyro-a	stdev	chl-b	stdev	chl-a	stdev	pptn-a	stdev
80	32.61	10.12	7.63	7.73	4.29	3.38	44.93	21.90	10.55	15.00
90	58.89	0.06	9.65	0.25	5.13	0.05	26.32	0.24	ND	ND
110	47.11	9.04	8.87	7.94	4.69	6.66	39.24	6.76	0.09	0.08
160	33.85	14.05	15.78	20.06	6.76	3.86	43.28	27.95	0.33	0.82
310	10.78	15.62	31.59	22.63	1.54	3.06	41.73	42.14	14.35	12.89
1000	18.85	26.16	17.98	21.60	7.03	16.68	54.56	42.35	1.59	3.89
1500	36.90	34.52	11.73	10.26	ND	ND	44.42	45.87	6.94	13.88
2000	27.24	31.37	25.99	27.36	1.07	3.03	43.73	48.26	1.97	5.57
2510	ND	ND	ND	ND	ND	ND	100	ND	ND	ND
3010	29.73	29.80	25.09	29.72	ND	ND	28.79	36.85	16.39	20.12
4010	51.62	37.67	14.62	13.92	5.46	12.20	28.30	40.25	ND	ND
4210	ND	ND	ND	ND	ND	ND	ND	ND	ND	ND

B.6.2 Niskin Bottle

Table 69: Pigment concentrations of in-situ pump samples collected on 1-μm filters during BaRFlux cruise 6 in ng/L. Depth is in meters.

ng/L

depth	ppb-a	stdev	pyro-a	stdev	chl-b	stdev	chl-a	stdev	pptn-a	stdev
80	28.21	18.78	3.76	4.02	5.11	5.85	60.65	44.30	7.42	10.09
90	513.48	30.81	76.02	6.63	68.59	4.81	345.82	17.97	ND	ND
110	140.08	91.21	10.85	6.68	29.71	37.67	170.38	134.60	0.21	0.21
160	24.74	18.04	14.78	21.53	6.57	5.59	25.92	25.23	0.10	0.24
310	5.60	8.16	7.29	9.76	0.16	0.17	0.76	0.69	5.16	7.09
1000	2.27	3.75	1.38	1.94	0.12	0.21	0.51	0.43	0.05	0.11
1500	8.47	10.75	2.11	2.53	ND	ND	0.41	0.15	0.10	0.20
2000	3.56	4.82	1.82	1.99	0.01	0.02	0.20	0.24	0.03	0.08
2510	ND	ND	ND	ND	ND	ND	0.45	ND	ND	ND
3010	2.72	4.76	1.30	1.63	ND	ND	0.18	0.10	0.18	0.25
4010	9.24	9.36	1.85	1.59	0.02	0.04	0.22	0.22	ND	ND
4210	ND	ND	ND	ND	ND	ND	ND	ND	ND	ND

Table 70: Pigment to POC ratios of in-situ pump samples collected during BaRFlux 6 cruise on 1-μm filter. Depth is in meters.

pigment/POC

depth	ppb-a	stdev	pyro-a	stdev
80	1.44×10^{-1}	9.62×10^{-2}	1.92×10^{-2}	2.06×10^{-2}
90	ND	ND	ND	ND
110	7.74×10^{-1}	5.04×10^{-1}	6.00×10^{-2}	3.69×10^{-2}
160	3.49×10^{-1}	2.55×10^{-1}	2.09×10^{-1}	3.04×10^{-1}
310	2.32×10^{-1}	3.38×10^{-1}	3.02×10^{-1}	4.04×10^{-1}
1000	3.18×10^{-1}	5.26×10^{-1}	1.93×10^{-1}	2.72×10^{-1}
1500	1.46E+00	1.85E+00	3.63×10^{-1}	4.36×10^{-1}
2000	1.32×10^{-1}	1.78×10^{-1}	6.75×10^{-2}	7.37×10^{-2}
2510	ND	ND	ND	ND
3010	1.48×10^{-1}	2.60×10^{-1}	7.11×10^{-2}	8.89×10^{-2}
4010	1.50×10^{-1}	1.52×10^{-1}	2.99×10^{-2}	2.58×10^{-2}
4210	ND	ND	ND	ND

Table 71: Pigment to POC ratios of in-situ pump samples collected during BaRFlux 6 cruise on 1-μm filter. Depth is in meters.

pigment/POC contd.

depth	chl-b	stdev	chl-a	stdev	pptn-a	stdev
80	2.62×10^{-2}	2.99×10^{-2}	3.11×10^{-1}	2.27×10^{-1}	3.80×10^{-2}	5.16×10^{-2}
90	ND	ND	ND	ND	ND	ND
110	1.64×10^{-1}	2.08×10^{-1}	9.42×10^{-1}	7.44×10^{-1}	1.17×10^{-3}	1.19×10^{-3}
160	9.02×10^{-2}	8.14×10^{-2}	3.77×10^{-1}	3.49×10^{-1}	1.38×10^{-3}	3.37×10^{-3}
310	6.80×10^{-3}	6.96×10^{-3}	3.16×10^{-2}	2.85×10^{-2}	2.14×10^{-1}	2.94×10^{-1}
1000	1.63×10^{-2}	2.93×10^{-2}	7.12×10^{-2}	6.00×10^{-2}	6.57×10^{-3}	1.61×10^{-2}
1500	ND	ND	7.10×10^{-2}	2.59×10^{-2}	1.70×10^{-2}	3.39×10^{-2}
2000	3.18×10^{-4}	8.99×10^{-4}	7.43×10^{-3}	8.73×10^{-3}	1.10×10^{-3}	3.12×10^{-3}
2510	ND	ND	1.98×10^{-2}	ND	ND	ND
3010	ND	ND	9.84×10^{-3}	5.49×10^{-3}	9.84×10^{-3}	1.37×10^{-2}
4010	3.25×10^{-4}	7.26×10^{-4}	3.60×10^{-3}	3.56×10^{-3}	ND	ND
4210	1.95×10^{-3}	ND	3.94×10^{-3}	ND	ND	ND

Table 72: Mole percent pigment compositions of in-situ pump samples collected on 70-μm filters during BaRFlux cruise 6. Depth is in meters.

70-μm filters

depth	ppb-a	stdev	pyro-a	stdev	chl-b	stdev	chl-a	stdev	pptn-a	stdev
60	50.35	0.41	21.50	4.17	20.40	3.90	4.37	0.53	3.37	0.16
80	48.49	0.30	23.82	2.08	4.66	0.14	19.06	3.32	3.98	1.09
140	24.31	0.51	41.57	0.69	8.60	0.35	24.01	0.18	1.51	0.71
160	11.61	1.38	40.18	4.04	21.22	2.24	20.78	0.42	6.21	0.84
1000	17.87	1.01	25.39	1.33	21.91	2.90	17.67	2.47	17.16	0.11
1500	31.37	9.31	36.94	11.71	ND	ND	3.42	2.00	28.26	4.40
2000	27.72	5.70	41.59	9.17	9.40	2.52	5.31	3.34	15.98	0.60
2490	ND	ND	ND	ND	49.92	5.99	23.59	1.09	26.49	7.07
2510	43.31	6.25	12.90	12.90	ND	ND	15.78	4.44	28.01	14.71
2990	78.65	6.23	ND	ND	7.75	2.16	12.36	2.44	1.25	1.76
3010	ND	ND	ND	ND	41.15	2.96	58.85	2.96	ND	ND

Table 73: Pigment concentrations of in-situ pump samples collected on 70-μm filters during BaRFlux cruise 6 in pg/L. Depth is in meters.

pg/L

depth	ppb-a	stdev	pyro-a	stdev	chl-b	stdev	chl-a	stdev	pptn-a	stdev
60	1552.27	315.29	619.58	232.36	925.70	4.00	198.11	15.25	151.15	22.69
80	711.35	32.53	316.26	39.98	104.50	0.96	418.53	56.82	86.66	26.87
140	327.14	23.20	506.29	54.85	178.21	23.62	488.27	48.53	28.57	11.35
160	50.69	1.70	161.23	29.78	141.98	2.88	138.38	14.63	39.82	2.00
1000	27.28	2.78	34.80	0.25	51.38	9.08	40.31	3.81	38.39	1.50
1500	72.45	10.67	99.97	65.40	ND	ND	17.03	13.77	102.54	29.64
2000	40.01	8.47	56.27	20.46	20.25	2.38	10.91	7.10	34.60	6.74
2490	ND	ND	ND	ND	140.38	30.19	64.85	9.28	68.86	11.97
2510	20.91	4.05	5.86	5.86	ND	ND	11.24	2.63	19.20	9.36
2990	893.69	231.52	ND	ND	125.88	12.91	201.10	5.66	15.63	22.10
3010	ND	ND	ND	ND	42.32	5.42	59.18	0.37	ND	ND

Table 74: Pigment to POC ratios of in-situ pump samples collected during BaRFlux 6 cruise on 70-μm filters. Depth is in meters.

pigment/POC

depth	ppb-a	stdev	pyro-a	stdev
60	4.34×10^{-3}	8.82×10^{-4}	1.73×10^{-3}	6.50×10^{-4}
80	9.56×10^{-4}	4.37×10^{-5}	4.25×10^{-4}	5.38×10^{-5}
140	3.76×10^{-4}	2.67×10^{-5}	5.82×10^{-4}	6.30×10^{-5}
160	1.41×10^{-4}	4.72×10^{-6}	4.48×10^{-4}	8.27×10^{-5}
1000	1.29×10^{-4}	1.31×10^{-5}	1.64×10^{-4}	1.15×10^{-6}
1500	2.73×10^{-4}	4.02×10^{-5}	3.77×10^{-4}	2.47×10^{-4}
2000	2.81×10^{-4}	5.94×10^{-5}	3.95×10^{-4}	1.43×10^{-4}
2490	ND	ND	ND	ND
2510	ND	ND	5.94×10^{-3}	5.94×10^{-3}
2990	3.41×10^{-3}	8.82×10^{-4}	ND	ND
3010	ND	ND	ND	ND

Table 75: Pigment to POC ratios of in-situ pump samples collected during BaRFlux 6 cruise on 70-μm filters. Depth is in meters.

pigment/POC contd.

depth	chl-b	stdev	chl-a	stdev	pptn-a	stdev
60	2.59×10^{-3}	1.12×10^{-5}	5.54×10^{-4}	4.26×10^{-5}	4.23×10^{-4}	6.34×10^{-5}
80	1.41×10^{-4}	1.29×10^{-6}	5.63×10^{-4}	7.64×10^{-5}	1.17×10^{-4}	3.61×10^{-5}
140	2.05×10^{-4}	2.71×10^{-5}	5.61×10^{-4}	5.57×10^{-5}	3.28×10^{-5}	1.30×10^{-5}
160	3.94×10^{-4}	7.99×10^{-6}	3.84×10^{-4}	4.06×10^{-5}	1.11×10^{-4}	5.55×10^{-6}
1000	2.42×10^{-4}	4.29×10^{-5}	1.90×10^{-4}	1.80×10^{-5}	1.81×10^{-4}	7.09×10^{-6}
1500	ND	ND	6.42×10^{-5}	5.19×10^{-5}	3.87×10^{-4}	1.12×10^{-4}
2000	1.42×10^{-4}	1.67×10^{-5}	7.65×10^{-5}	4.97×10^{-5}	2.43×10^{-4}	4.72×10^{-5}
2490	7.43×10^{-4}	1.60×10^{-4}	3.43×10^{-4}	4.91×10^{-5}	3.65×10^{-4}	6.34×10^{-5}
2510	1.43×10^{-3}	1.43×10^{-3}	1.43×10^{-2}	1.21×10^{-2}	ND	ND
2990	4.80×10^{-4}	4.92×10^{-5}	7.66×10^{-4}	2.16×10^{-5}	5.96×10^{-5}	8.42×10^{-5}
3010	3.43×10^{-4}	4.40×10^{-5}	4.80×10^{-4}	3.00×10^{-6}	ND	ND

Table 76: Mole percent pigment compositions of Niskin bottle samples collected during BaRFlux cruise 6. Depth is in meters.
*Indicates Chlorophyll maximum

depth	ppb-a	stdev	pyro-a	stdev	chl-b	stdev	chl-a	stdev	pptn-a	stdev
10	15.33	15.33	ND	ND	4.61	1.75	80.06	13.58	ND	ND
25	ND	ND	ND	ND	5.60	ND	94.40	ND	ND	ND
50	22.98	19.47	ND	ND	5.90	1.74	71.12	17.84	ND	ND
68*	33.79	ND	ND	ND	9.01	ND	57.19	ND	ND	ND
70	49.60	ND	ND	ND	5.85	ND	44.56	ND	ND	ND
75	39.09	3.27	ND	ND	9.74	0.45	51.17	2.82	ND	ND
80	42.74	1.48	ND	ND	9.59	0.28	47.67	1.20	ND	ND
100	30.47	30.47	ND	ND	2.01	2.01	17.52	17.52	ND	ND
150	ND	ND	ND	ND	ND	ND	ND	ND	ND	ND
200	ND	ND	ND	ND	14.46	ND	85.54	ND	ND	ND
300	ND	ND	ND	ND	ND	ND	66.67	47.14	ND	ND
500	ND	ND	ND	ND	ND	ND	ND	ND	ND	ND
800	ND	ND	ND	ND	ND	ND	100	ND	ND	ND
1000	ND	ND	ND	ND	37.43	37.43	12.57	12.57	ND	ND
1500	ND	ND	ND	ND	ND	ND	ND	ND	ND	ND
2000	ND	ND	ND	ND	ND	ND	ND	ND	ND	ND
2500	ND	ND	ND	ND	66.96	ND	33.04	ND	ND	ND
3000	ND	ND	ND	ND	ND	ND	ND	ND	ND	ND
3500	ND	ND	ND	ND	ND	ND	ND	ND	ND	ND
4000	ND	ND	ND	ND	ND	ND	ND	ND	ND	ND
4200	ND	ND	ND	ND	ND	ND	ND	ND	ND	ND
4573	ND	ND	ND	ND	ND	ND	100	ND	ND	ND

Table 77: Piigment concentrations of Niskin bottle samples collected during BaRFlux cruise 6. Depth is in meters.
*Indicates Chlorophyll maximum

ng/L

depth	ppb-a	stdev	pyro-a	stdev	chl-b	stdev	chl-a	stdev	pptn-a	stdev
10	31.91	31.91	ND	ND	12.47	3.34	218.94	10.30	ND	ND
25	ND	ND	ND	ND	63.49	ND	1053.53	ND	ND	ND
50	108.21	106.10	ND	ND	33.85	5.55	399.85	27.95	ND	ND
68	280.53	ND	ND	ND	114.57	ND	715.73	ND	ND	ND
70	991.41	ND	ND	ND	178.90	ND	1342.78	ND	ND	ND
75	676.27	95.42	ND	ND	256.01	3.19	1323.58	4.03	ND	ND
80	602.10	50.25	ND	ND	206.10	4.15	1009.40	24.07	ND	ND
100	267.31	267.31	ND	ND	27.06	27.06	231.65	231.65	ND	ND
150	ND	ND	ND	ND	ND	ND	ND	ND	ND	ND
200	ND	ND	ND	ND	2.30	ND	13.37	ND	ND	ND
300	ND	ND	ND	ND	ND	ND	2.10	1.63	ND	ND
500	ND	ND	ND	ND	ND	ND	ND	ND	ND	ND
800	ND	ND	ND	ND	ND	ND	0.77	ND	ND	ND
1000	ND	ND	ND	ND	1.20	1.20	0.40	0.40	ND	ND
1500	ND	ND	ND	ND	ND	ND	ND	ND	ND	ND
2000	ND	ND	ND	ND	ND	ND	ND	ND	ND	ND
2500	ND	ND	ND	ND	2.31	ND	1.12	ND	ND	ND
3000	ND	ND	ND	ND	ND	ND	ND	ND	ND	ND
3500	ND	ND	ND	ND	ND	ND	ND	ND	ND	ND
4000	ND	ND	ND	ND	ND	ND	ND	ND	ND	ND
4200	ND	ND	ND	ND	ND	ND	ND	ND	ND	ND
4573	ND	ND	ND	ND	ND	ND	0.64	ND	ND	ND

Table 78: Pigment to POC ratios of Niskin bottle samples collected during BaRFlux 6 cruise. Depth is in meters.
*Indicates Chlorophyll maximum.

pigment/POC

depth	ppb-a	stdev	pyro-a	stdev
10	3.40×10^{-4}	3.40×10^{-4}	ND	ND
25	ND	ND	ND	ND
50	–	–	–	–
68	–	–	–	–
70	1.15×10^{-2}	ND	ND	ND
75	–	–	–	–
80	1.11×10^{-2}	9.27×10^{-4}	ND	ND
100	4.86×10^{-3}	4.86×10^{-3}	ND	ND
150	ND	ND	ND	ND
200	ND	ND	ND	ND
300	ND	ND	ND	ND
500	ND	ND	ND	ND
800	ND	ND	ND	ND
1000	–	–	–	–
1500	ND	ND	ND	ND
2000	ND	ND	ND	ND
2500	ND	ND	ND	ND
3000	ND	ND	ND	ND
3500	ND	ND	ND	ND
4000	ND	ND	ND	ND
4200	ND	ND	ND	ND
4573	ND	ND	ND	ND

Table 79: Pigment to POC ratios of Niskin bottle samples collected during BaRFlux 6 cruise. Depth is in meters.
*Indicates Chlorophyll maximum.

pigment/POC contd.

depth	chl-b	stdev	chl-a	stdev	pptn-a	stdev
10	1.33×10^{-4}	3.56×10^{-5}	2.33×10^{-3}	1.10×10^{-4}	ND	ND
25	9.12×10^{-4}	ND	1.51×10^{-2}	ND	ND	ND
50	–	–	–	–	–	–
68	–	–	–	–	–	–
70	2.08×10^{-3}	ND	1.56×10^{-2}	ND	ND	ND
75	–	–	–	–	–	–
80	3.80×10^{-3}	7.66×10^{-5}	1.86×10^{-2}	4.44×10^{-4}	ND	ND
100	4.92×10^{-4}	4.92×10^{-4}	4.21×10^{-3}	4.21×10^{-3}	ND	ND
150	ND	ND	ND	ND	ND	ND
200	4.29×10^{-5}	ND	2.50×10^{-4}	ND	ND	ND
300	ND	ND	3.89×10^{-5}	3.02×10^{-5}	ND	ND
500	ND	ND	ND	ND	ND	ND
800	ND	ND	1.62×10^{-5}	ND	ND	ND
1000	–	–	–	–	–	–
1500	ND	ND	ND	ND	ND	ND
2000	ND	ND	ND	ND	ND	ND
2500	4.97×10^{-5}	ND	2.42×10^{-5}	ND	ND	ND
3000	ND	ND	ND	ND	ND	ND
3500	ND	ND	ND	ND	ND	ND
4000	ND	ND	ND	ND	ND	ND
4200	ND	ND	ND	ND	ND	ND
4573	ND	ND	1.50×10^{-5}	ND	ND	ND

References

L. Abramson, C. Lee, Z. Liu, S. G. Wakeham, and J. Szlosek. Exchange between suspended and sinking particles in the northwest mediterranean as inferred from the organic composition of in situ pump and sediment trap samples. *Limnology and Oceanography*, 55(2):725, 2010.

Alice L. Alldredge, Granada T.C., C.C. Gotschalk, and T.D. Dickey. The physical strength of marine snow and its implications for particle disaggregation in the ocean. *Limnology and Oceanography*, 35(7):1415–1428, 1990.

Josephine Y. Aller and Robert C. Aller. Evidence for localized enhancement of biological activity associated with tube and burrow structures in deep-sea sediments at the hebble site, western north atlantic. *Deep Sea Research*, 33(6):755–790, 1986.

R.C. Aller. The effects of macrobenthos on chemical properties of marine sediments and overlying waters. In P.L. McCall and M.J.S. Tevesz, editors, *Animal-Sediment Relations: The Biogenic Alteration of Sediments.*, pages 53–102. Plenum Press; N.Y., 1982.

M. A. Altabet, J. K. B. Bishop, and J. J. McCarthy. Differences in particulate nitrogen concentration and isotopic composition for samples collected by bottles and large-volume pumps in gulf stream warm-core rings and the sargasso sea. *Deep Sea Research Part I: Oceanographic Research Papers*, 39:S405–S417, 1992.

R. A. Armstrong, C. Lee, J. I. Hedges, S. Honjo, and S. G. Wakeham. A new, mechanistic model for organic carbon fluxes in the ocean based on the quantitative association of poc with ballast minerals. *Deep Sea Research Part II: Topical Studies in Oceanography*, 49(1):219–236, 2002.

R.A. Armstrong, M.L. Peterson, C. Lee, and S.G. Wakeham. Settling velocity spectra and the ballast ratio hypothesis. *Deep Sea Research Part II*, 56:1470–1478, 2009.

F. Azam and F. Malfatti. Microbial structuring of marine ecosystems. *Nature Reviews Microbiology*, 5(10):782–791, 2007.

M. P. Bacon and R. F. Anderson. Distribution of thorium isotopes between dissolved and particulate forms in the deep sea. *J. Geophys. Res.-Oceans*, 87:2045–2056., 1982.

M. J. Behrenfeld and E. S. Boss. Resurrecting the ecological underpinnings of ocean plankton blooms. *Annual review of marine science*, 6:167–194, 2014.

T. S. Bianchi and E. A. Canuel. *Chemical biomarkers in aquatic ecosystems.* Princeton University Press, 2011.

T. S. Bianchi, J. E. Bauer, E. R. Druffel, and C. D. Lambert. Pyrophaeophorbide-a as a tracer of suspended particulate organic matter from the ne pacific continental margin. *Deep Sea Research Part II: Topical Studies in Oceanography*, 45(4):715–731, 1988a.

T. S. Bianchi, R. Dawson, and P. Sawangwong. The effects of macrobenthic deposit-feeding on the degradation of chloropigments in sandy sediments. *Journal of Experimental Marine Biology and Ecology*, 122(3):243–255, 1988b.

Pierre E. Biscaye and Stephen L. Eittreim. Suspended particulate loads and transports in the nepheloid layer of the abyssal atlantic ocean. *Developments in Sedimentology*, 23:155–172, 1977.

J. K. B Bishop, D.R. Ketten, and J.M. Edmond. Chemistry, biology and vertical flux of particulate matter from the upper 400 m of the cape basin in the southeast atlantic ocean. *Deep Sea Research*, 25(12):1121–1161, 1978.

K. O. Buesseler, A. N. Antia, M. Chen, S. W. Fowler, W. D. Gardner, O. Gustafsson, and T. Trull. An assessment of the use of sediment traps for estimating upper ocean particle fluxes. *Journal of Marine Research*, 65:345–416, 2007a.

K. O. Buesseler, C. H. Lamborg, P. W. Boyd, P. J. Lam, T. W. Trull, R. R. Bidigare, and S. Wilson. Revisiting carbon flux through the ocean's twilight zone. *Science*, 316 (5824):567–570, 2007b.

J. Bustillos-Guzman, D. Lopez-Cortes, M. Mathus, and F. Hernandez. Dynamics of pigment degradation by the copepodite stage of pseudodiaptomus euryhalinus feeding on tetraselmis suecica. *Marine Biology*, 140(1):143–149, 2002.

S. R. Carpenter, M. M. Elser, and J. J. Elser. Chlorophyll production, degradation, and sedimentation: Implications for paleolimnology. *Limnology and Oceanography*, 31: 112–124, 1986.

P. Cartaxana, B. Jesus, and V. Brotas. Pheophorbide and pheophytin-a like pigments as useful markers for intertidal microphytobenthos grazing by hydrobia ulvae. *Estuarine, Coastal and Shelf Science*, 58(2):293–297, 2003.

N. Chen, T. S. Bianchi, and J. M. Bland. Implications for the role of pre-versus post-depositional transformation of chl-a in the lower mississippi river and louisiana shelf. *Marine Chemistry*, 81(1):37–55, 2003.

B. C. Cho and F. Azam. Major role of bacteria in biogeochemical fluxes in the ocean's interior. *Nature*, 332(6163):441–443, 1988.

R. J. Daley and S. R. Brown. Chlorophyll, nitrogen, and photosynthetic patterns during growth and senecense of two blue-green algae. *Journal of Phycology*, 9(4):395–101, 1973.

G. B. Deevey and A. L. Brooks. Copepods of the sargasso sea off bermuda: species composition, and vertical and seasonal distribution between the surface and 2000 m. *Bulletin of Marine Science*, 27(2):256–291, 1977.

J. Dymond, K. Fischer, M. Clauson, R. Cobler, W. Gardner, M. J. Richardson, and R. Dunbar. A sediment trap intercomparison study in the santa barbara basin. *Earth and Planetary Science Letters*, 53(3):409–418, 1981.

C. B. Eckardt, B. J. Keely, J. R. Waring, M. I. Chicarelli, J. R. Maxwell, J. W. De Leeuw, and J. D. Hudson. Preservation of chlorophyll-derived pigments in sedimentary organic matter [and discussion]. philosophical transactions of the royal society of london. *Series B: Biological Sciences*, 333(1268):339–348, 1991.

Steven Emerson and John Hedges. *Chemical oceanography and the marine carbon cycle*. Cambridge University Press, 2008.

W. D. Gardner, J. B. Southard, and C. D. Hollister. Sedimentation, resuspension and chemistry of particles in the northwest atlantic. *Marine Geology*, 65(3):199–242, 1985.

W.D. Gardner, M.J. Richardson, C.A. Carlson, D. Hansell, and A.V. Mishonov. Determining true particulate organic carbon: bottles, pumps and methodologies. *Deep-Sea Research II*, 50:655–674, 2003.

A. Hagström, F. Azam, A. Andersson, J. Wikner, and F. Rassoulzadegan. (1988). microbial loop in an oligotrophic pelagic marine ecosystem: possible roles of cyanobacteria and nanoflagellates in the organic fluxes. *Marine ecology progress series*, 49(1):171–178, 1988.

G. W. Hallegraeff. Seasonal study of phytoplankton pigments and species at a coastal station off sydney: Importance of diatoms and the nanoplankton. *Marine Biology*, 61: 107–118, 1981.

E. J. H. Head and L. R. Harris. Chlorophyll destruction by calanus sp. grazing on phytoplankton: Kinetics, effects of ingestion rate and feeding history, and a mechanistic interpretation. *Marine Ecology Progress Series*, 35(1):223–235, 1996.

C. Hoek. *Algae: an Introduction to Phycology.* Cambridge University Press, 1995.

S. Honjo, J. F. Connell, and P. L. Sachs. Deep-ocean sediment trap; design and function of parflux mark ii. *Deep Sea Research Part I: Oceanographic Research Papers*, 27(9): 745–753, 1980.

S.W. Jeffrey, S.W. Wright, and M. Zapata. Recent advances in hplc analysis of phytoplankton. *Marine and Freshwater Research*, 50(8):879–896, 1999.

L. L. King. *Chlorophyll diagenesis in the water column and sediments of the Black Sea*. PhD thesis, MIT-WHOI Joint Program, 1993.

C. Klaas and D. E. Archer. Association of sinking organic matter with various types of mineral ballast in the deep sea: Implications for the rain ratio. *Global Biogeochemical Cycles*, 16(4):63, 2002.

B. W. Klein, W. C. Gieskes, and G. G. Kraay. Digestion of chlorophylls and carotenoids by the marine protozoan oxyrrhis marina - studies of hplc analysis of algal pigments. *Journal of Plankton Research*, 8(5):827–836, 1986.

C. Lee, S. G. Wakeham, and J. I. Hedges. Composition and flux of particulate amino acids and chloropigments in equatorial pacific seawater and sediments. *Deep Sea Research Part I*, 47:1535–1568, 2000.

Z. Liu, G. Stewart, J.K. Cochran, C. Lee, R. A. Armstrong, D. J. Hirschberg, and J. C Miquel. Why do poc concentrations measured using niskin bottle collections sometimes differ from those using in-situ pumps? *Deep Sea Research Part I: Oceanographic Research Papers*, 52(7):1324–1344, 2005.

Z. Liu, J.K. Cochran, C. Lee, B. Gasser, J.C. Miquel, and S.G. Wakeham. Further investigations on why poc concentrations differ in samples collected by niskin bottle and in situ pump. *Deep Sea Research Part II: Topical Studies in Oceanography*, 2009.

M. W. Lomas and S. B. Moran. Evidence for aggregation and export of cyanobacteria and nano-eukaryotes from the sargasso sea euphotic zone. *Biogeosciences*, 8:203–216, 2011.

William J. Louda, J. W. Loitz, D. T. Rudnick, and E. W. Baker. Early diagenetic alteration of chl-a and bacteriochl-a in a contemporaneous marl ecosystem; florida bay. *Organic Geochemistry*, 31(12):1561–1580, 2000.

I. McCave. The vertical flux of particles in the ocean. *Deep Sea Research and Oceanographic Abstracts*, 22(7):491–502, July 1975.

A.F. Michaels, D.A. Caron, N.R. Swanberg, F.A. Howse, and C.M. Michaels. Planktonic sarcodines (acantharia, radiolaria, formnifera) in surface waters near bermuda: abundance, biomass and vertical flux. *Journal of Plankton Research*, 17:131–163, 1995.

S. Monk and R. Johnson. Bermuda atlantic time-series study (bats). `http://batsftp.bios.edu/BATS/bottle/bats_pigments.txt`, March 2014.

S. B. Moran, M. A. Charette, S. M. Pike, and C. A. Wicklund. Differences in seawater particulate organic carbon concentration in samples collected using small-and large-volume methods: the importance of doc adsorption to the filter blank. *Marine Chemistry*, 67 (1):33–42, 1999.

Uta Passow. Transparent exopolymer particles (tep) in aquatic environments. *Progress in Oceanography*, 55(3):287–333, 2002.

M. L. Peterson, D.S. Thoreson, J.I. Hedges, C. Lee, and S.G. Wakeham. Field evaluation of a valved sediment trap. *Limnol. Oceanography*, 38:1741–1761, 1993.

Michael L. Peterson, S.G. Wakeham, C. Lee, M.A. Askea, and J.C. Miquel. Novel techniques for collection of sinking particles in the ocean and determining their settling rates. *Limnology and Oceanography: Methods 3*, pages 520–532, 2005.

C. H. Pilskaln, K. Hayashi, B. A. Keafer, D. M. Anderson, and D. J. McGillicuddy Jr. Benthic nepheloid layers in the gulf of maine and alexandrium cyst inventories. *Deep Sea Research Part II: Topical Studies in Oceanography*, 103:55–65, 2014.

N. Reuss, D. J. Conley, and T. S. Bianchi. Preservation conditions and the use of sediment pigments as a tool for recent ecological reconstruction in four northern european estuaries. *Marine Chemistry*, 95(3):283–302, 2005.

R. B. Rivkin and M. R. Anderson. Inorganic nutrient limitation of oceanic bacterioplankton. *Limnology and Oceanography*, 42(4):730–740, 1997.

Y. Satoh and T. Hama. Stepwise alteration from fluorescent to non-fluorescent chlorophyll derivatives during early diagenesis of phytoplankton in aquatic environments. *Journal of Experimental Marine Biology and Ecology*, 449:36–44, 2013.

C. C. Sheridan. Suspended particles in the equatorial pacific ocean: Organic concentration, composition, and relation to cycling processes. Master's thesis, Stony Brook University - School of Marine and Atmospheric Sciences., 2000.

F. Randolph Shuman and Carl J. Lorenzen. Quantitative degradation of chlorophyll by a marine herbivore. *Limnology and Oceanography*, 20(4):580–586, 1975.

Craig R. Smith, D. J. Hoover, S. E. Doan, R. H. Pope, D. J. Demaster, F. C. Dobbs, and M. A. Altabet. Phytotdetritus at the abyssal seafloor across $10^{c}irc$ of latitute in the central equatorial pacific. *Deep Sea Research Part II: Topical Studies in Oceanography*, 43(4-6):1309–1338, 1996.

D.C. Smith, M. Simon, A. Alldredge, and F. Azam. Intense hydrolytic enzyme activity on marine aggregates and implications for rapid particle dissolution. *Nature,*, 359:10, 1992.

D. K. Steinberg, C. A. Carlson, N. R. Bates, R. J. Johnson, A. F. Michaels, and A. H. Knap. Overview of the us jgofs bermuda atlantic time-series study (bats): a decade-scale look at ocean biology and biogeochemistry. *Deep Sea Research Part II: Topical Studies in Oceanography*, 48(8):1405–1447, 2001.

A. D. Steinman, K. E. Havens, J. W. Louda, N. M. Winfree, and E. W. Baker. Characterization of the photoautotrophic algal and bacterial communities in a large shallow subtropical lake using hplc-pda based pigment analysis. *Canadian Journal of Fisheries and Aquatic Science*, 55:206–219, 1998.

S.L. Strom. Production of pheopigments by marine protozoa: Results of laboratory experiments analysed by hplc. *Deep Sea Research Part I*, 40(1):57–80, 1993.

M. Sun, R. C. Aller, and C. Lee. Early diagenesis of chl-a in long island sound sediments: A measure of carbon flux and particle reworking. *Journal of Marine Research*, 49(2): 379–401, 1991.

M. Szymczak-Zyła, G. Kowalewska, and J. W. Louda. The influence of microorganisms on chlorophyll a degradation in the marine environment. *Limnol. Oceanography*, 53(2): 851–862, 2008.

R. Turnewitsch, B.M. Springer, K. Kiriakoulakis, J.C. Vilas, J. Aristegui, G. Wolff, F. Peine, S. Werk, G. Graf, and J.J. Waniek. Determination of particulate organic carbon (poc) in seawater: the relative methodological importance of artificial gains and losses in two glass-fiber-filter-based techniques. *Marine Chemistry*, 105:208–228, 2007.

M. Vernet and C. J. Lorenzen. The relative abundance of pheophorbide a and pheophytin a in temperate marine waters. *Limnology and oceanography,*, 32(2):352–358, 1987.

P. R. Vogt and W. Y. Jung. Origin of the bermuda volcanoes and the bermuda rise: history, observations, models, and puzzles. *Geological Society of America Special Papers*, 430:553–591, 2007.

S. G. Wakeham and E. A. Canuel. Organic geochemistry of particulate matter in the eastern tropical north pacific ocean: Implications for particle dynamics. *Journal of Marine Research*, 46(1):183–213, 1988.

S. G. Wakeham and C. Lee. Organic geochemistry of particulate matter in the ocean: The role of particles in oceanic sedimentary cycles. *Organic Geochemistry*, 14(1):83–96, 1988.

S. G. Wakeham, J. I. Hedges, C. Lee, M. L. Peterson, and P. J. Hernes. Compositions and transport of lipid biomarkers through the water column and surficial sediments of the equatorial pacific ocean. *Deep Sea Research Part II: Topical Studies in Oceanography*, 44(9):2131–2162, 1997.

S. G. Wakeham, C. Lee, M. L. Peterson, Z. Liu, J. Szlosek, I. F. Putnam, and J. Xue. Organic biomarkers in the twilight zone - time series and settling velocity sediment traps during medflux. *Deep Sea Research Part II: Topical Studies in Oceanography*, 56 (18):1437–1453, 2009.

R. Ziegler, A. Blaheta, N. Guha, and B. Schonegge. Enzymatic formation of phaeophorbide and pyrophaeophorbide during chlorophyll degradation in a mutant of chlorella fusca. *Journal of Plant Physiology*, 132(3):327–332, 1988.